

POLITECNICO DI TORINO

Master of Science in Mechanical Engineering



Master Thesis

Meanline, Streamline and FEM Analyses for an industrial Gas Turbine unit

Supervisors

Prof.ssa Daniela Anna Misul

Prof. Mirko Baratta

Company Supervisors

Ing. Luca Forno

Ing. Marco Toppino

Candidate

Francesco Sorgi

ACADEMIC YEAR 2019/2020

Index

1	Industrial Turbines for Power Generation.....	2
1.1	Electricity generation.....	2
1.2	Thermal power station in the world, European and Italian context	3
1.3	Gas Turbine Power Plants.....	5
2	Case Study – FR1625.....	7
2.1	Thermodynamic Principles	7
2.2	NOx abatement.....	10
2.3	Fuel.....	10
2.3.1	LHV calculation.....	11
2.4	Compressor air extraction.....	12
2.5	Valuation compressor thermodynamic properties for each stage	14
2.6	Estimated power generated by the turbine.....	16
2.7	Turbine cooling system definition.....	17
2.7.1	Cooling system purpose.....	17
2.7.2	Cooling system description.....	19
2.8	Main parameters used in pre-analysis	21
3	AxSTREAM Analysis	22
3.1	Software description.....	22
3.2	3D Turbine model generation	23
3.3	AxSLICE elaboration of 3D model.....	25
3.3.1	3D CAD model import and Slicing operation	25
3.3.2	Profile correction.....	27
3.4	Creation of the calculation model in AxSTREAM	31
3.4.1	Machine configuration.....	32
3.4.2	Definition of the main and cooling fluid properties.....	34
3.4.3	Loss models	36
3.4.4	Cooling model set up on AxSTREAM.....	36
3.4.5	Boundary conditions definition.....	40
3.5	Meanline analysis.....	41

3.5.1	Output and validation	41
3.6	Streamline analysis.....	43
3.6.1	Output and validation	43
3.6.2	Other results.....	45
4	Compressor thermo-structural FEA.....	50
4.1	Mathematical model	51
4.2	Numerical solution – FEM	52
4.3	Creation of the calculation model in Ansys.....	54
4.4	Post-processing	57
4.4.1	Aft stub shaft.....	58
4.4.2	Wheel 15.....	63
4.4.3	Wheel 14 – 13	69
5	Conclusions and further Developments.....	73
	Bibliografia	74
	Figure Index.....	75
	Table Index	77

Abstract

This thesis work stems from a partnership project between Politecnico di Torino and Ethos Energy Italia S.p.A., a turbine services provider specialized in design, production, and maintenance of gas turbines.

The main goal of the project is the creation of a predictive model in steady state operating conditions for an industrial gas turbine used for generator drive applications. Flow path Meanline (1D) and Streamline (2D) analyses are performed using AxSTREAM software, in order to obtain integral turbomachinery information (power, efficiency, mass flow rate) as well as distribution of kinematics and thermodynamics parameters in both streamwise and spanwise directions. The latter represent the set of boundary conditions to implement in a thermo-structural Finite Element Analysis (FEA) useful for rotor components lifetime evaluation.

First, an estimate of the flow rates involved, and power generated by the turbine is made. The set of all parameters defined in this preliminary analysis process and data already known are an important input or comparison information for the subsequent AxSTREAM model implemented.

AxSTREAM calculation model is defined starting from 3D models elaboration of the turbine components. Meanline and Streamline output parameters are presented in tabular and graphical form, leading to a perfect match with target data.

The work ends with thermo-structural FEA of the last four compressor rotor components, conducted through Ansys software and followed by creep and Low Cycle Fatigue (LCF) evaluation for component life prediction.

The thesis project was developed in a context of comprehensive study of the turbomachinery, and is part of a larger company program called Life Time Extension (LTE), whose main goal is the re-design of rotor parts and definition of an opportune maintenance plan allows to extend the useful life beyond that recommended by the OEM.

1 Industrial Turbines for Power Generation

Heavy duty industrial turbines are motor machine transforms an input source of primary energy into mechanical energy output. They are used in a vast number of industrial fields including electrical utilities power producers, industrial cogeneration (CHP - Combined Heat and Power) or mechanical drive applications in oil and gas refineries.

Turbines are one of the most flexible products in the industry, being able to act both in simple and combined cycle configuration; in the latter plant efficiency is considerably increased by recovering waste heat through a heat recovery steam generator and thus power a conventional steam turbine.

For these reasons, turbines are closely integrated with the devices they power, such as electric generator, secondary-energy equipment or gearbox connected to any operating machines.

1.1 Electricity generation

The importance of this production and distribution lies in the fact that modern society is fundamentally based on the consumption and exploitation of energy, of which a significant part is represented by electricity. Since electricity is not freely available in nature in large amounts, it must be necessarily produced, i.e. transformed from other forms of primary energy.

Almost all commercial electrical power on Earth is generated using electromechanical generators (except for solar PV), which efficiently convert mechanical energy into electrical energy (AC) using the electromagnetic induction principle. Generators are usually driven by a turbine, put in rotation by a working fluid. There are many types of turbines that base their operation on different sources of primary energy [1]:

- Steam turbines currently generate most of the electric power in the world using a variety of heat sources:
 - Combustion of fossil fuels (non-renewable sources) such as coal, oil, and other hydrocarbons.
 - Renewable fuels, such as biogas, biomass, urban solid waste, or wood waste.
 - Solar thermal energy or geothermal power.
 - Nuclear fission heat created in a nuclear reactor.
- Gas turbines directly driven by combustion gases. At least 20% of the world's electricity is generated by natural gas. Gas and steam turbines are usually located in the so-called thermal power station.
- Hydraulic turbines that exploit falling water potential energy or tides kinetic energy.
- Wind turbines that exploit wind kinetic energy.

1.2 Thermal power station in the world, European and Italian context

Thermal power plants represent the most widespread type of power plants and the primary energy source mainly used is that deriving from the combustion of fossil fuels.

In them, the thermal energy of an expanding fluid is exploited through gas or steam turbines to produce electricity. This process still represents the backbone of the production of electricity worldwide as it is possible to supply large powers, with rather high efficiency, in a wide and constant production regime.

The figures below show the evolution over the years of the use of various primary energy sources in different contexts, worldwide (figure 1.1), European (figure 1.2) [2] and Italian (figure 1.3) [3].

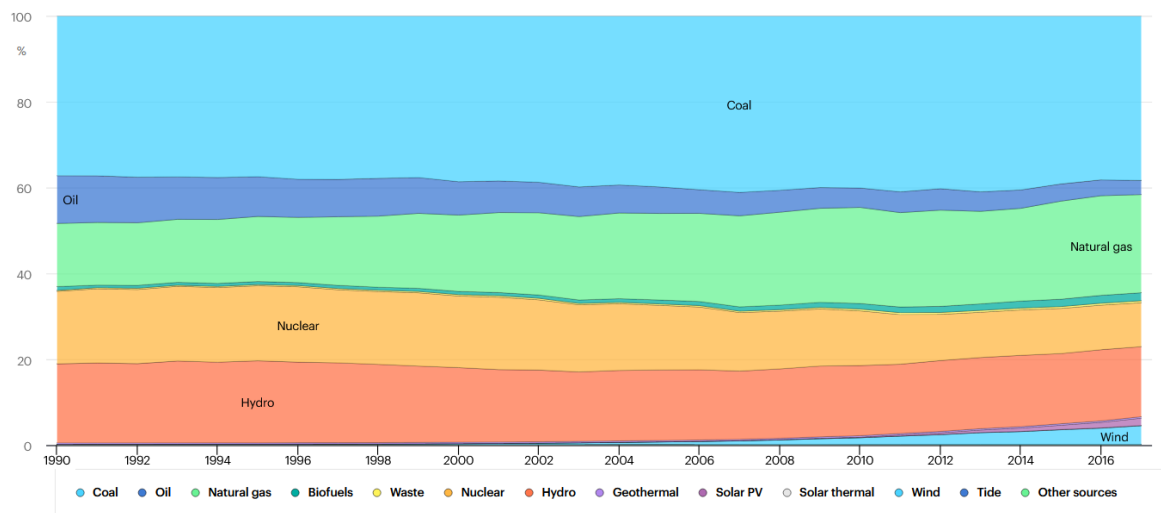


Figure 1.1: Electricity generation by source in the world – 1990-2017

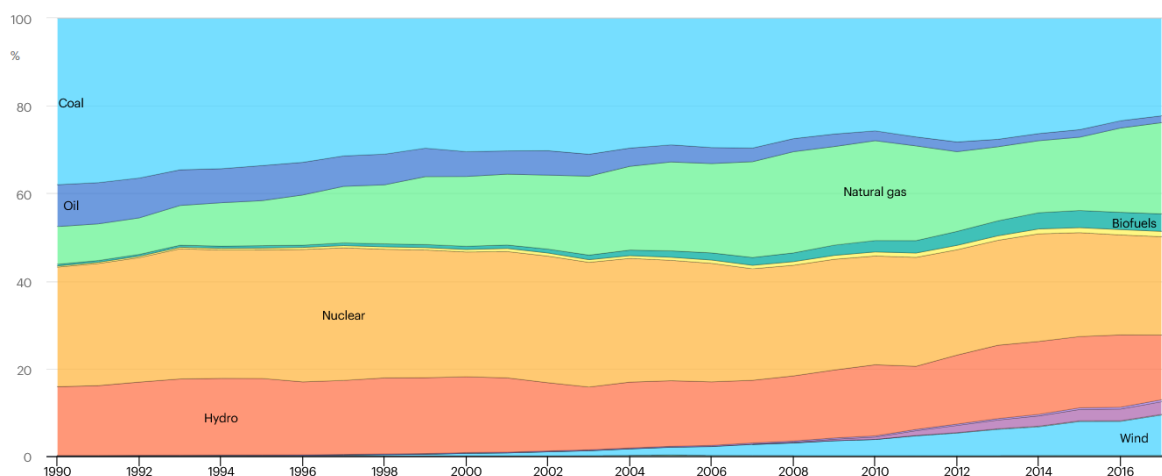


Figure 1.2: Electricity generation by source in Europe – 1990-2017

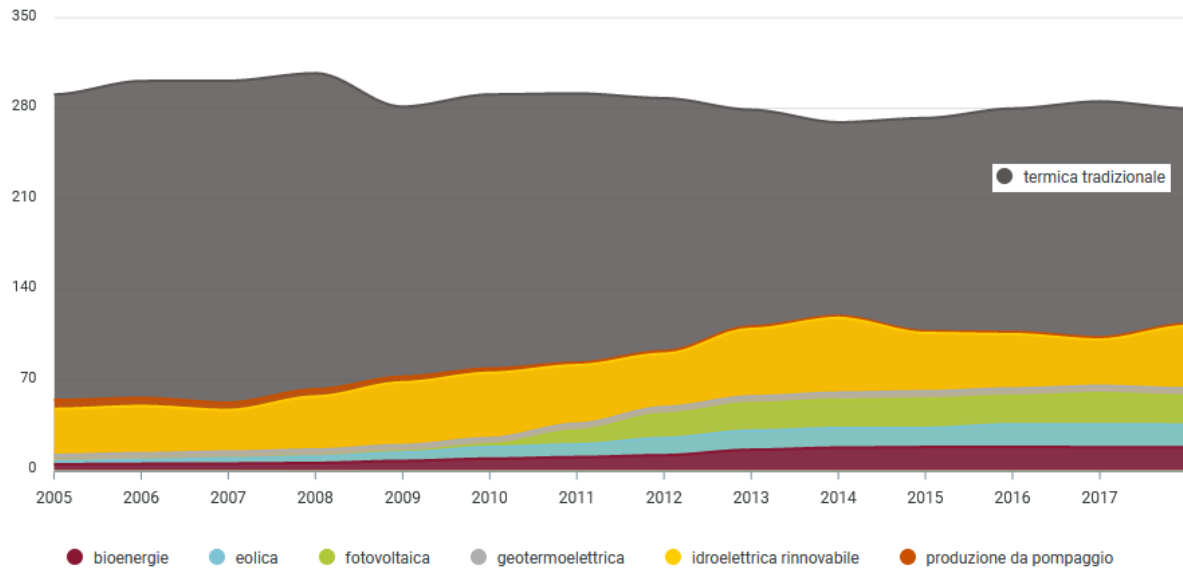


Figure 1.3: Electricity generation by source in Italy [TWh] – 2005-2018

The graphs confirm that regardless of the context, energy production is heavily dependent on the use of non-renewable sources despite the progressive development of technologies based on renewable sources. The growing attention to air pollution and consequences of climate change related mainly to the burning of oil and coal (to a lesser extent natural gas), combined with the variability of the price of fuel from politically unstable regions, have pushed the European Union to approval of heavy investments in the renewable sector.

In November 2018, the European Commission updated the objectives with a view to decarbonisation, so that the share of energy from renewable sources for final consumption should go from the current 17% to 32% [4]. This important goal was already achieved by Italy in 2012 and has been constantly improved up to the 40% share in 2018 (latest available data - figure 1.4) [3].

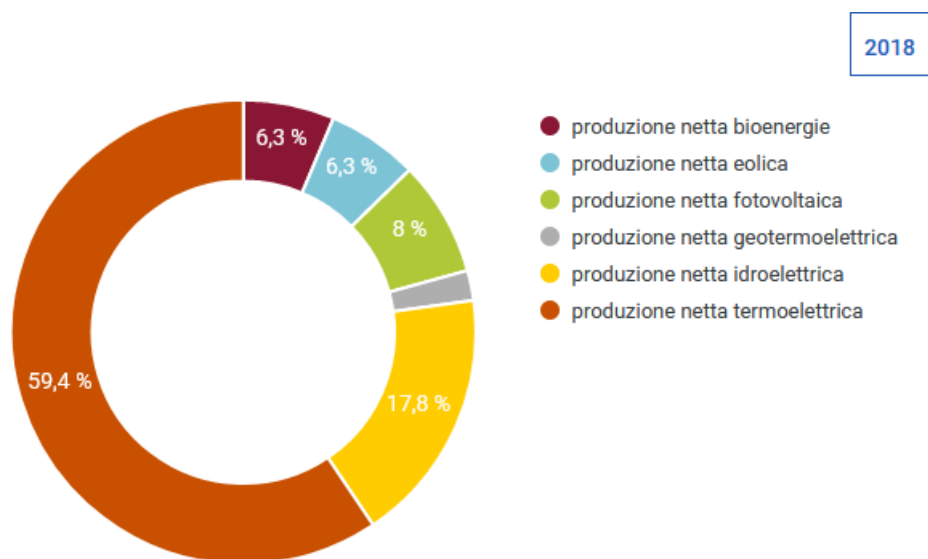


Figure 1.4: Electricity generation by source in Italy – 2018

Finally, at national level, it is interesting to observe how the percentages relating to the main fuels have changed radically over the years: there has been a radical reversal of the relative importance between oil and natural gas, the use of which has grown strongly in both absolute and percentage terms, bringing a great development to the market of gas turbine systems.

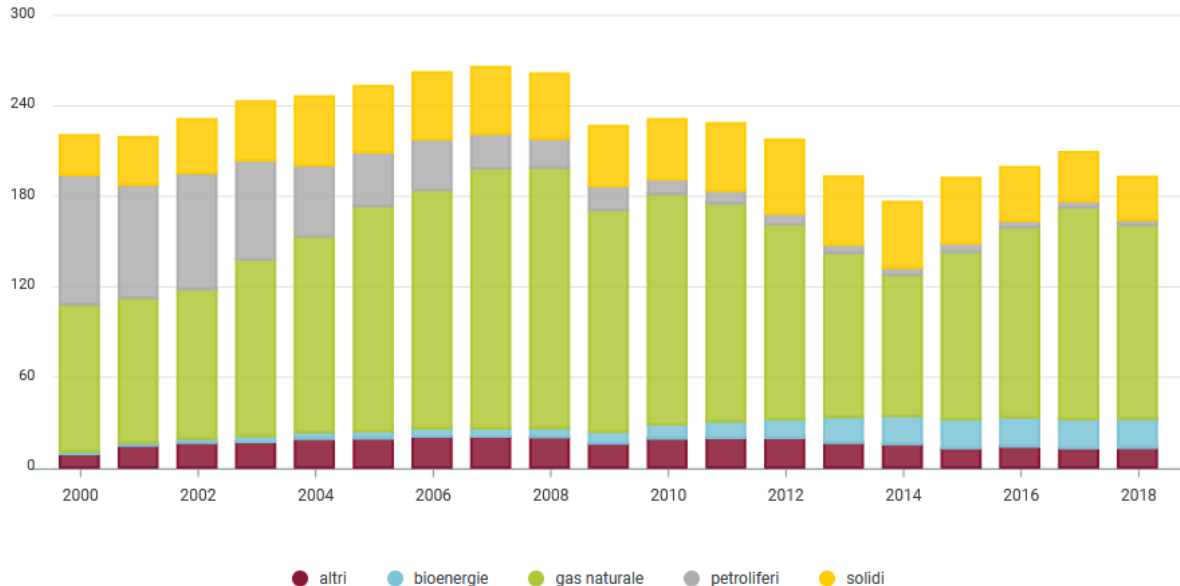


Figure 1.5: Electricity generation for fuel in Italy [GWh] – 2000-2018 [3]. Most of the Italian thermal power stations are currently powered by natural gas

1.3 Gas Turbine Power Plants

Natural gas is the fastest growing fossil fuel, accounting for nearly a quarter of global electricity generation. Its growth, in a sustainable development scenario, is estimated to continue until 2030 before reverting to present levels by 2040, thus gradually replacing the use of coal and oil [5]. According to estimates by the International Energy Agency, gas-fired power generation increased globally 4% in 2018, led by strong growth in the United States and China (figure 1.6).

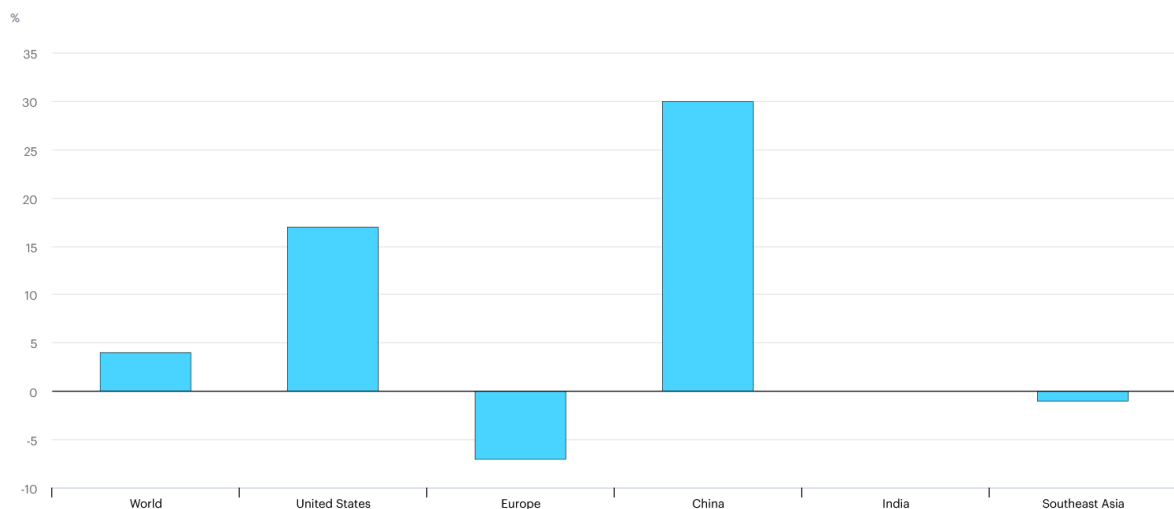


Figure 1.6: Changes in natural gas-fired power generation by region - 2018 [6]

There are many reasons for such an important growth in power generation sector:

- From the environmental impact point of view, it is the least harmful system based on fossil fuels since the combustion of natural gas does not produce dust and sulfur compounds (responsible for acid deposition). Moreover, switching from coal and oil burning plants to gas-fired plants could greatly reduce emissions of carbon dioxide and NO_x if relative prices and regulation support this potential.
- New technologies for combined cycle gas turbines plants allow a very high global efficiency (close to 60%). The possibility of exploiting increasingly advanced technologies makes it possible to reach higher temperatures and enthalpies variations compared to traditional steam plants, resulting in the opportunity to get higher power outputs with the same mass flow rate.
- Gas turbines operational flexibility allows to respond to short term demand fluctuations, thus they can offer supplement or support function to power systems with a growing share of variable renewables [5].
- Natural gas market is becoming increasingly globalized, supported by continuous development of storability systems, transmission, and distribution pipelines. “Despite the strong worldwide growth in demand, the reserves continue to rise, thanks to improvements in gas exploration technologies. The exploitable proven reserves are of around 150 Tm³, with a residual life, at present consumption rate, of around 65 years; considering another 200 Tm³ of potential discoveries, gas has a future potential nearly twice that of oil [7]”.

2 Case Study – FR1625

FR1625 is a simple-cycle single shaft gas turbine, a typical configuration used for generator drive applications where significant speed variation is not required.

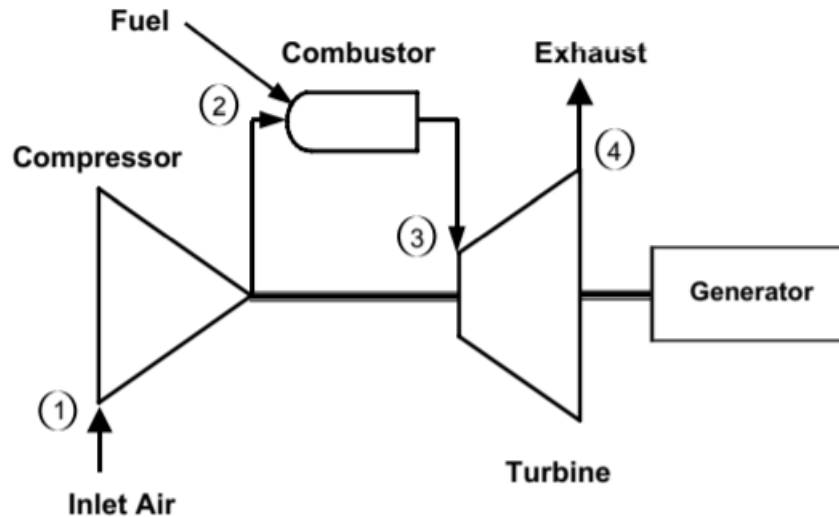


Figure 2.1: Single cycle, single shaft gas turbine

Gas turbine power plants generally have two different operating conditions dependent on both starts and hours of operation. Peaker plants generally run only when there is a high demand for electricity and operate at higher power factors or temperature rises. On the other hand, base load plants supply continuously a consistent amount of electricity, to meet the minimum demand. As the former supply power only occasionally, the power supplied results a much higher price per kilowatt hour than base load plants.

In this analysis, we focus exclusively on the Base Load condition operation.

2.1 Thermodynamic Principles

The thermodynamic cycle upon which all gas turbines operate is called the Brayton cycle (figure 2.2).

Air entering the gas turbine at the compressor inlet (point 1) is compressed to achieve the most favourable conditions in terms of temperature and pressure for the following combustion. In each stage, it is first accelerated by rotating blades, then stator stationary blades convert the gained kinetic energy into a pressure rise.

Air enters the combustion system at point 2 where fuel is injected, and combustion occurs. The combustion process occurs at essentially constant pressure.

Then, the hot exhaust gases are expanded through the turbine to produce the mechanical power (path 3-4). Regarding energy conversion, the chemical energy present in the combustion

reactants is transferred to the gas flow during combustion. This energy, measured in terms of gas enthalpy, is then converted into the mechanical work by expanding the gas through the turbine. This conversion takes place in two steps: in the nozzle section of the turbine, a portion of the thermal energy is converted into kinetic energy, whereas in the subsequent bucket section of the turbine, a portion of the kinetic energy is transferred to the rotating buckets and converted to work. Some of the work developed by the turbine is used to drive the compressor, and the remainder - available for useful work at the output flange of the gas turbine - is thus derived ultimately from the combustion process.

The path from 4 back to 1 indicates a constant-pressure cooling process. This cooling is done by the atmosphere, which provides fresh, cool air at point 1 in exchange for the hot gases exhausted to the atmosphere at point 4. The actual cycle is therefore an “open” rather than “closed” cycle.

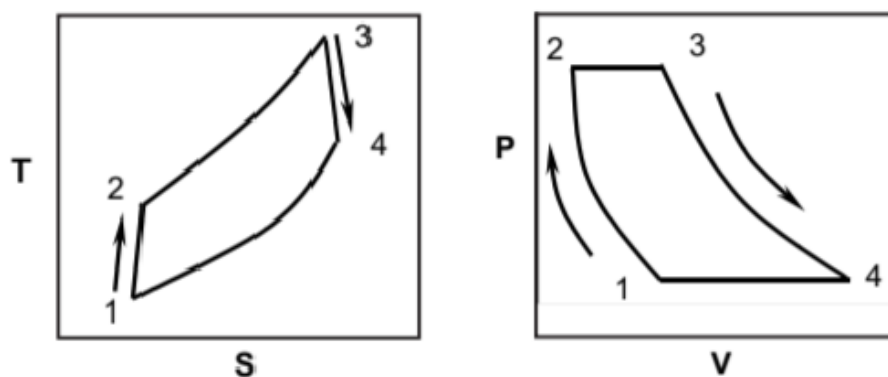


Figure 2.2: Temperature-entropy (TS) and pressure-volume (PV) diagrams for Brayton cycle

Every Brayton cycle can be characterized by two significant parameters: pressure ratio and firing temperature [8].

The pressure ratio of the cycle is the pressure at point 2 (compressor discharge pressure) divided by the pressure at point 1 (compressor inlet pressure). In an ideal cycle, this ratio is also equal to the pressure at point 3 divided by the pressure at point 4. However, in an actual cycle there is some slight pressure loss in the combustion system and hence, the pressure at point 3 is slightly lower than that at point 2.

The other significant parameter, firing temperature, is usually defined as the flow mean total temperature at the stage 1 nozzle trailing edge plane.

They strongly affect gas turbine performance (figure 2.3): the pressure ratio resulting in maximum output and maximum efficiency change with firing temperature, and the higher the pressure ratio, the greater the benefits from increased firing temperature. Increases in firing temperature provide power increases at a given pressure ratio, although there is an increase in cooling air requirement to maintain parts lives.

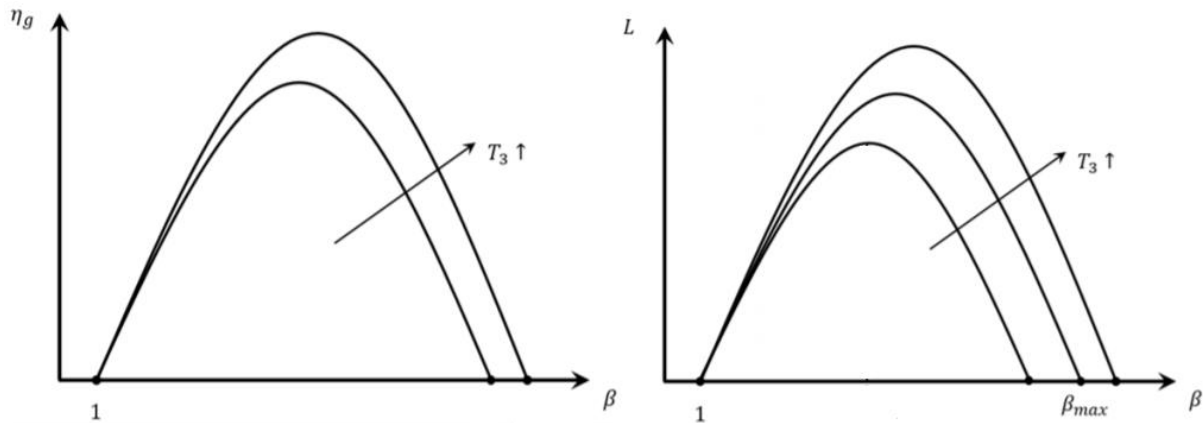


Figure 2.3: Global efficiency and specific power dependence over β and firing temperature

In our case study, their values are known through specific data supplied to the company and will be an important source of comparison and validation of the results obtained by simulation. They are subsequently referred to as β and T_{ir}° respectively.

Since the gas turbine is an air-breathing engine, its performance is changed by anything that affects the density and/or mass flow of the air intake to the compressor. Figure 2.4 shows how ambient temperature affects the output, heat rate, heat consumption, and exhaust flow of a single-shaft gas turbine [8]. Each turbine model has its own temperature-effect curve.

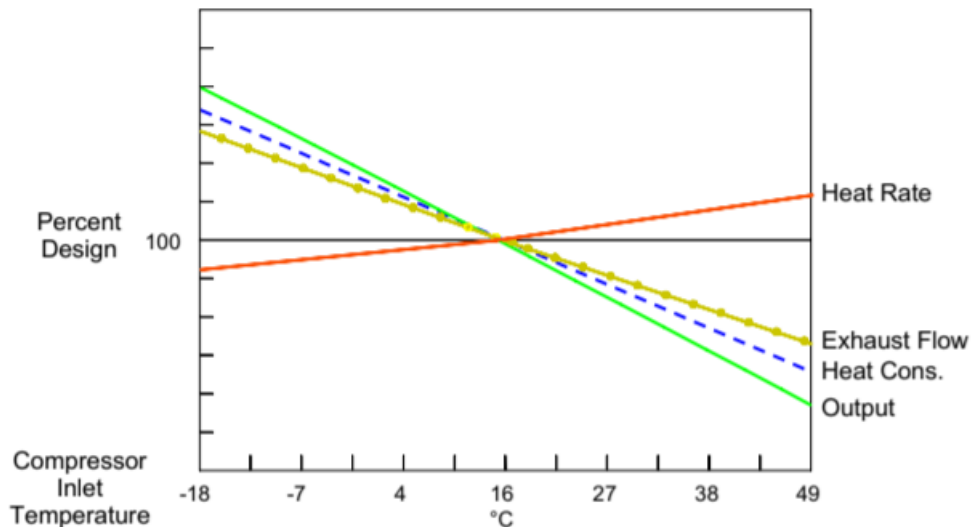


Figure 2.4: Effect of ambient temperature

Turbine performance are also sensible both to the effect of humid air, which is less dense than dry air, and to the altitude or barometric pressure since air density reduces as the site elevation increases. Since these conditions vary from day to day and from location to location, it is convenient to consider some standard conditions for our analysis. The standard conditions used by the gas turbine industry are 59 F/15 C, 14.7 psia/1.013 bar and 60% relative humidity, which are established by the International Standards Organization (ISO) and frequently referred to as

ISO conditions. Only the inlet pressure value assumed is different from that established by ISO standards: it is set equal to 1,003 bar, accounting for pressure losses at the entrance of the machine due to the presence of air filters and assumed equal to 100 mm H₂O (10 mbar).

2.2 NOx abatement

The control of NOx emissions is a crucial aspect in the design and maintenance of a gas turbine. The amount of NOx produced strictly depends on the combustion temperature: when the combustion takes place at a lower temperature the NOx emissions are reduced. For this purpose, two main technologies have been developed:

- Wet Low Emission (WLE) technology injects steam or water into the head end of the combustor. Generally, the amount of diluent is limited to the amount required to meet the NOx local requirement in order to minimize operating cost and impact on combustor and turbine parts life. Depending on the amount of water or steam injected, power output increase because of the additional mass flow.
- Dry low emission (DLE) technology reduces combustion temperature without using water or steam injection. This solution can reach lower levels of NOx emissions (less than 25 ppm).

In our analysis we consider a DLE technology approach.

2.3 Fuel

The chemical characterization of the fuel is very important as it directly affects the physico-chemical properties including the enthalpy value of the combustion gases entering the turbine, and therefore the power output value. In particular, the determination of the lower heating value (paragraph 2.5.1) is of crucial importance both in defining the flow rate of burnt fuel and the flow rate of air sucked by the compressor.

$$HR[KJ/KWh] = \frac{G_{fuel}[Kg/h] * \overline{LHV}[KJ/Kg]}{PU[KW]} \quad 2.1$$

$$G_{in,comp} = G_{exh} - G_{fuel} \quad 2.2$$

HR, PU, G_{exh} indicate respectively heat rate, useful power and turbine exhaust flow rate. They are known by specific data supplied to the company.

2.3.1 LHV calculation

Estimate of the fuel composition in molar percentage:

Fuel composition - x_i	
Nitrogen	0.82
Methane	74.43
Carbon Dioxide	9.51
Ethane	9.57
Propane	5.12
I-butane	0.48
I-pentane	0.07

Table 2-1: Fuel molar percentage

Components molar masses M_i [g/mol]:

Molar masses	
Nitrogen	28
Methane	16
Carbon Dioxide	44
Ethane	30
Propane	44
I-butane	58
I-pentane	72

Table 2-2: Components molar masses

Estimate of the fuel average molar mass:

$$\bar{M} = \sum_i x_i * M_i = 21.78 \text{ g/mol} \quad 2.3$$

Components LHVs [9]:

LHV [KJ/Kmol]	
Nitrogen	0
Methane	802600
Carbon Dioxide	0
Ethane	1428600
Propane	2043100
I-butane	2649000
I-pentane	3239500

Table 2-3: Components LHVs

Estimate of the fuel average LHV:

$$\overline{LHV} = \frac{\sum_i x_i * LHV_i}{\bar{M}} = 39204 \text{ KJ/Kg} \quad 2.4$$

2.4 Compressor air extraction

FR1625 has a 17 stages axial compressor. The compressor stator consists of four main components:

- The inlet casing located at the forward end of the gas turbine. It contains the variable Inlet guide vanes which control the amount of airflow across the compressor.
- The forward casing which contains the first four compressor stator vanes.
- The aft casing which contains the 5th to the 10th compressor stator vanes.
- The discharge casing which contains the last seven stages of compressor veins and two rows of exit guide vanes. It connects the compressor to the turbine section and supports the combustion system.

The compressor rotor is composed of 2 stub shafts and 15 individual wheels held together with tie bolts and nuts. The forward stub shaft (located at compressor air inlet) is machined both to prevent any axial movements and to connect the gas turbine shaft to the auxiliary gearbox through the forward flange. On the other hand, aft stub shaft (located at air exit) connect the compressor rotor to the turbine rotor through the aft flange.

The first of the three main air extractions takes place in the gap between the sixteenth wheel and the aft stub shaft: a fan (figure 2.5), machined on the forward side of the aft stub shaft, draws air from the gap and leads it to the hollow part of rotor to cool 1st and 2nd turbine buckets and pressurize 2nd stage aft and 3rd stage forward wheel spaces (blue path figure 2.6).

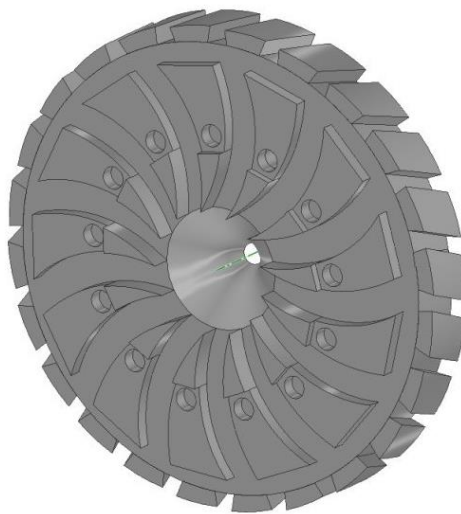


Figure 2.5: Fan in the forward side of the aft stub shaft

The second extraction (red path in figure 2.6) comes from compressor discharge air leakages that do not participate in the combustion process: they are responsible for 1st and 2nd turbine vanes cooling and pressurization of 1st stage aft and 2nd stage forward wheel spaces.

The last extraction, quantitatively less important than the previous ones, comes from air leakages passing through the clearance between the compressor discharge casing inner barrel and the compressor aft stub shaft (again red path in figure 2.6). Here there is a seal arrangement which regulate the cooling airflow into the 1st forward wheel space.

The total amount of air extracted is set as 15.1% of the turbine exhaust flow rate - a value that agrees with experience level for technology level of unit - opportunely divided into the three extractions to satisfy the cooling and pressurization requirements described in paragraph 2.7.

It is finally possible to define both turbine inlet flow rate and that entering the combustor:

$$G_{in,turb} = G_{exh} - G_{cool} \quad 2.5$$

$$G_{out,comp} = G_{exh} - G_{fuel} - G_{cool} \quad 2.6$$

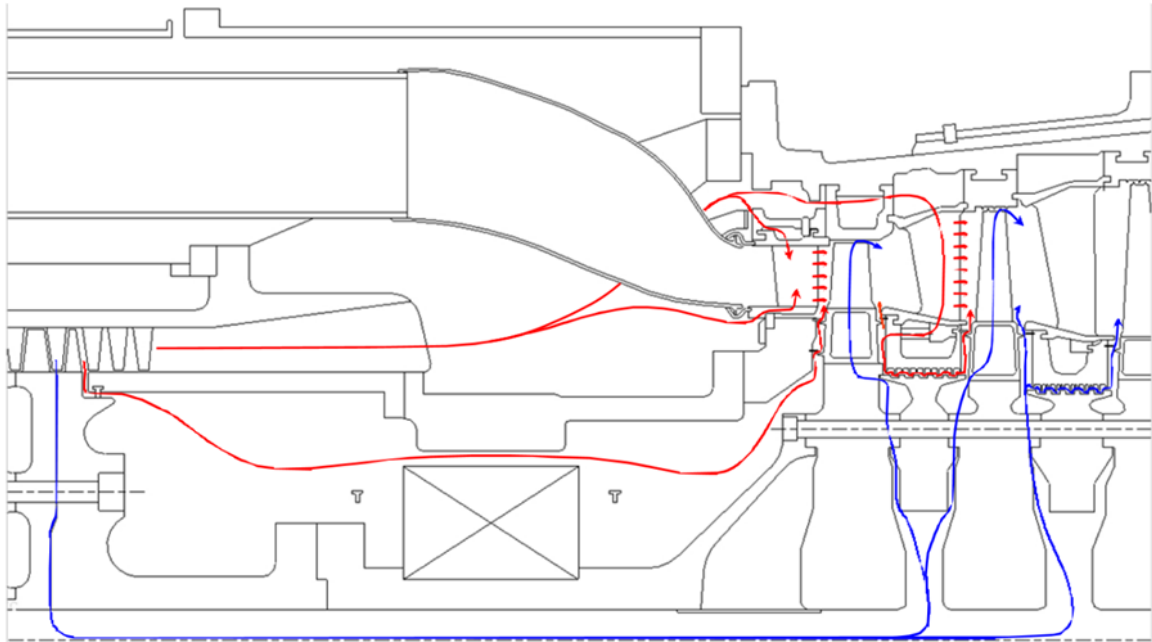


Figure 2.6: Air extraction for cooling and pressurization process

2.5 Valuation compressor thermodynamic properties for each stage

The purpose of this section is to determine temperature and discharge pressure of each stage of the compressor so that the enthalpy values at the extraction points can be estimated later (paragraph 2.6).

First, the compressor discharge temperature is evaluated, by adopting the known β value and a value of the polytropic coefficient “m” estimated through operational experience:

$$T_2 = T_1 * \beta^{\frac{m-1}{m}} \quad 2.7$$

Having no data available regarding the discharge temperature of each intermediate stage, a known trend of another similar machine (17 stages axial compressor) is used. Again, thanks to the operational experience, it is considered possible to assume that this trend is similar in the FR1625.

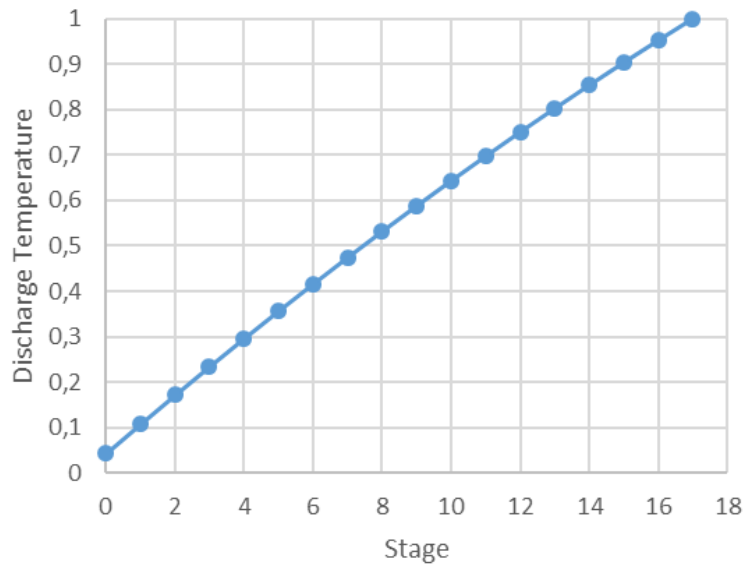


Figure 2.7: Dimensionless discharge temperature for each stage

As regards the pressures, a theoretical approach is followed: assuming the compressor as a series of 17 compressions, we keep constant both the flow (Φ) and the load coefficient (Ψ) in each stage, in order to maximize polytropic efficiency. Consider the first coefficient, being the fluid compressible, we obtain that as the specific volume decreases, the diameter must also decrease according to a cubic law:

$$\Phi = \frac{c_a}{u} \propto \frac{v}{D^3} = cost$$

Diameters values are extrapolated graphically and reported dimensionless in the table below.

Stage	D	Stage	D
0	1	9	0.867
1	0.984	10	0.867
2	0.944	11	0.867
3	0.903	12	0.867
4	0.872	13	0.867
5	0.8675	14	0.867
6	0.867	15	0.867
7	0.867	16	0.867
8	0.867	17	0.867

Table 2-4: Dimensionless compressor diameter

Once specific volumes are obtained in each stage, whose values at the compressor inlet and outlet were already known, pressures are easily computed through the perfect gases law (figure 2.8).

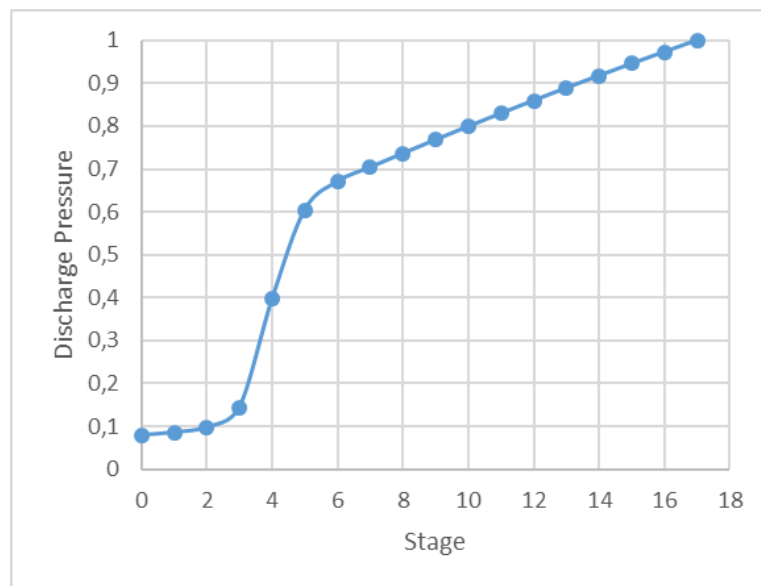


Figure 2.8: Dimensionless discharge pressure for each stage

2.6 Estimated power generated by the turbine

Once the thermodynamic properties are defined in the various compressor stages, it is possible to evaluate the enthalpy values of the compressed air at the extraction points, useful for calculating the power absorbed by the compressor. Tables supplied to the company define the enthalpy values of the air as a function of pressure and temperature.

The absorbed power is calculated below as:

$$PC = G_{in,comp} * (h_{16} - h_{in,comp}) + (G_{in,comp} - G_{16}) * (h_{out,comp} - h_{16}) \quad 2.8$$

where G_{16} and h_{16} are respectively extracted flow rate and enthalpy value of air in the gap between the sixteenth wheel and the aft stub shaft, whereas $h_{in,comp}$ and $h_{out,comp}$ are air enthalpy value at the compressor inlet and outlet.

The power generated by the turbine is therefore evaluated by the balance equation to the drive shaft:

$$PU = \eta_{tot} * (PT - PC) - P_{mech} \quad 2.9$$

Total efficiency is given by the product of transmission and generator efficiency and is assumed to be equal to:

$$\eta_{tot} = \eta_{gen} * \eta_{gear} = 0.98^2 \quad 2.10$$

The P_{mech} value considers the mechanical losses associated with the bearings and is assumed equal to 1.5 MW. Both values are determined based on operational experience with similar turbines.

The result obtained confirms what typically occurs: more than 50% of the power developed by the turbine is used to drive the axial compressor.

2.7 Turbine cooling system definition

2.7.1 Cooling system purpose

An efficient cooling system is of fundamental importance for the regular operation of the FR1625. First it is important to maintain a reasonable temperature value both for turbine rotor, to ensure a longer service life, and for turbine shell as it controls radial and axial position of all turbine stator parts. For this purpose, they must be isolated from the hot gas flow through opportune thermal resistances:

- Buckets are not directly attached to the wheel, but they are connected by means of shanks.
- Bucket tips don't run directly against the stator casing but against curved hollow segments called shrouds. The first shroud is different from the following ones (which are toothed): being hit by gas at higher temperature, it is treated by thermal barrier coating and cooled by the compressor discharge air leakage.
- The inner sidewall of the second and third nozzle are attached to segments called diaphragms.

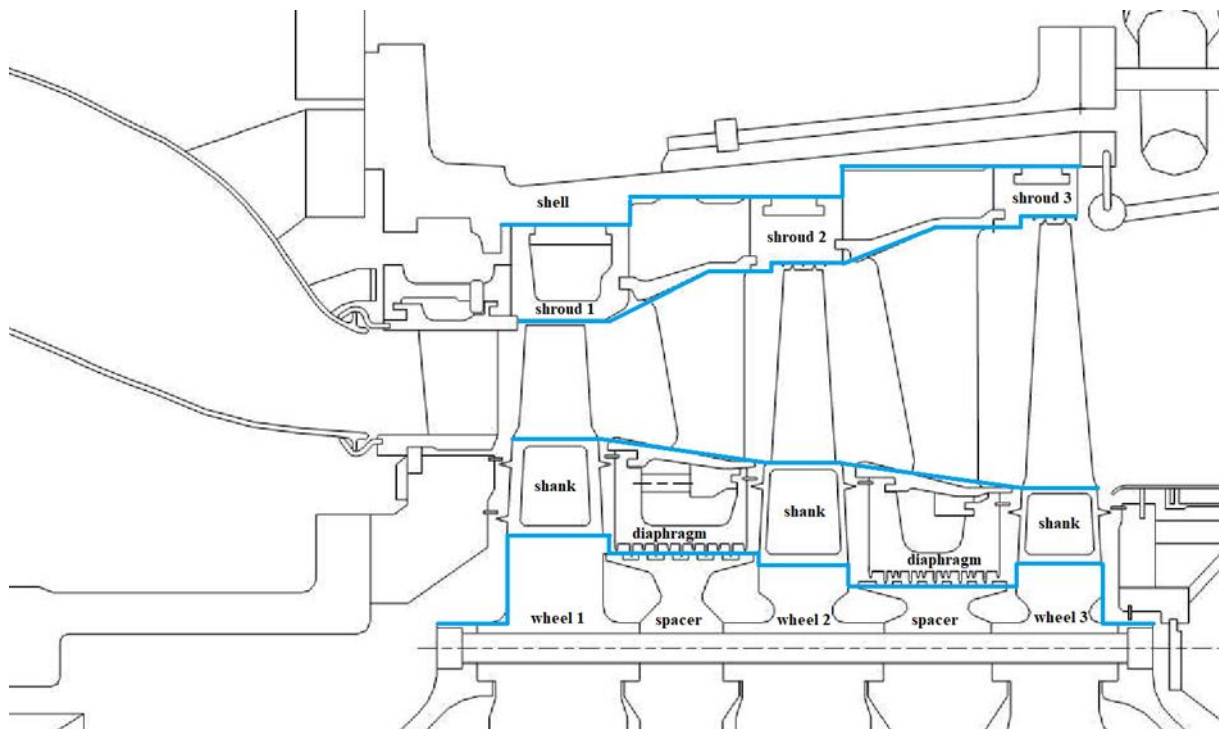


Figure 2.9: Thermal resistances isolate hot gas flow

Cooling air flow from the compressor is used for internal cooling of buckets and nozzles and for pressurization and cooling of spaces below the flow path, between the shanks and the diaphragm. These spaces, called wheel spaces (figure 2.10), must necessarily be pressurized by means of compressed air flow radially discharged outward to prevent part of the main flow from encountering the rotor wheels. They can be damaged and worn because the materials with which they are made are different from those of the buckets and therefore cannot withstand such high temperatures. To avoid this phenomenon, called gas ingestion, sealing wings installed on the first stage nozzle support, on the exhaust frame and on both sides of each diaphragm and each bucket shank are also used (figure 2.10).

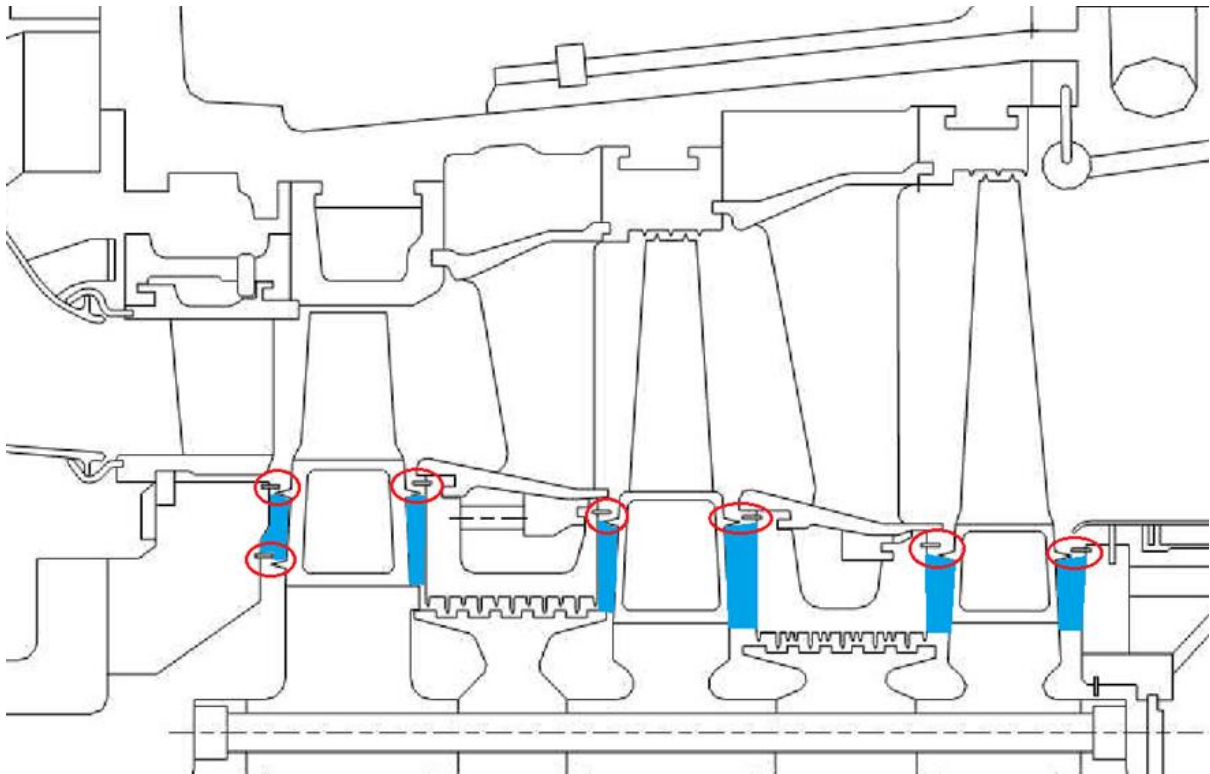


Figure 2.10: Wheel spaces pressurization and sealing wings

2.7.2 Cooling system description

The pressurization and cooling model subsequently elaborated in AxSTREAM is summarized below:

- 1st stage nozzles: compressor discharge leakage air internally cools the hollow nozzle segments by entering from the upper impingement plates and exiting through holes on the trailing edge into the hot gas path (figure 2.11). By creating “ribbed” holes, cooling airflows becomes turbulent, resulting in improved cooling effectiveness: this design allows to reach high temperature drops between leading and trailing edge, while maintaining the desired firing temperature level.
- 1st stage forward wheel space is cooled and pressurized by discharge leakage air also used to cool the second bearing.
- 1st stage buckets: when the bucket is attached to the wheel a small air plenum is formed in between (figure 2.12). Rotor internal cooling air passes through apposite slots on the forward face of the first wheel spacer, enters the plenums, internally cool buckets through a series of longitudinal air passages and exits at the bucket tip.
- 2nd stage nozzles: internally cooled by compressor discharge leakage air passing through the first stage shroud. Some of this air exits through holes on the airfoils trailing edges, while the remaining one is directed to the first stage aft wheel space through three cooling air tubes assembled on the diaphragm (figure 2.11). A labyrinth seal on the diaphragm inside diameter mate with opposite sealing on the turbine rotor spacer to control the amount of the cooling air passing from the 1st stage aft wheel space to the 2nd stage forward wheel space ensuring precise cooling and pressurization.
- 2nd stage buckets are internally cooled by rotor internal cooling air which passes through slots on the aft face of the first wheel spacer with a process like that of the first stage buckets.
- 2nd stage aft wheel space is cooled and pressurized by rotor internal cooling air which first passes through slots on the forward face of the second wheel spacer and then through a gap at the mating surface with the 2nd stage wheel. Some of this air is sent to the 3rd stage forward wheel space in similar way to that of 2nd stage forward wheel space.
- 3rd stage nozzles and buckets are not internally cooled.
- 3rd stage aft wheel space is cooled and pressurized by exhaust frame air.

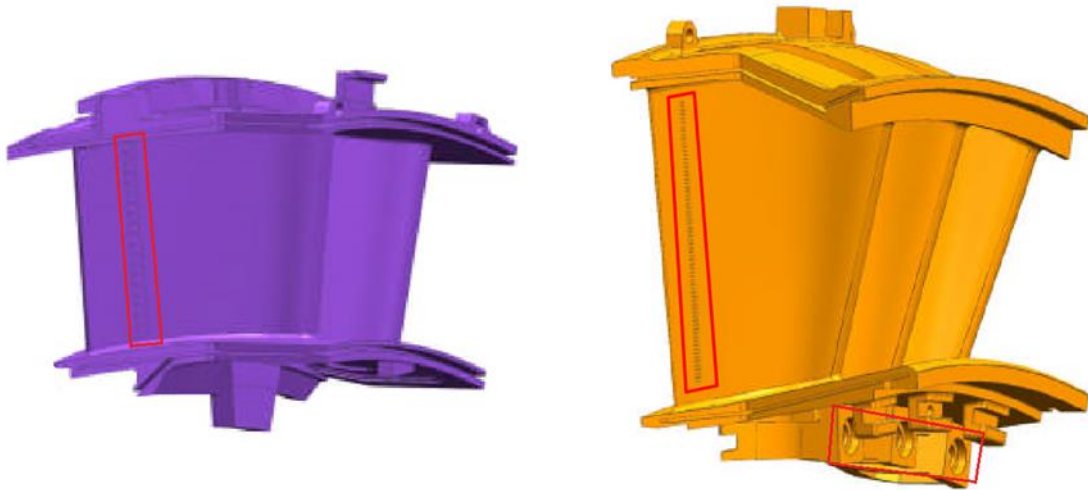


Figure 2.11: On the left the first stage nozzle with highlighted holes on the trailing edge, on the right the second stage nozzle with highlighted holes on the trailing edge and three tubes assembled on the diaphragm

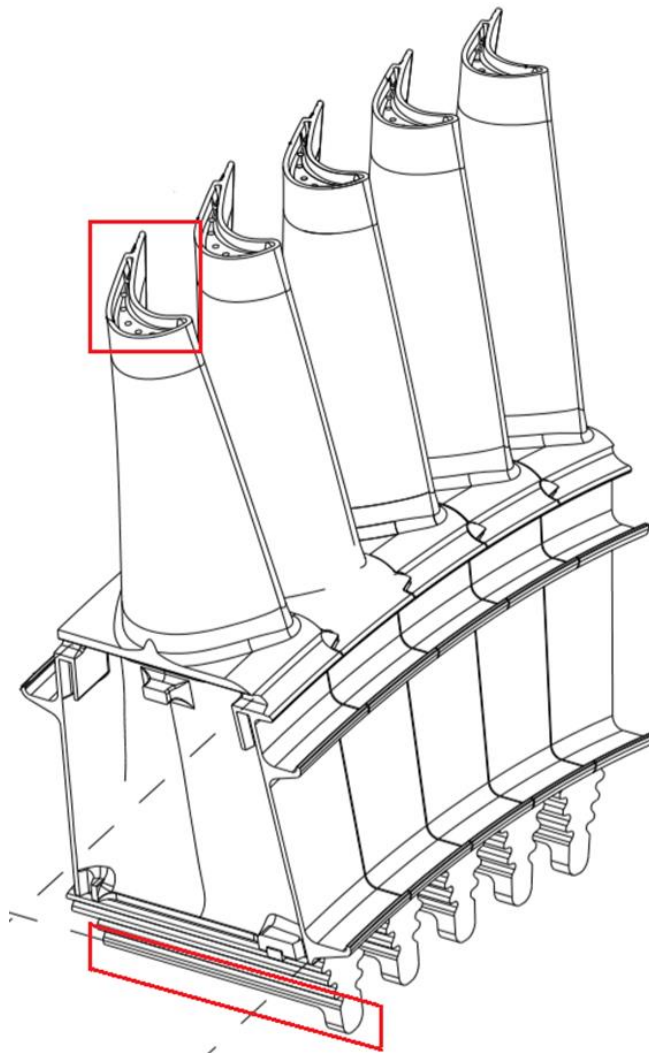


Figure 2.12: First stage buckets with highlighted air plenum and holes on the tip

2.8 Main parameters used in pre-analysis

The main parameters defined in the preliminary analysis process of the turbomachinery are here briefly summarized. They will be important input or comparison data in the AxSTREAM model implemented.

Known values:

- Heat Rate - HR
- Useful Power – PU
- Turbine exhaust flow rate - G_{exh}
- Compression ratio – β
- Firing total temperature - T_{ir}° - to be matched
- Turbine exhaust total temperature – T_{exh}° – to be matched

Estimated values:

- Fuel average lower heating value – LHV
- Fuel mass flow rate – G_{fuel}
- Extracted cooling air flow rate – G_{cool}
- Combustor inlet air flow rate = compressor outlet air flow rate – $G_{out,comp}$
- Turbine inlet mass flow rate – $G_{in,turb}$
- Turbine inlet total pressure – $P_{it}^{\circ} = \beta * P_{in,comp}$ – It will be compared to the AxSTREAM simulation output.
- Turbine output power – PT – starting from the estimate of the power absorbed by the compressor (PC). It will be compared to the AxSTREAM simulation output.

3 AxSTREAM Analysis

3.1 Software description

AxSTREAM is a software suite developed by SoftInWay Inc. for multidisciplinary design, analysis, and optimization of all types of turbomachines, as well as for thermo-fluid dynamic calculation of existing flow paths on design and off-design operation.

There are two main working modes in AxSTREAM:

- Design mode
- Analysis mode

One of AxSTREAM's features is high integration of all software components which allows users to combine separate phases of design to create a single processing chain. Specially the various software modules can provide support for [10]:

- Design of new thermodynamic systems and compare the cost of one or many projects/configurations to determine the economic viability of a system throughout their life cycle.
- Rotor design process conducted through structural checks (such as centrifugal and thermal stresses) and rotor dynamics analyses. The design process can be completed with an accurate modelling of bearings, determining hydrodynamic and mechanical characteristics for different types of journal, rolling, and thrust bearings.
- Production of flow path geometries, including the airfoils profile, that satisfy user-defined boundary conditions and geometric parameters within given constraints.
- Optimization of geometry based on performance, size, and manufacturability requirements.

On the other hand, the analysis mode is mainly related to performance prediction for design and off-design points, through Meanline (1D) and Streamline (2D) calculation modules that allow getting integral turbomachinery information (power, efficiency, mass flow rate) as well as distribution of kinematics and thermodynamics parameters in both streamwise and spanwise directions.

The work carried out and presented below therefore required the exclusive use of the second mode.

Finally, it is also possible to study the performance and flow behaviour via Computational Fluid Dynamics (by running 3D RANS equations) or evaluate stress condition on blades and attachments through 3D Finite Element Analysis.

3.2 3D Turbine model generation

It represents the starting point for the AxSTREAM analysis of the FR1625. This procedure first requires the 3D models generation of the turbine individual components through an appropriate process of reverse engineering.

Using the dimensions and drawings held by the company, it is possible, at least potentially, to manually enter all the geometric characteristics of the components in a 3D CAD software. However, this option is not considered as it is very expensive, complex, and long.

Since in our case we have access to real models, the acquisition of three-dimensional geometry is carried out using 3D scanning laser tools from which it is possible to obtain a digital file containing a dense cloud of points of the scanned component and, starting from this, derive the 3D CAD model. Still, it should be remembered that the acquisition phase and therefore the result of the analysis, are strictly linked to the quality of the instrumentation, to the skill of the operator and to the physical accessibility of the components.

We thus obtain the following 3D models:

- 1st stage nozzle row directly sealed to the transition pieces. It consists of 18 cast segments and each of them contains two airfoils hollow partitions. Segments are in turn contained on a retaining ring on the external side wall and supported by an appropriate support ring on the inner side wall.
- 1st stage bucket row made up of 92 elements attached axially to the first wheel by a dovetail arrangement.
- 2nd stage nozzle row consists of 16 segments and each of them contains three hollow airfoils partitions. They are assembled between the first and second stage shrouds.
- 2nd stage bucket row made up of 92 elements and attached to the second wheel in the same way as the first stage.
- 3rd stage nozzle row consists of 16 segments and each of them contains four hollow airfoils partitions. They are assembled between the second and third stage shrouds.
- 3rd stage bucket row made up of 92 elements and attached to the second wheel in the same way as the first and second stage.

They are suitably assembled using the CAD software Creo, developed by PTC. With reference to the 2D drawings of the turbine unit, it is necessary to fix the relative position between the nozzles and rotating buckets in axial, radial and circumferential direction. This is a crucial phase since the correct position of these parts is critical for the turbine performance prediction. Furthermore, it allows to considerably simplify the insertion of numerous geometric data subsequently requested by AxSTREAM during the analysis process.

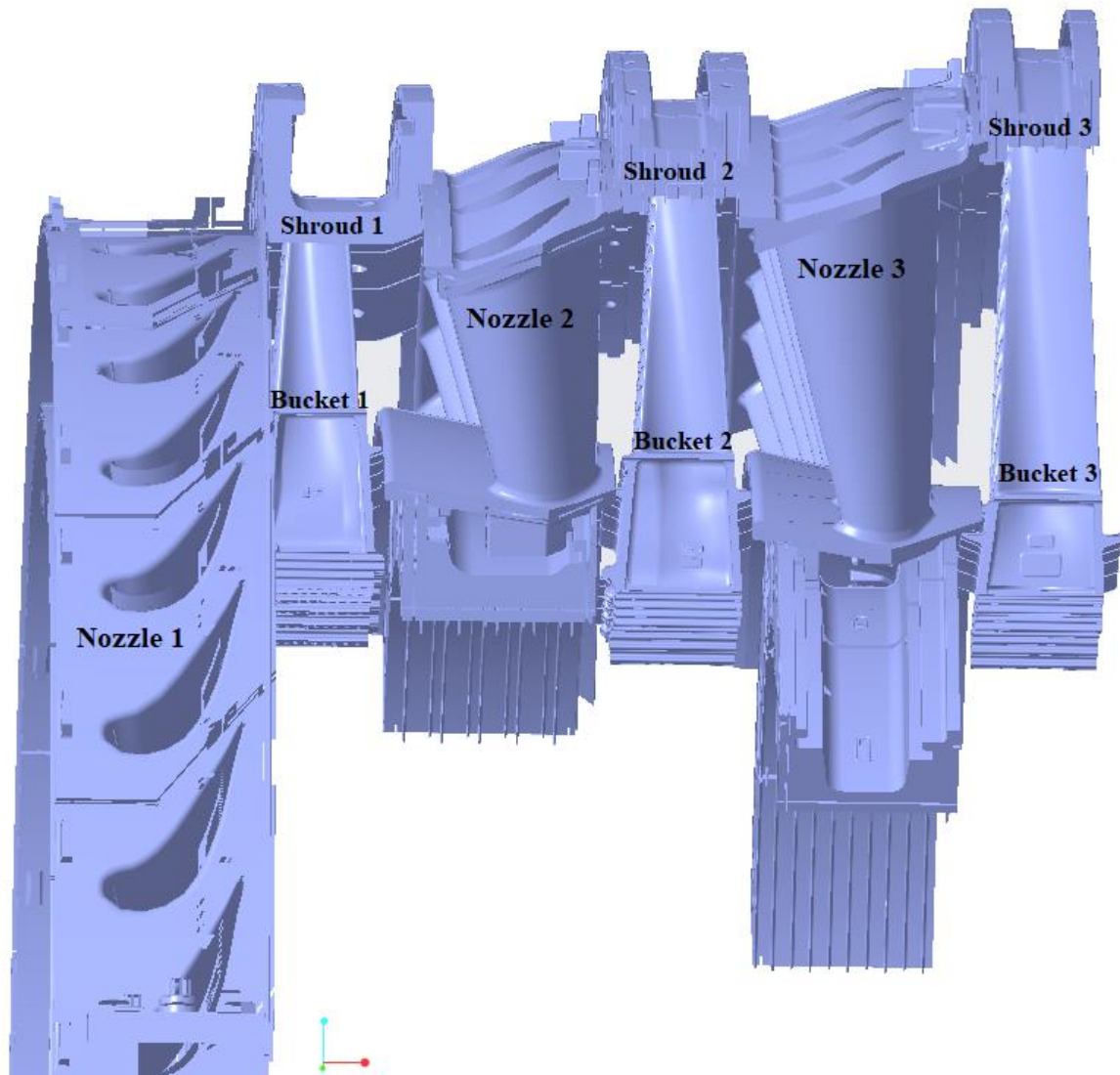


Figure 3.1: 3D model assembly

3.3 AxSLICE elaboration of 3D model

AxSLICE is a module enables elaborating 3D CAD models geometries in STL or IGES formats or cloud of points generated from 3D laser scans, to extract the profile geometry information for further turbomachines analysis in the AxSTREAM software platform.

3.3.1 3D CAD model import and Slicing operation

Unfortunately, it is not possible to import the entire row of buckets / vanes on AxSLICE, but only the individual blades whose it is composed. For this reason, it is necessary to create suitably sectioned 3D models. Once the different components of the turbine are imported individually, the module automatically recognizes their relative position in the various directions, as they were previously imposed on Creo.

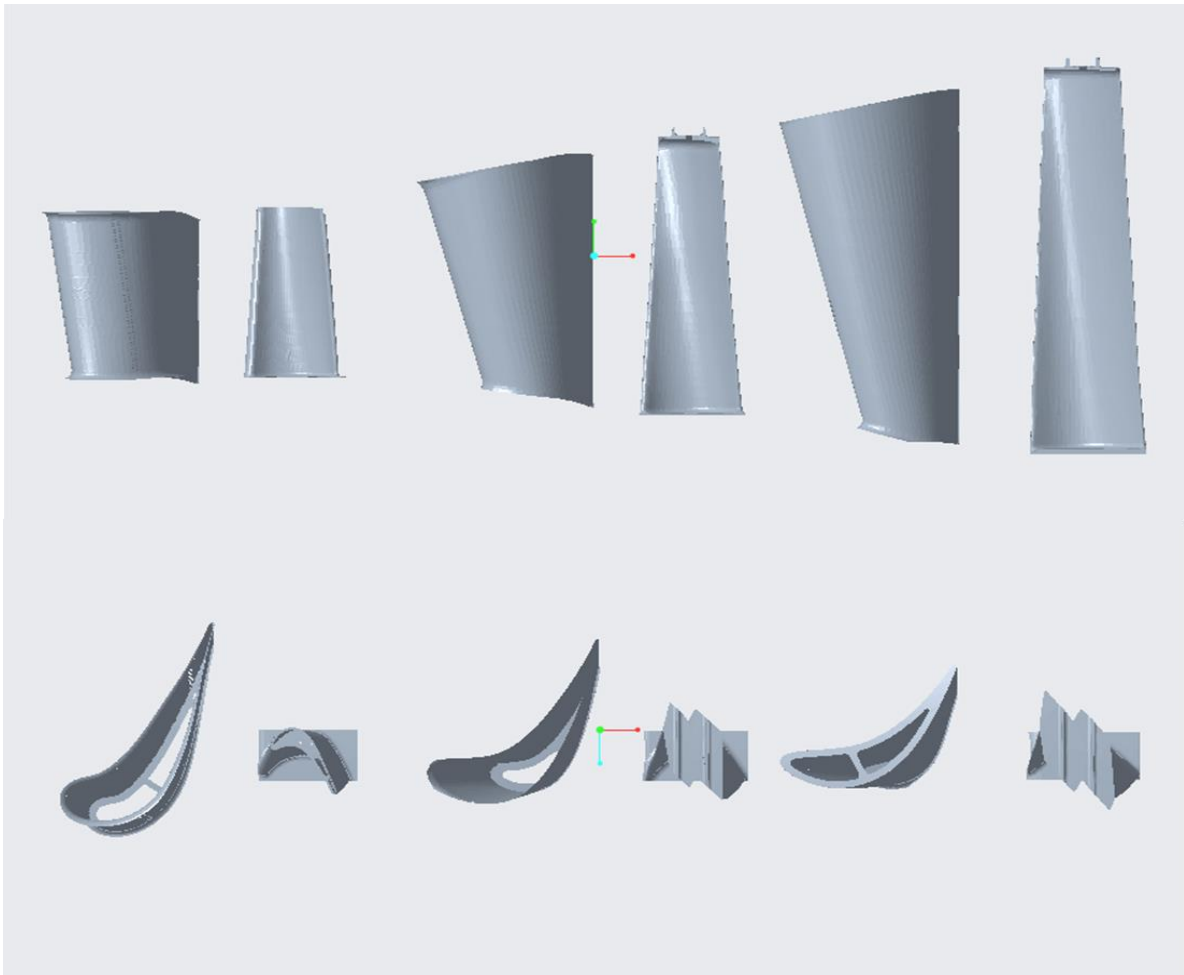


Figure 3.2: Sectioned 3D models imported on AxSLICE

AxSLICE allows to extract the geometry of several chosen profiles obtained from different sections along the bucket/vane height. This operation is called slicing. The number of sections

is decided by the user, from 3 up to 49 (an odd number of sections is mandatory to always keep a hub, mean and tip section), however, it is important to keep in mind that it must be the same number of sections used for subsequent streamline analysis in AxSTREAM.

This choice was made based on previous company experience, in addition to the information obtained in the manual [11]: 3 sections are usually not accurate enough, whereas a too large number of sections slow down the calculations more than it increases their accuracy. Therefore, recommended values are in the range of 7, 9, 11 sections spanwise. In our study we adopt 9, usually this is enough to get accurate results in a reasonable calculation time.

We get in this way 54 profiles. For convenience, the figure below shows only 4 of the 9 airfoils obtained by automatic slicing for the second stage vane.

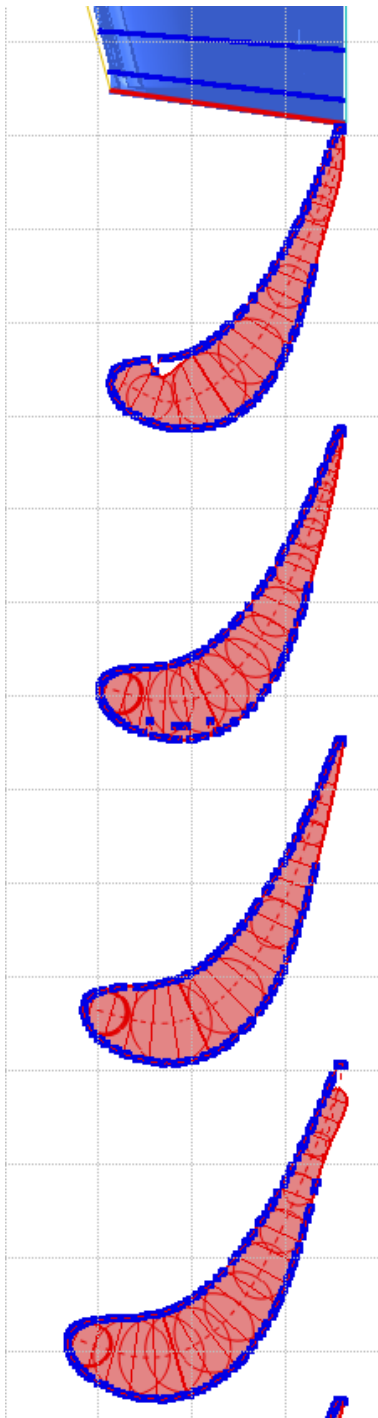


Figure 3.3: 4 of 9 airfoils for the second stage vane

The set of points represents the portion of the profile actually recognized by the module. As we can notice, there are many inaccuracies and some features are not even recognized. This is due to various factors, including, as mentioned above, the quality of the 3D scan. It is therefore necessary to analyze and correct the geometry of each profile through specific AxSLICE functions.

3.3.2 Profile correction

The correction operation is carried out following principles dictated by previous company experiences: the geometry of each profile must be as regular as possible; it must also be approximated by a single circumference at the leading edge and one at the trailing edge.

In figures 3.4 this process is presented concerning one of the airfoil of the second stage vane:

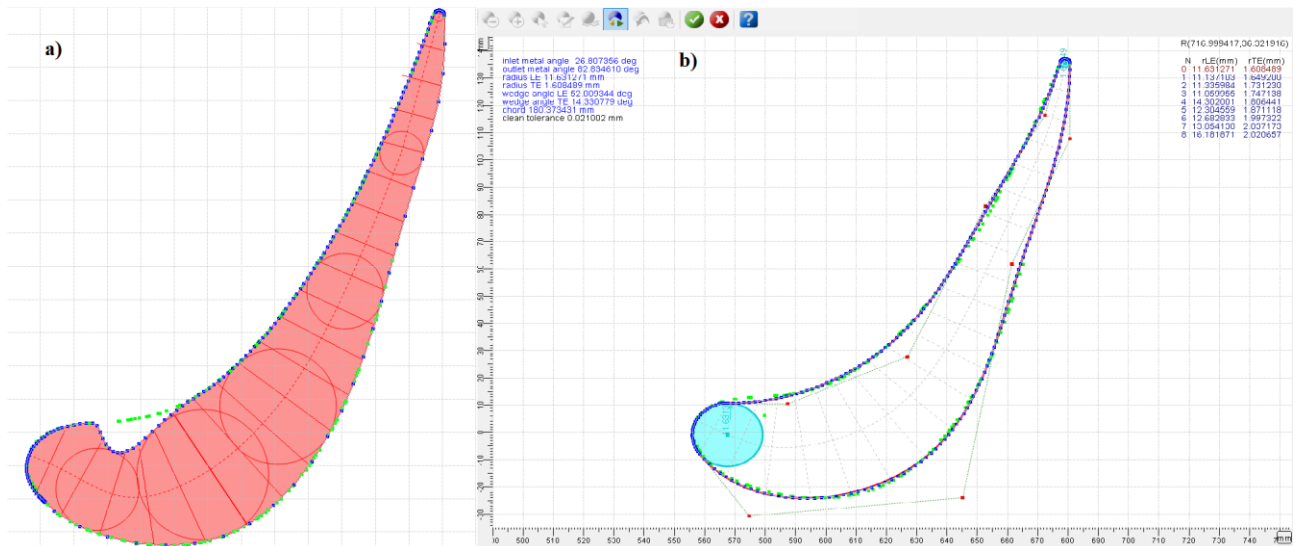


Figure 3.4: a) Initial profile obtained with automatic slicing. b) Correction process by splines

A fundamental criterion for validating the correction made is the analysis of the trend of some geometric parameters of the blade along its height, mainly the inlet and the outlet metal angle: if they are too irregular, the correction process must be repeated in order to obtain a more consistent trend.

In figures 3.5, 3.6, 3.7 they are shown respectively for the second stage vane, for the first and the third stage bucket.

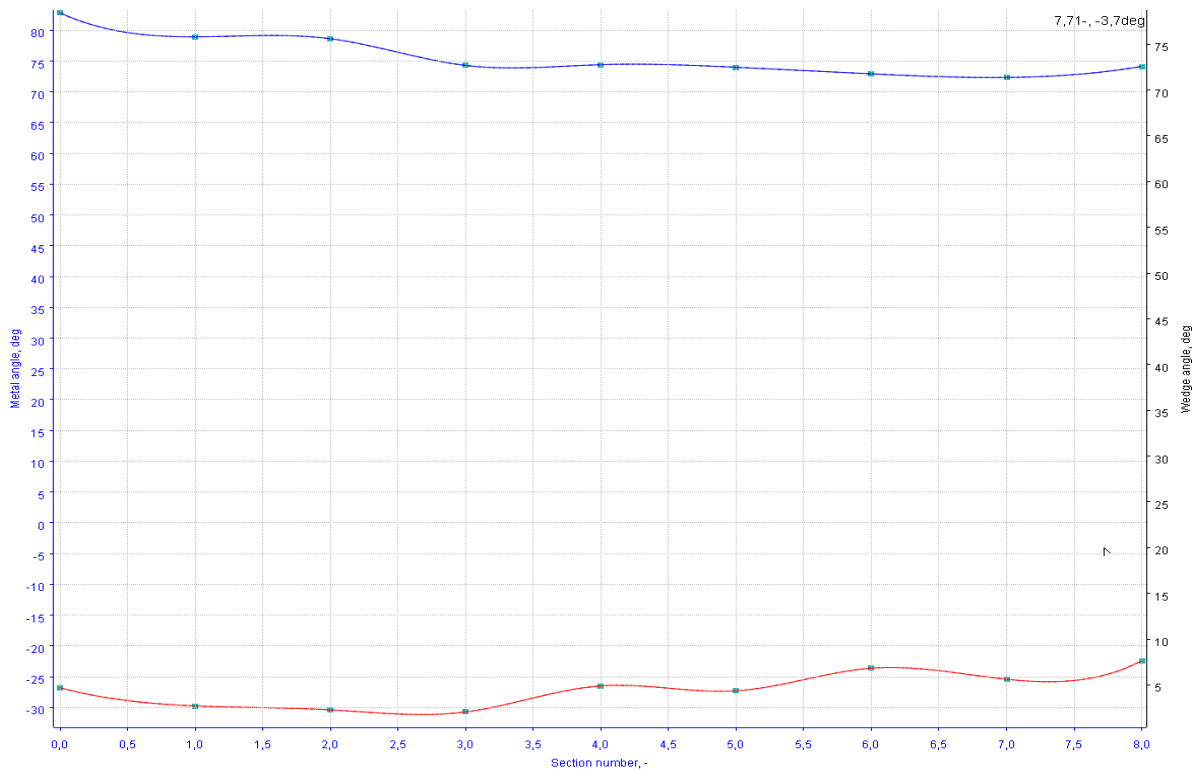


Figure 3.5: Trend of the inlet (red) and the outlet (blue) metal angle along the height for the second stage vane

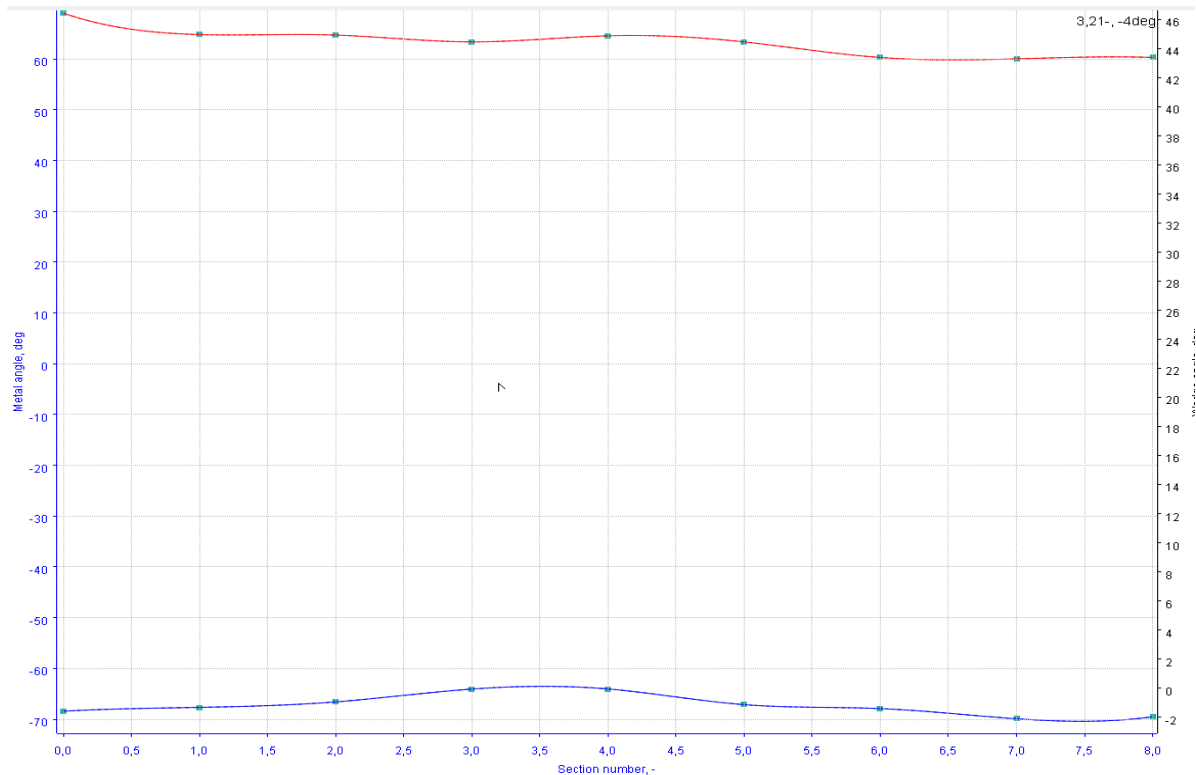


Figure 3.6: Trend of the inlet (red) and the outlet (blue) metal angle along the height for the first stage bucket

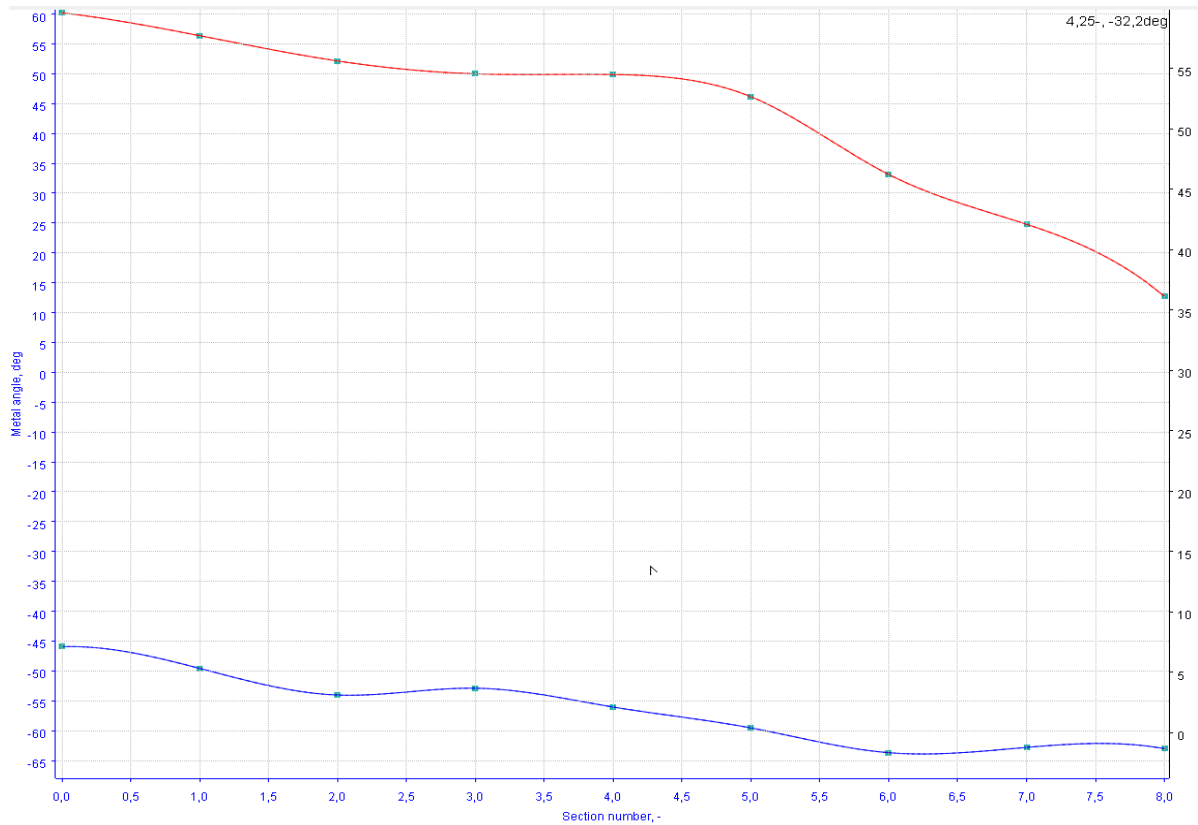


Figure 3.7: Trend of the inlet (red) and the outlet (blue) metal angle along the height for the third stage bucket

It is thus possible to get the following general conclusions:

- The vanes of the three stages present along the height a slightly increasing inlet metal angle value and a slightly decreasing outlet metal angle value. A small relaxation of the profile curvature along the height is thus obtained.
- First stage buckets have a slightly decreasing trend of the inlet metal angle along the height and an almost constant value of the outlet metal angle; second and third stage buckets show similar tendencies: stronger and slighter decrease of the inlet and outlet metal angle respectively.

Finally, figure 3.8 shows the 54 correct airfoils together with the 3D model developed by AxSLICE. The output generated by the module is a .xbs format file containing information regarding both the geometries of all the correct profiles that will then be used for streamline analysis, and the 2D geometry of the flow path to which the clearances data must be subsequently added in AxSTREAM.

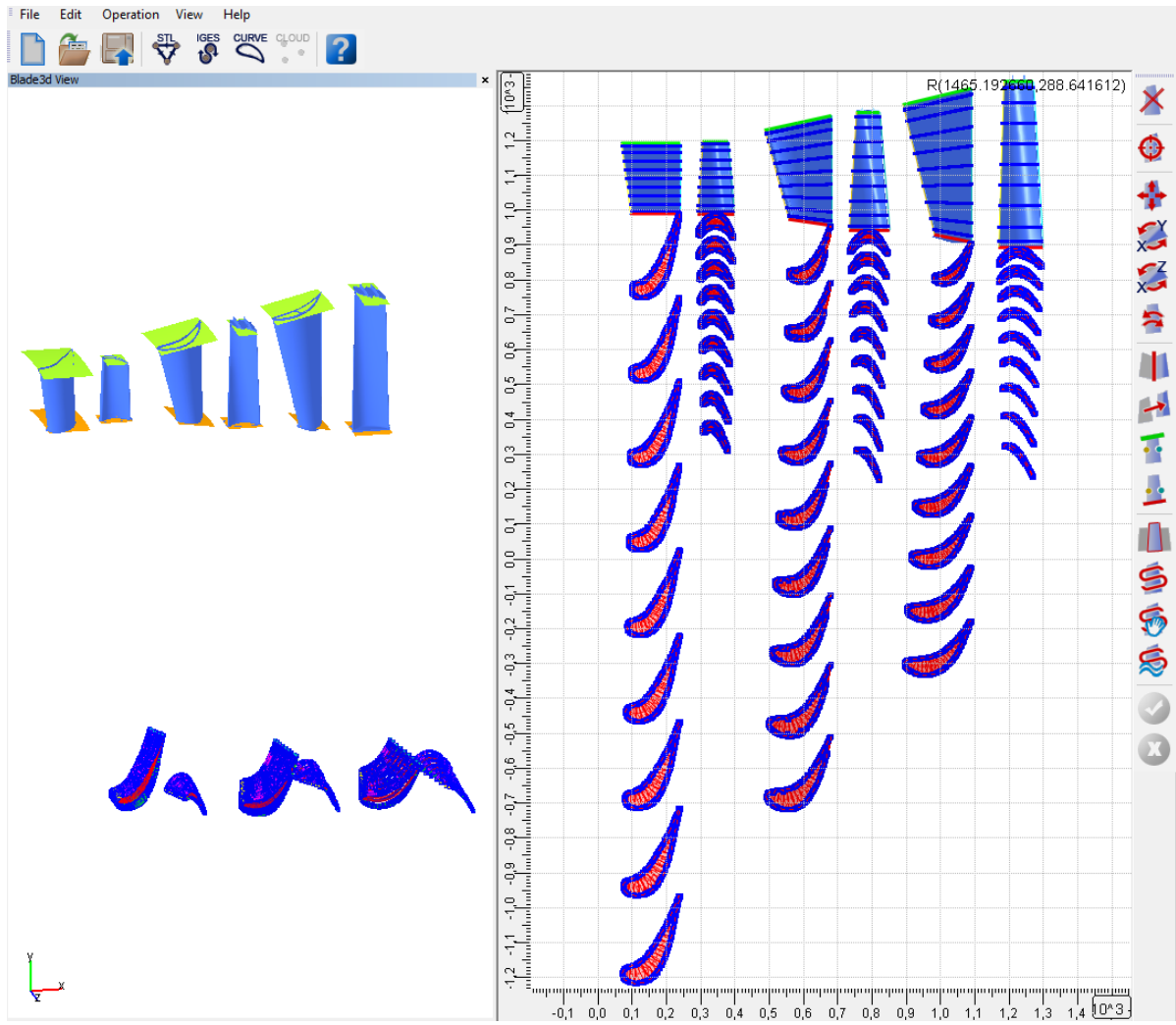


Figure 3.8: Final AxSLICE output

3.4 Creation of the calculation model in AxSTREAM

The definition of the turbomachinery on which the thermo-fluid dynamics analysis must be conducted, is carried out in the main database of the software. AxSTREAM structure consists of the main database and a few local databases connected to the main one like the Solver database, which provides the results of the last simulation performed.

The main database contains all the data that belongs to the current project:

- Machine configuration – information about elements (stators and rotors, ducts, volutes, etc.), clearance data.
- Geometry of all the elements listed, cascade geometry information on selected sections.
- Working and cooling fluid information.
- Loss models.
- Information about extractions, injections, cooling, and other changes of flow path.
- Boundary conditions – inlet, outlet BCs.
- Calculation outputs – all set of data loaded from the Solver database such as integral results, losses, thermodynamic and kinematic results.

The screenshot displays the AxSTREAM software interface. On the left, a tree view shows the project structure under 'Turbine_AT 2D_Calc', including 'Working fluid', 'Cooling fluid', 'Shaft_1', 'Inlet_0', 'Solution Inlet_0', 'Outlet Station Solution Inlet_0', 'Module_1', 'Duct axial_1', 'Stage_1', 'Stator axial_2-1', 'Rotor axial_3-1', 'Calculation models', 'Cooling data', 'Strength', 'Clearances', 'Blade Rotor axial_3-1', 'Solution Rotor axial_3-1', 'Stage_2', 'Stator axial_4-2', 'Rotor axial_5-2', 'Stage_3', 'Stator axial_6-3', and 'Rotor axial_7-3'. On the right, the 'Properties' tab is active, showing a table of properties for 'Turbine_AT'.

		Property	Unit
1	type	machine type	-
2	Gin	mass flow rate at inlet	kg/s
3	Gout	mass flow rate at outlet	kg/s
4	N	power	MW
5	eff_tt	internal total-to-total efficiency	-
6	eff_ts	internal total-to-static efficiency	-
7	effd_tt	diagram total-to-total efficiency	-
8	effd_ts	diagram total-to-static efficiency	-
9	uCo_	averaged isentropic velocity ratio	-
10	psi_	averaged work coefficient	-
11	phi_	averaged flow coefficient	-
12	ti_in	total enthalpy at inlet	J/kg
13	Tt_in	total temperature at inlet	°C
14	Pt_in	total pressure at inlet	bar
15	Tout	total temperature at outlet	°C
16	Pt_out	total pressure at outlet	bar
17	Pst_out	stat. pressure at outlet	bar
18	psr	total-static pressure ratio	-
19	ptr	total-total pressure ratio	-
20	H	isentropic heat drop total-to-static	J/kg
21	Ht	isentropic heat drop total-to-total	J/kg
22	Lu	specific work	J/kg
23	mass	total blades mass	lbm
24	eff_BSC	internal efficiency by BSC formulation	-
25	coolTask	cooling data set type	-
26	eff_cool_ts	cooled turbine total-to-static efficiency	-
27	eff_cool_tt	cooled turbine total-to-total efficiency	-
28	kToxi	temperature irregularity coefficient at machine inlet	-
29	Gvin	volume flow rate at inlet	m³/s

Figure 3.9: Main AxSTREAM database

3.4.1 Machine configuration

The process of importing the 3 stator and rotary elements from the .xbs format file is straightforward and intuitive: the main database will automatically have available all the geometric information of the turbine previously defined, including the spanwise cascade geometry parameters.

Clearances definition

The software manual specifies that clearances data of the fixed and rotating parts must be assigned in AxSTREAM supposing that the turbine is in its hot state (under running conditions). As the data are obtained from the drawings available to the company and therefore refer to the cold condition of the turbomachinery, they should be corrected to get the corresponding hot state conditions. The cold data are therefore appropriately scaled by a factor suggested by the company's previous experience with the analysis of turbomachinery operating in conditions similar to the FR1625.

The figures 3.10, 3.11 show the auxiliary setup windows for the insertion of the first stage clearances.

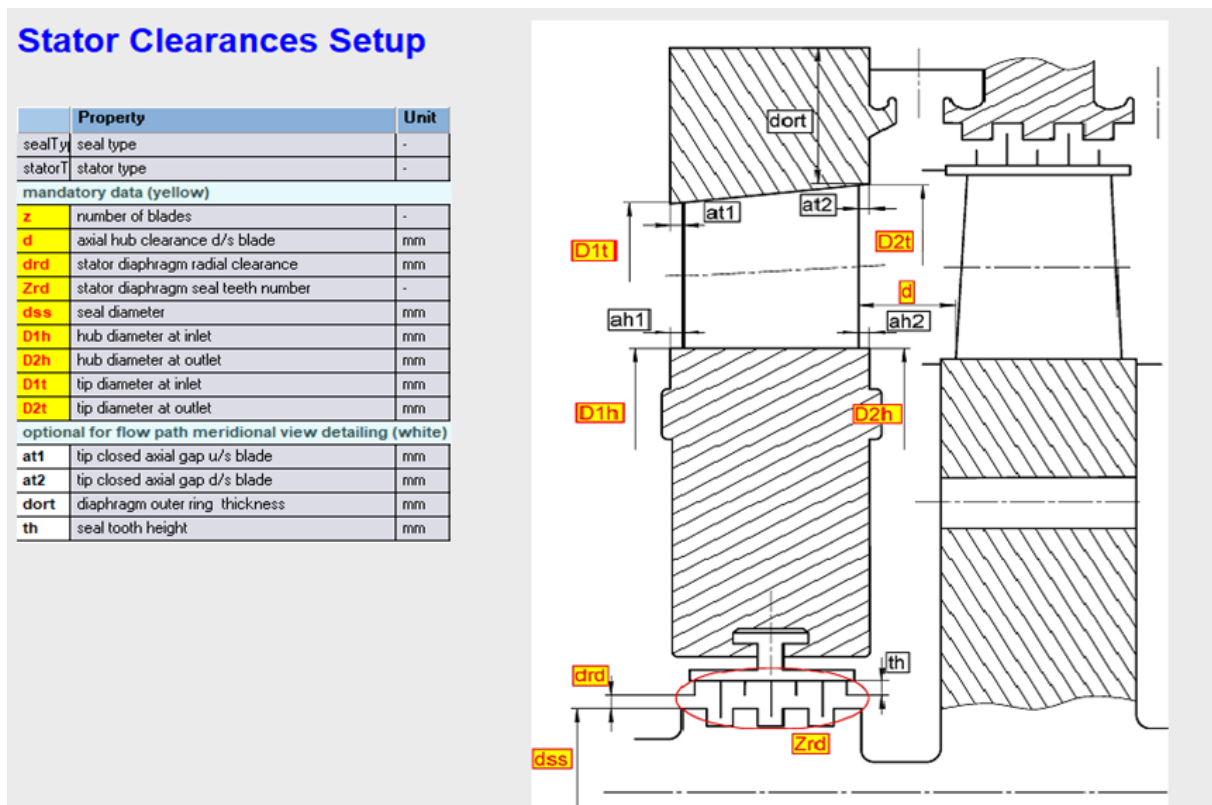


Figure 3.10: Setup window for first stage vane clearances

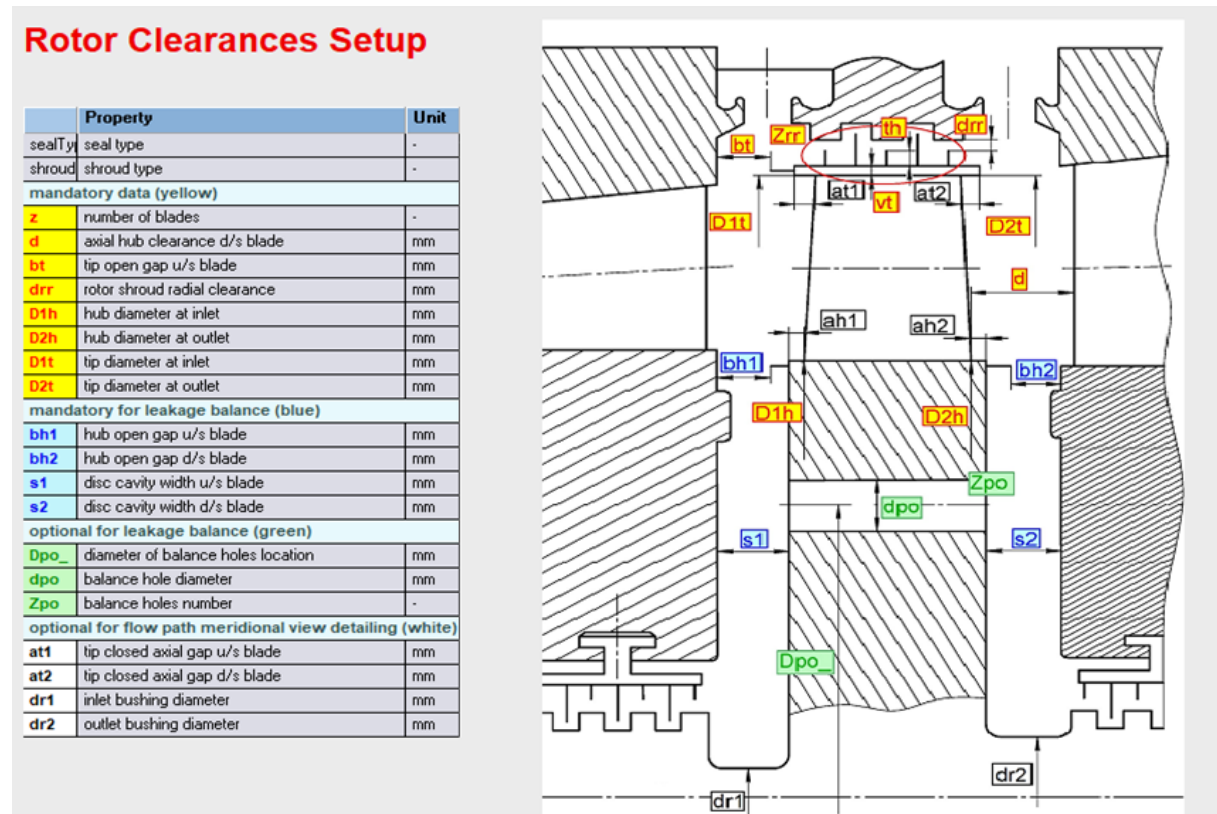


Figure 3.11: Setup window for first stage bucket clearances

To simulate absence of leakage through the first vane a large number of seal teeth and a small value of clearance are specified. However, the construction characteristics of subsequent stages are different, for example the first stage blade is the only one not properly equipped with a shroud, for this reason the definition of clearances is carried out in a slightly different way. The characterisation of the two-dimensional flow path is thus completed and shown in the figure below.

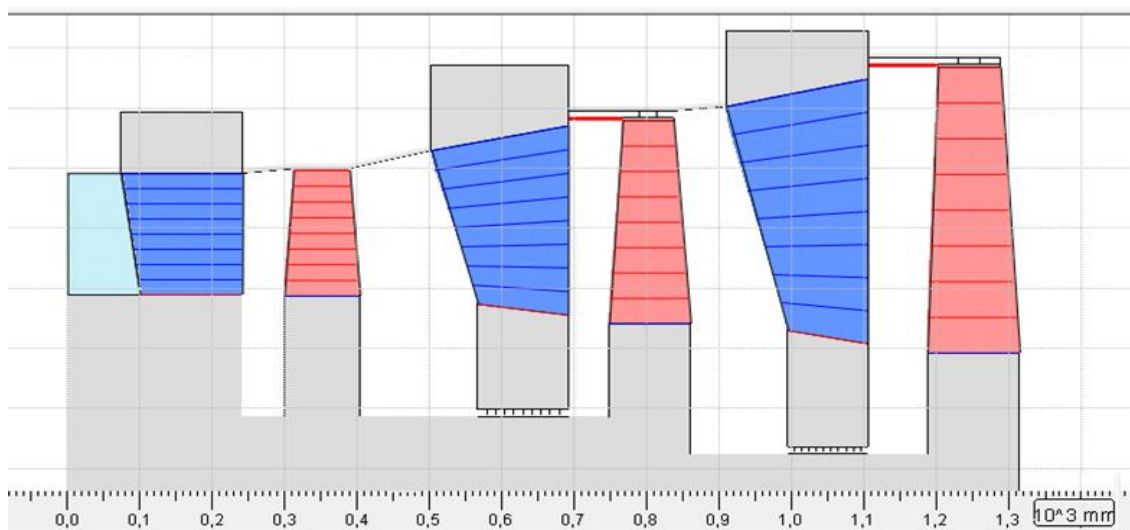


Figure 3.12: 2D flow path

3.4.2 Definition of the main and cooling fluid properties

On AxSTREAM it is possible to choose between different fluid models and it is also possible to create customized fluid models: in our case, in fact, we chose both for the main fluid (consisting of a mixture of gases burned in excess of air), and for the cooling fluid (composed by only air), the fluid “AxS FLG Ethos_Fuel 4” suitably created by the collaboration between SoftInWay Inc. and Ethos Energy S.p.a.

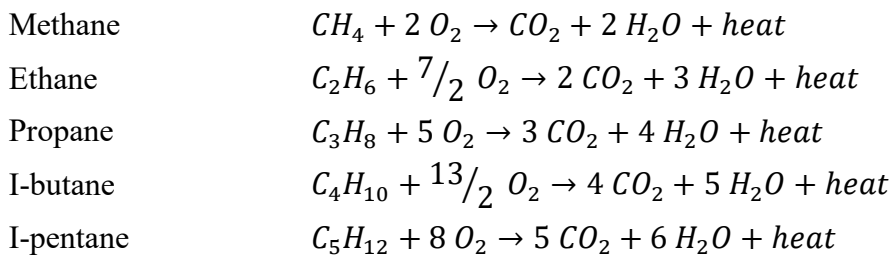
For both, software requires the insertion of an Air Excess Factor, defined as the ratio of the actual air-to-fuel ratio to the stoichiometric air-to-fuel ratio:

$$af = \frac{\alpha}{\alpha_{st}} = \frac{G_{out,comp} / G_{fuel}}{\alpha_{st}} \quad 3.1$$

Its precise determination is very important as it directly affects the enthalpy value of the combustion gases entering the turbine. In fact, by applying the first principle to the combustion system, it is obtained that as the air-to-fuel ratio increases, the enthalpy value of the gases and consequently the temperature profile in the turbine decreases:

$$h_{in,turb} = h_{out,comp} + \frac{HC}{(1 + \alpha)} \quad 3.2$$

The numerator of eq. 3.1 is easily computed, having all the data available, while the estimation of the denominator required an in-depth analysis on the composition of the fuel considered. First, the exothermic and stoichiometric combustion reactions of all the components are reported:



In stoichiometric reactions it is necessary that 1 mole of fuel burns with “x” moles of oxygen, or equivalently with $\frac{x}{0.21}$ moles of air being in fact the percentage of oxygen in the air of 21%

	Methane	Ethane	Propane	I-butane	I-pentane
Air [mol]	9.52	16.67	23.81	30.95	38.1

Table 3-1: Stoichiometric moles of air in the combustion reactions

The various combustion proceeds in the following weight proportions:

$$air [g] = \frac{M_{air} * mol_{air,st}}{M_i} \quad 3.3$$

where:

- $M_{air} = 28.97 \text{ g/mol}$
- $mol_{air,st}$ from table 3.1
- M_i from table 2.2

	Methane	Ethane	Propane	I-butane	I-pentane
Air [g]	17.24	16.09	15.68	15.46	15.33

Table 3-2: Grams of air required for each gram of i-th fuel

Now considering the composition of the fuel (table 2.1) and the molar mass of each of its components (table 2.2), each mole of fuel is composed as follows:

Nitrogen	0.23
Methane	11.91
Carbon Dioxide	4.18
Ethane	2.87
Propane	2.25
I-butane	0.28
I-pentane	0.05
TOT - \bar{M}	21.78

Table 3-3: Fuel composition [g]

which requires the following quantities of air:

Nitrogen	0
Methane	205.36
Carbon Dioxide	0
Ethane	46.21
Propane	35.32
I-butane	4.3
I-pentane	0.77
TOT	291.96

Table 3-4: Air required

Based on the ratio between quantities, it can be deduced that under ISO conditions, about 13.55 kg of air are needed per kilogram of fuel.

		Property	Unit	Value
1	name	fluid name	-	AxS FLG Ethos_FUEL4 ...
2	af	air excess factor	-	2.605000
3	lo	stoichiometric	-	13.552900
4	dscr	fluid description	-	

Figure 3.13: Main fluid properties

Finally, the properties of the cooling flow are differentiated from those of the main flow only by means of a different AF value, set equal to 1000. Such assignment is suggested by the manual [11] and should provide entropy and enthalpy reference points' coordination between the two fluids.

3.4.3 Loss models

The software includes some industry-approved loss models for profile losses, secondary losses, blockage losses, leakage losses, also allowing users to customize or implement their own models. For our purposes we retain the default settings, except for the fluid deviation angle model in the rotating buckets. A maximum value has been set for this, which is useful for matching the turbine exhaust temperature.

3.4.4 Cooling model set up on AxSTREAM

The thermodynamic cooling processes described in chapter 2.7 are actually very complex and are modelled in AxSTREAM in a simplified way using a 0-D model:

- The cooling process for fixed parts is described in the H-S diagram as an isenthalpic lamination with corresponding pressure drop (represented by ptr) starting from the compressor extraction (T_{cool0} , P_{cool0}) to the cooling holes position, followed by an isobaric heat exchange process (represented by sigma) between the cooling flow and the cooled parts. The final state of cooling flow is represented by (T_{cool} , P_{cool}).
- The cooling process for the moving parts is described in the H-S diagram as isentropic transformation of total enthalpy drop into rotor shaft work starting from the compressor extraction to the compressor rotor axis, followed by an isenthalpic total pressure drops along the turbine rotor axis. The cooling flow is so pumped to the turbine cooling hole position (T_{w_pump} , P_{cool}) due to the centrifugal effect of the turbine rotor. Finally, an isobaric heat exchange process between the cooling flow and the cooled rotor blades.

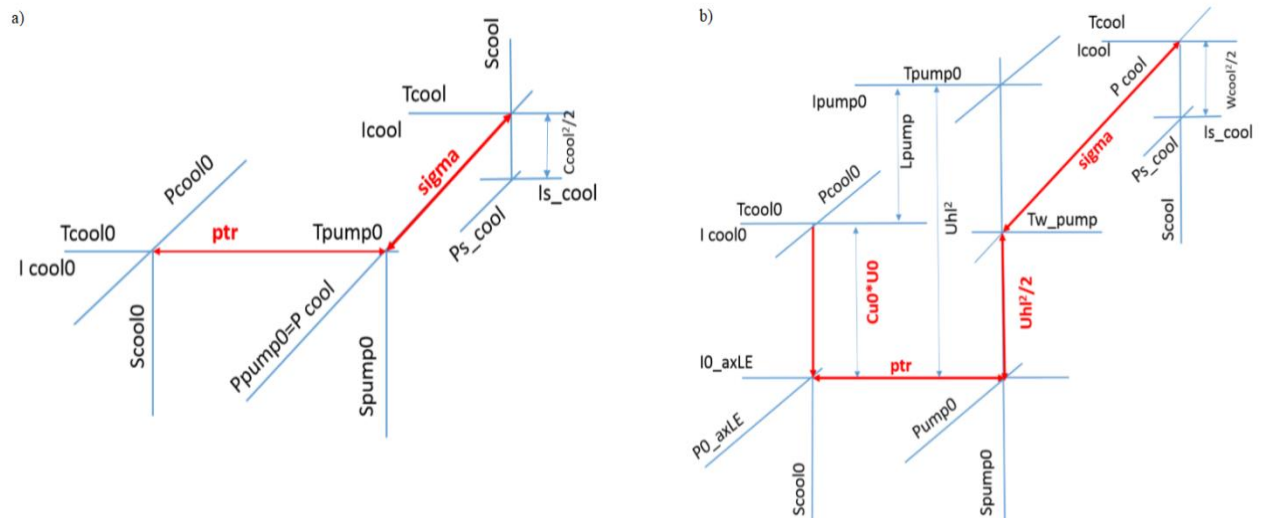


Figure 3.14: a) Thermodynamic cooling process for stator components. It does not contain any pumping effect because the cooling flows pass through the casing components and therefore there is no work exchange with the rotor. b) Thermodynamic cooling process for rotor components

AxSTREAM uses three different "cooling data set types" which differ from each other in the input data to be provided. In our case study the "G-sigma data set" is chosen which requires the desired cooling mass flow rate as input and returns the corresponding pressure ratio (ptr) needed.

The set of input data to be entered for each cooling flow can be grouped by their functionality:

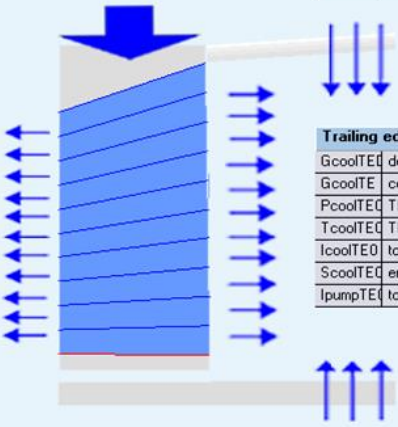
- Thermodynamics properties
 - Desired cooling air flow rate through the corresponding cooling holes.
 - Total pressure and temperature at compressor extraction.
- Geometry properties
 - Total cooling holes cross sectional area.
 - Cooling flow velocity angle with respect to a certain reference frame.
 - Compressor extraction position diameter.
 - Other coefficients.
- Non dimensional coefficients
 - Coefficient sigma indicates the effectiveness of the isobaric heat exchange. It is the ratio between cooling flow temperature increase in the cooled parts and the temperature difference between the inlet main flow and cooling flow at the beginning of the cooling process. It is a very important parameter and is obtained based on the company operational experience.
 - Other coefficients.

With the aim of making the introduction of the input data as intuitive as possible, AxSTREAM provides graphic "set up templates" for both stator and rotor components (Figure 3.15, Figure 3.16). They are filled for each component of the turbine, trying to comply as much as possible with the real inlet criteria in the main flow path. The setup template contains four (stator parts) or five (rotor parts) groups of cooling flows:

- Leading edge (LE), cooling flows except rotor tip located upstream from the throat.
- Trailing edge (TE), cooling flows downstream from the throat.
- Tip, only for rotor parts.
- External enwall downstream from the throat.
- Internal enwall downstream from the throat.

Stator Cooling Setup

Stator Cooling Setup



Leading edge cooling		
GcoolLE	desired cooling air flow rate through LE	kg/s
GcoolLE	cooling air flow rate through LE	kg/s
PcoolLE	LE total pressure in absolute frame at the	bar
TcoolLE	LE total temperature in absolute frame at	°C
IcoolLE	total enthalpy in absolute frame at the cooling	J/kg
ScoolLE	entropy in absolute frame at the cooling	J/kg
IpumpLE	total enthalpy in absolute frame with pump	J/kg
PpumpLE	total pressure in absolute frame with pump	bar

External Endwall Cooling		
GcoolSD	desired cooling air flow rate on external en	kg/s
GcoolS	cooling air flow rate on external endwall	kg/s
PcoolS0	external endwall total pressure in absolute	bar
TcoolS0	external endwall total temperature in abso	°C
IcoolS0	total enthalpy in absolute frame at the cooling	J/kg
ScoolS0	entropy in absolute frame at the cooling	J/kg
IpumpS0	total enthalpy in absolute frame with pump	J/kg

Trailing edge cooling		
GcoolTE	desired cooling air flow rate through TE	kg/s
GcoolTE	cooling air flow rate through TE	kg/s
PcoolTE	TE total pressure in absolute frame at the	bar
TcoolTE	TE total temperature in absolute frame at	°C
IcoolTE	total enthalpy in absolute frame at the cooling	J/kg
ScoolTE	entropy in absolute frame at the cooling	J/kg
IpumpTE	total enthalpy in absolute frame with pump	J/kg

Internal Endwall Cooling		
GcoolHD	desired cooling air flow rate on internal en	kg/s
GcoolH	cooling air flow rate on internal endwall	kg/s
PcoolH0	internal endwall total pressure in absolute	bar
TcoolH0	internal endwall total temperature in abso	°C
IcoolH0	total enthalpy in absolute frame at the cooling	J/kg
ScoolH0	entropy in absolute frame at the cooling	J/kg
IpumpH0	total enthalpy in absolute frame with pump	J/kg

Figure 3.15: Stator set up template

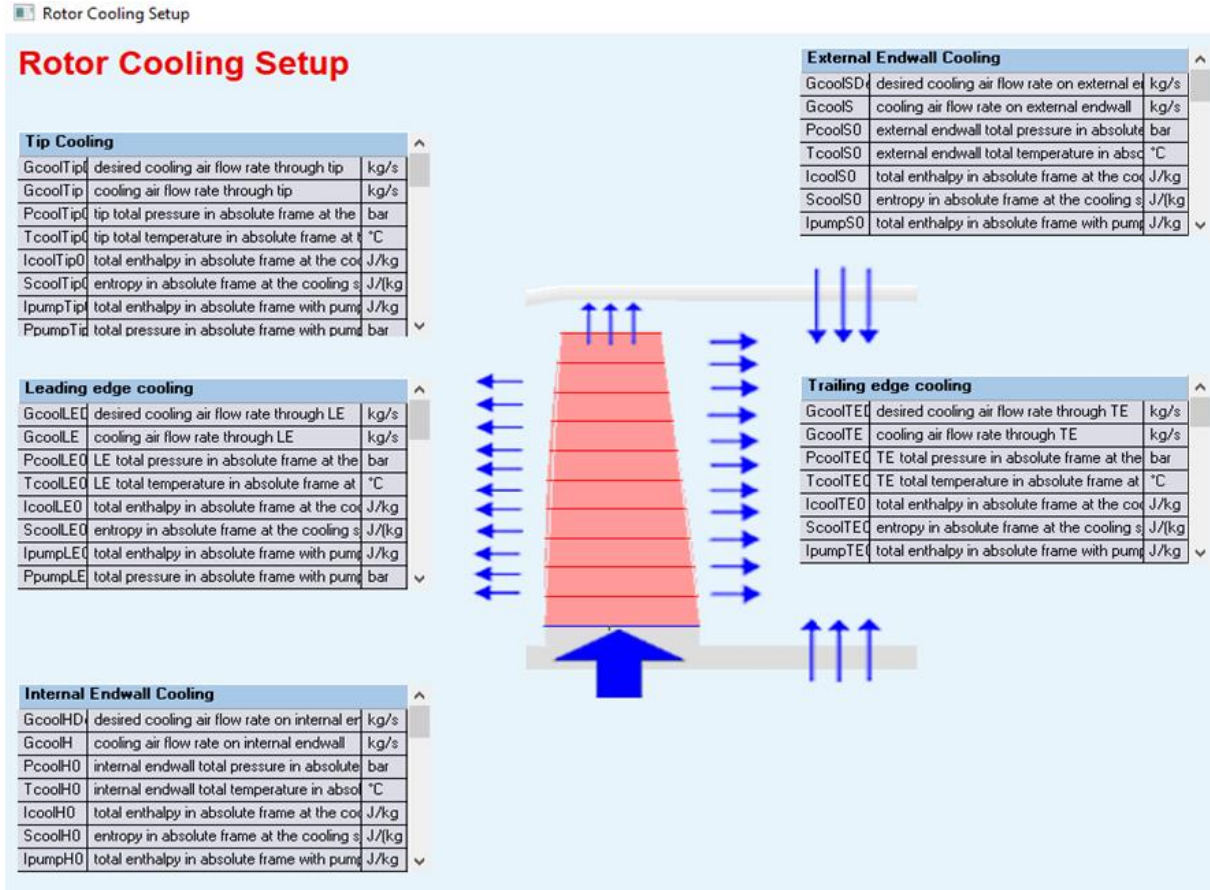


Figure 3.16: Rotor set up template

The values of the cooling and pressurization flow rates are obtained starting from the resolution of the cooling flow network [12]. They are suitably scaled to better adapt them to current operating conditions.

Once the simulation has been carried out, AxSTREAM provides as additional output data all the thermodynamic properties of the different cooling flows when they enter the main flow and two further parameters:

- Ptr is the pressure ratio between the total pressure of cooling flow input into the main flow path and the total pressure in the compressor extraction point.
- Actual cooling mass flow rate based on cooling flow velocity and cooling holes area. This value must be compared with the desired mass flow rate to check if pressure in the compressor extraction point is high enough to let cooling flow rates to enter the main flow path. If this does not happen, it will be necessary to change the extraction conditions or the cooling holes area so that the desired mass flow rate is reached.

3.4.5 Boundary conditions definition

Turbine inlet total temperature

It is defined as T_{it}° and like any other inlet condition in AxSTREAM it is assigned to the inlet of the duct, upstream of the first nozzle and before the inlet cooling flows. Together with firing temperatures, it represents extremely important operating parameters, as they are linked to the materials with which the main components of the turbine are built.

For meanline simulation, a single input value of T_{it}° is required: it is obtained through a series of simulations to get the desired firing temperature at the first bucket inlet.

On the other hand, in the streamline simulation, a variable temperature profile is imposed along the height of the duct, inserting a total temperature value for each streamline. The trend is strictly dependent on the shape of the duct connects the combustion chamber to the turbine inlet, and having no data available, we can only rely on the company's experience in this area. DLE and standard combustors can have significantly different patterns. DLE systems generally have a more uniform temperature across the cross section to make emissions low. Also, they make much less use of cooling air at the liner walls. Both tend to produce a flatter profile than a standard system. There are two case studies reported:

- The first one considers the same pattern factor of an OEM unit with standard combustor system (yellow curve – figure 3.17).
- The second considers an optimized profile, more common to DLE systems (blue curve).

Their average value is the same as that imposed in the meanline analysis.

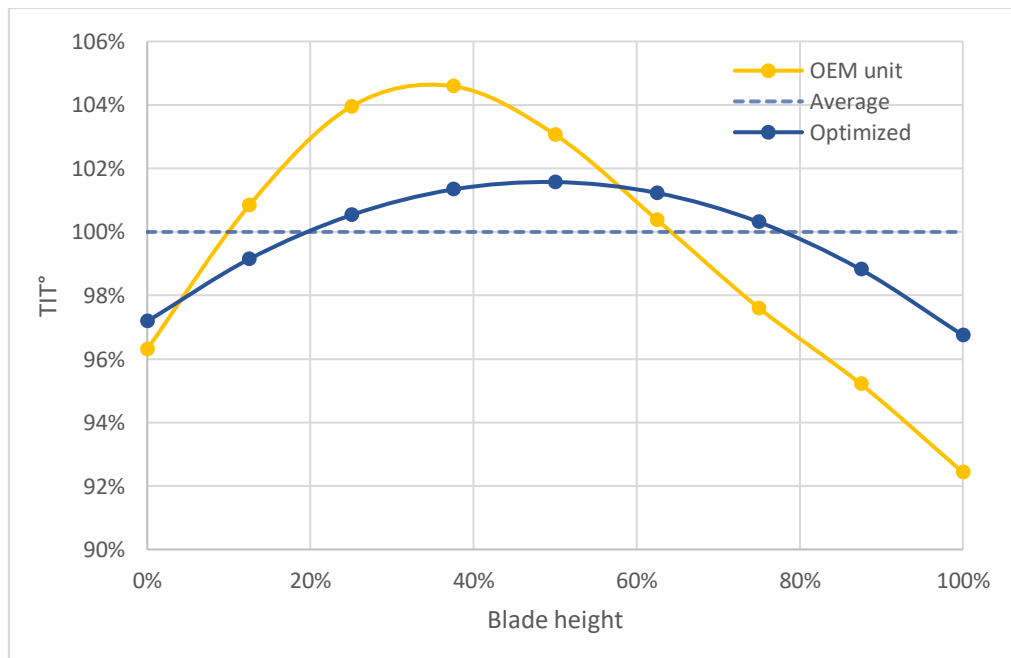


Figure 3.17: T_{it}° profiles along duct height, dimensionless with respect to average value

Turbine inlet mass flow rate

The same previously defined in paragraph 2.8

Turbine exhaust total pressure

Defined as P°_{exh} from experimental data supplied to the company. It is assigned at the last rotor exit after the last rotor cooling flow.

Turbine inlet total pressure

It is the same as defined in paragraph 2.8 unless pressure losses in the combustion chamber. In our case it is an indicative input value to which the solver tries to converge for given MFR and outlet total pressure. Eventually the solver finds the solution in a close range to the selected one.

Shaft rotational speed and inlet flow angle

FR1625 is used for 50 Hz applications, thus having a rotational speed of 3000 rpm.

Turbine inlet flow angle is assumed equal to 90° .

3.5 Meanline analysis

The meanline approach is a 1D calculation at the pitch (mean) line with extrapolation of the flow properties at hub and shroud. Representing a one-dimensional analysis, it provides only punctual results of the thermo-fluid dynamic properties calculated in each section and therefore, by the nature of the analysis itself, any consideration is limited to the trend of the average properties along the axis of the machine, depriving the analysis of the further degree of radial detail.

Meanline simulations have a significantly shorter calculation time than is necessary for streamline simulations. Despite this, as we will see later, the output parameters show a full similarity with the average output parameters obtained in the streamline analysis.

3.5.1 Output and validation

Table 3.5 summarizes the percentage deviations between outputs of the quantities of interest returned by the software and the respective target to be matched.

	$\Delta \%$
Pit°	1.38
PT	0.06
Tir°	0.12
Texh°	- 0.52

Table 3-5: Meanline analysis output deviations with respect to targets

It is noted that temperatures and power developed by the turbine are practically coincident to the estimated ones. The greater deviation value, even if within acceptable tolerances, refers to the total pressure at the turbine inlet. This was however expected as the estimated value is affected by two main uncertainties:

- The slight but unknown pressure drop in the combustion chamber.
- The β value corresponding to the current case study. The value used in the analysis, the only one available, in fact refers to FR1625 in working conditions other than those of study, i.e. at reduced power output with lower fuel consumption requirement. In this regard, it is recalled from theory that reduction of fuel consumption produces a reduction of T_{it} and hence in the line slope on the compressor map (figure 3.18). Plant operating point is moved to the left along constant speed compressor characteristic and the current β will therefore be different and slightly higher than that entered in the simulation. The excess total pressure value returned by the software is thus justifiable.

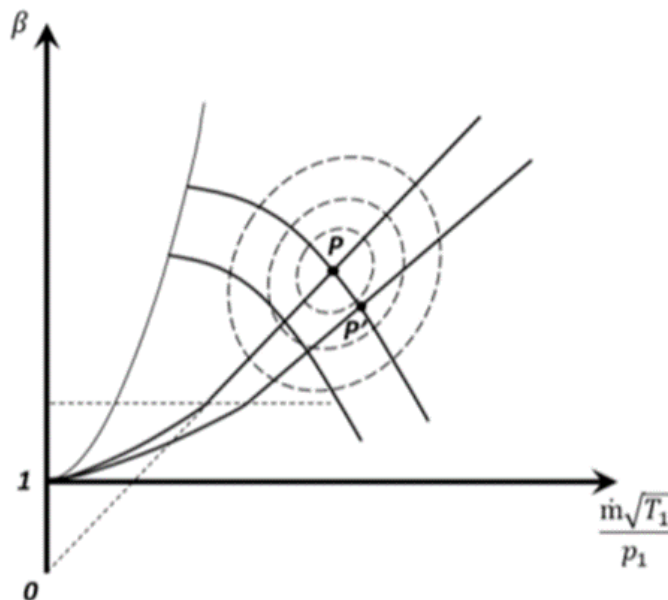


Figure 3.18: Actual plant operating point (P) on the compressor map

3.6 Streamline analysis

The streamline approach is a 2D calculation accounting to real blade angles at each spanwise location. It is especially useful for the study of long blades, as in our case [11]¹.

In this scenario, the change in the blade speed along the radius produces a variation in the velocity diagram along the radius due to the change in the balance between the pressure and the centrifugal force acting on the fluid element. The balance of these forces is referred to as the radial equilibrium and the classical approach to satisfying it in AxSTREAM is the use of the free vortex variation in the velocity diagram. Its main features are:

- $\frac{dp}{dr} = \rho * \frac{c_u^2}{r}$ – pressure varies along radius.
- $c_r = 0$
- Constant c_a along radius.
- Constant $r * c_u$ along radius.
- Constant specific work along radius.

3.6.1 Output and validation

Table 3.6 summarizes the percentage deviations between outputs of the quantities of interest returned by the software and the respective target to be matched.

	Δ % OEM profile	Δ % Opt. profile
Pit°	1.25	1.08
PT	- 0.24	- 0.33
Tir°	0.17	0.04
Texh°	- 0.41	- 0.46

Table 3-6: Streamline analysis output deviations with respect to targets

First, in terms of performance, the change in the input profile does not generate great differences. As already anticipated, there is a congruence with results from the meanline analysis, except for the power outputs that now deviate negatively from the target values. This effect is mainly due to the slightly higher exhaust temperature values reached in the streamline cases, being the flow rate processed in the two types of simulation unchanged. Probably, the loss models used are now more precise, thus allowing a slightly lower flow expansion than in the previous case.

Again, temperatures and power generated by the turbine deviate negligibly from targets.

The trend of the two main temperatures along the height of the bucket is shown in the figure

¹ A blade is considered long if (mean diameter)/(blade height) ≤ 10

below with respect to the average matched value. Both profiles generally follow that imposed by the T_{it} . For OEM profile, trends differ most in the lower part of the blading, reach a maximum around 40% of the height and then decrease in a similar way up to the tip.

On the other hand, the optimized profiles show, with the same average temperatures, peak values a few tens of degrees lower than in the previous cases. This in turn produces a slight decrease in the value of power generated and therefore a lower expansion in the turbine, although it leads to an almost perfect matching with the target firing temperature.

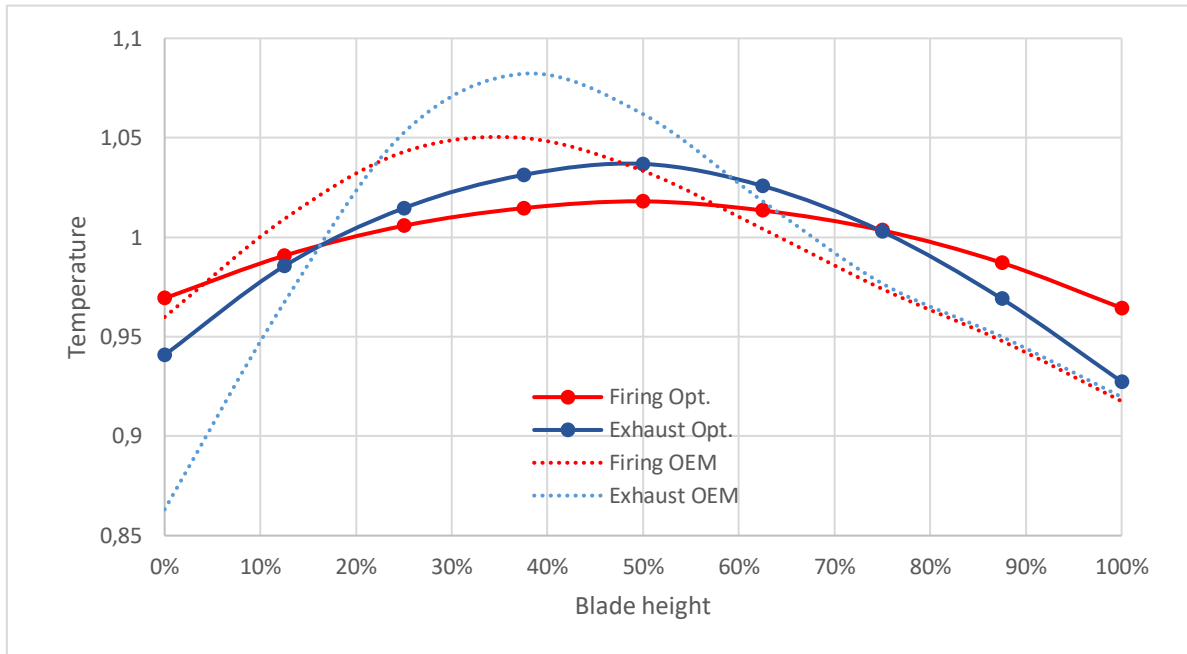


Figure 3.19: Firing and exhaust total temperature trend along blade height

Additionally, contours of static and total quantities (pressure, temperature, enthalpy) can be displayed on the turbomachinery in both absolute and relative frames of reference. Figures 3.20, 3.21 illustrate dimensionless total temperature contours with respect to firing temperature.

Streamline results are used to define boundary condition for turbine component CFD analyses, heat transfer and structural evaluation, ultimately resulting in rotor components life prediction [13].

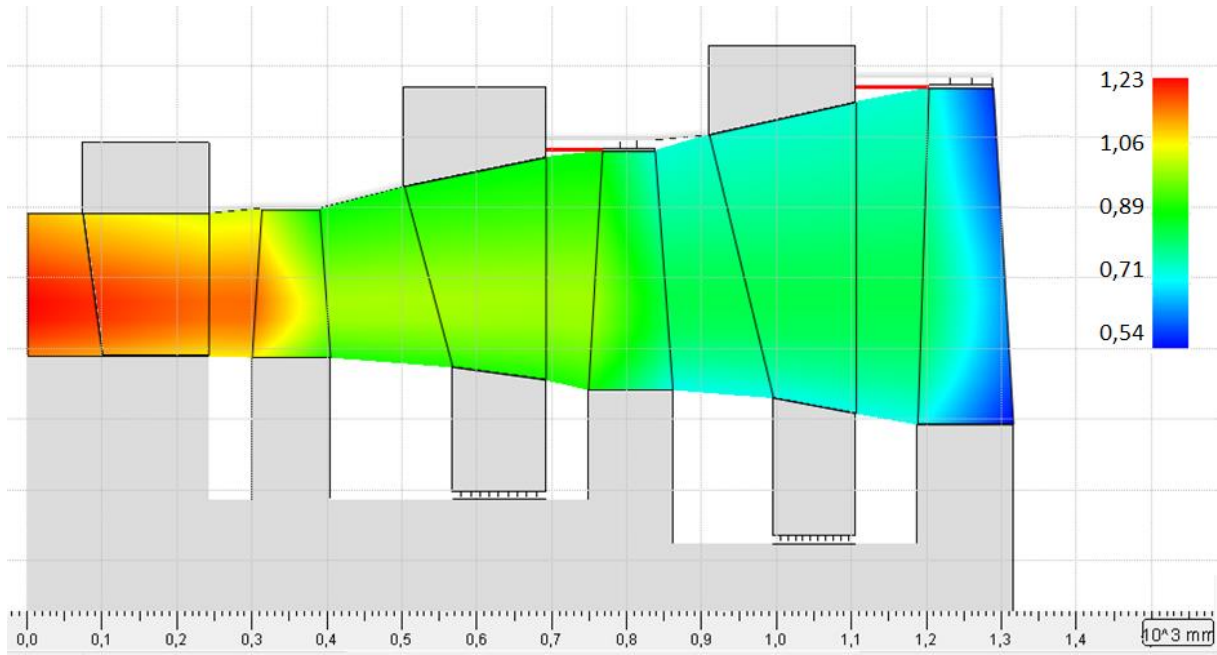


Figure 3.20: Total temperature contour – OEM profile

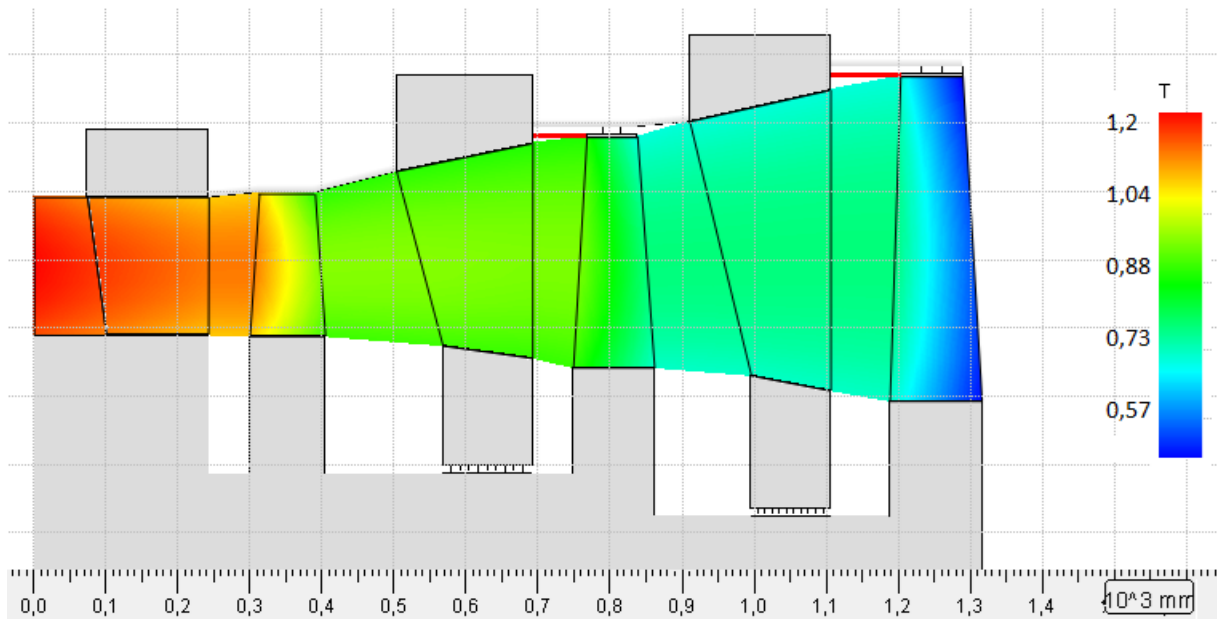


Figure 3.21: Total temperature after optimization – Opt. profile

3.6.2 Other results

Streamline solver window allows not only to check the performance, but also streamwise graphical or tabular representations of many parameters such as velocities, Mach number, losses and reaction as well as velocity triangles for any calculated spanwise sections.

Figure 3.22 shows the value of the absolute Mach number obtained at the vanes output sections. It varies significantly along the height due to the variability of the thermodynamic (temperature,

density, pressure) and kinematic (absolute, sound speed) properties. Unlike the previous two, the third stage vane shows an average value greater than unit: in this regard, it is underlined that the section where the Mach number is computed by the software is not known, but it must necessarily be in the uncovered region of the blades where the phenomenon of post-expansion occurs. However, it is useful to observe how the lower expansion elaborated in the optimized configuration produces a more uniform trend of the Mach numbers, with lower peak values. On the other hand, the exit sections of the buckets are not characterized by high Mach number values.

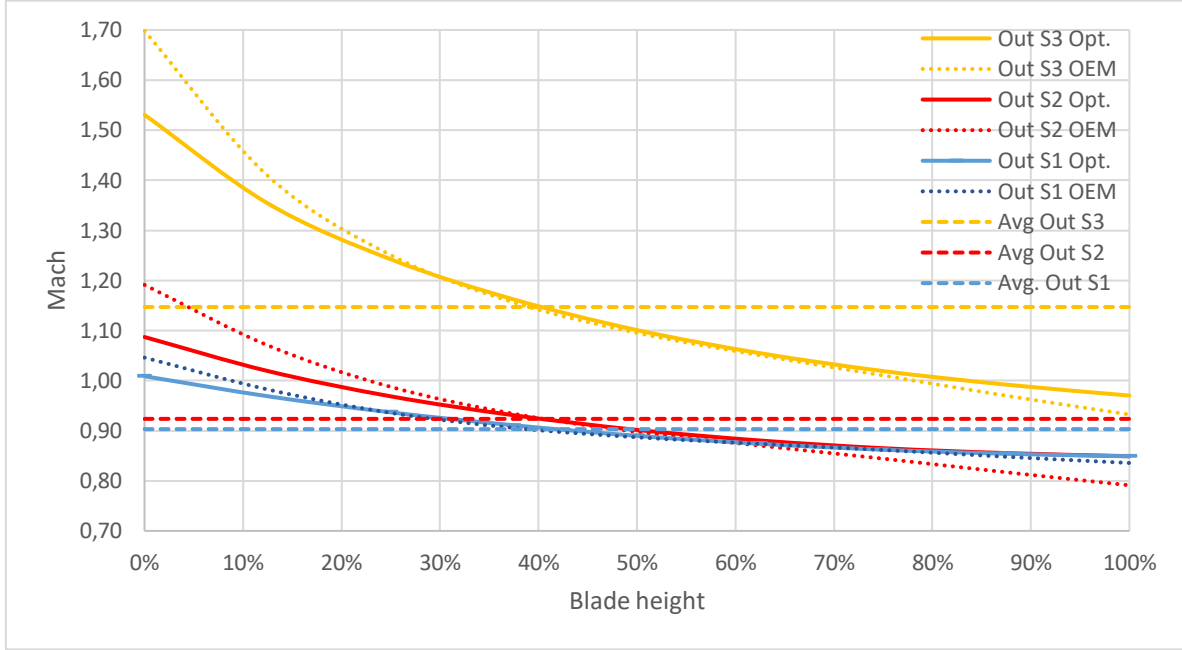


Figure 3.22: Mach number

Another parameter shown is the degree of reaction defined as:

$$R = \frac{\Delta h_{rotor}}{\Delta h_{stage}^{\circ}} \quad 3.4$$

In reaction machines like the FR1625 the degree of reaction indicates how the turbine stage expansion process is split between rotor and stator.

From figure 3.23 it is observed that the trend of R is similar for all the stages, it increases towards the tip of the blade as a consequence of the increase of the enthalpy drop elaborated in the rotor part of each stage as the height of the streamline increases.

The average value of R deviates in negative from the optimal value 0.5, the ideal condition with the greatest efficiency; in the current case, therefore, the fluid is accelerated more in the stator than in the rotor part.

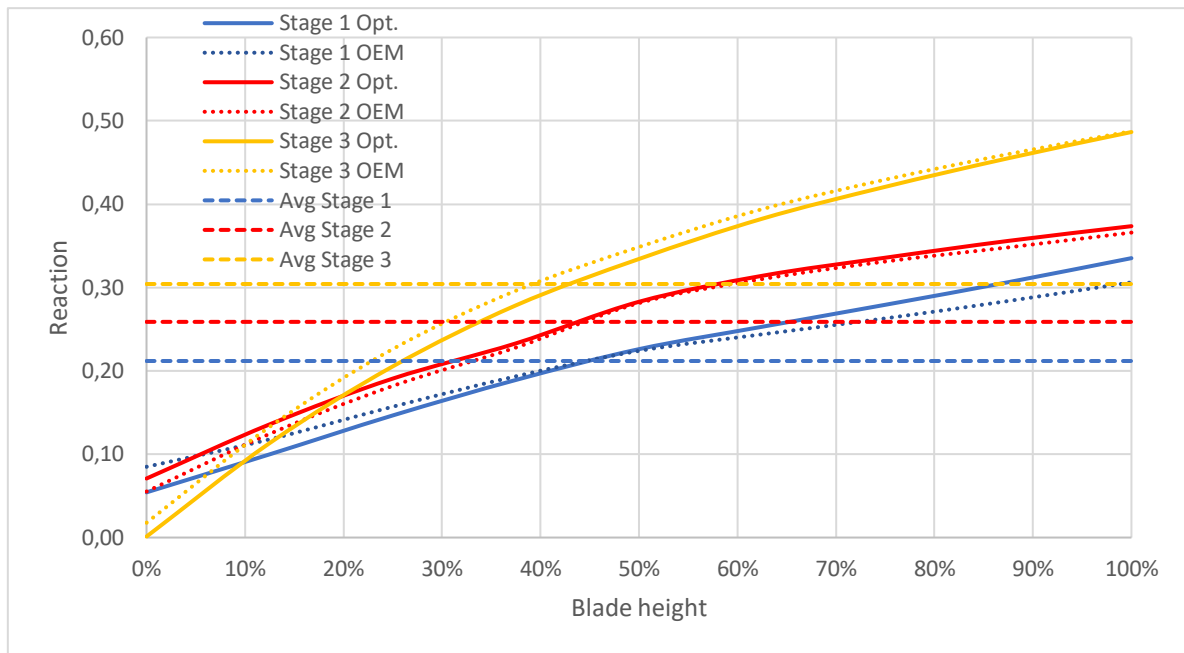


Figure 3.23; Reaction degree

Other figures of interest can be displayed for each streamline, such as the h-s diagram or velocity triangles with their numerical values of speed, angles, incidences, and deviations. Figure 3.24, 3.25 show those relating to the mean section.

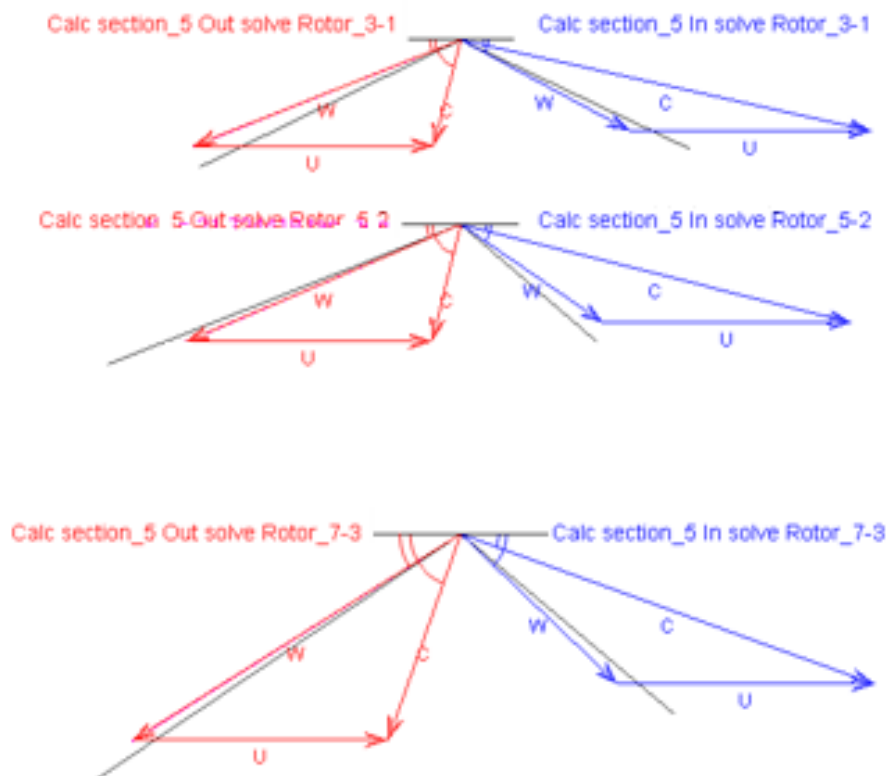


Figure 3.24: Velocity triangles for streamline 5

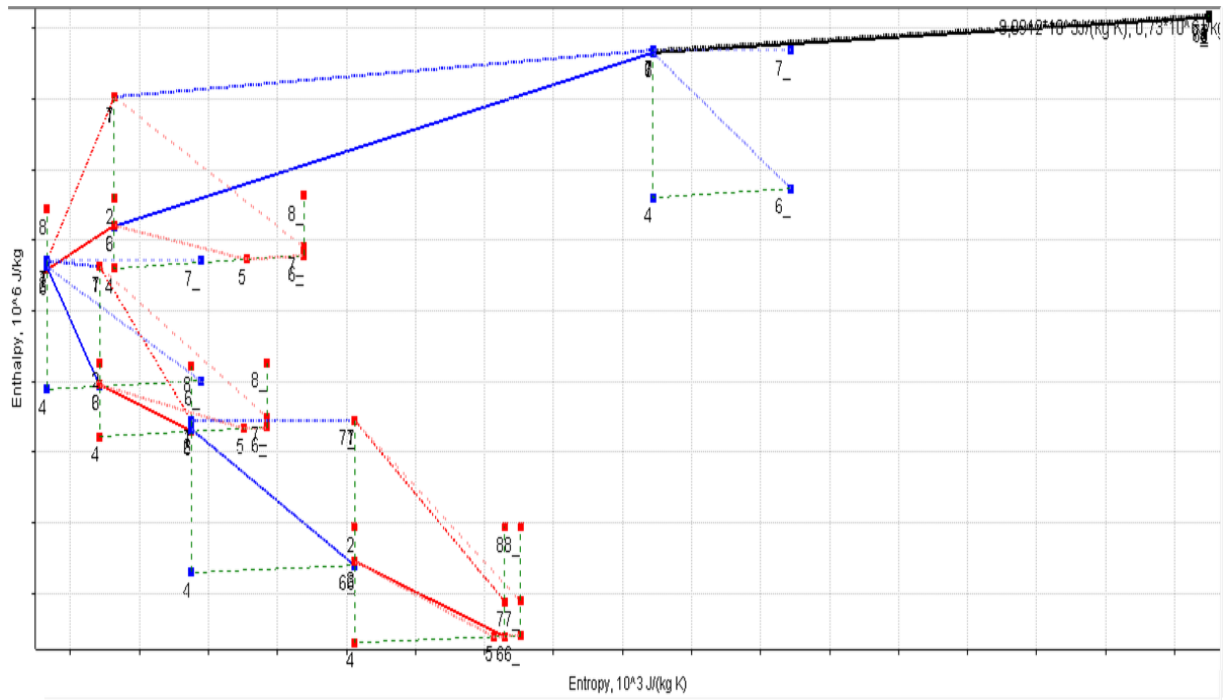


Figure 3.25: h - s diagram for streamline 5

The diagram appears very complex because several thermodynamic points are represented which do not/consider mixing processes of leakages and secondary flow rates with the main flow.

The transformations take place through the stator channels are represented by blue lines, while those that take place through the rotor ones by red lines. For each row, the total and static upstream conditions are represented by two points, blue or red, with the same entropy and different enthalpy. Starting from each of them, a lighter and a thicker line branch out. The lightest line connects the upstream conditions (total or static) with the downstream ones without considering the mixing processes. The thicker line connects the upstream conditions with the downstream ones, considering the mixing process of the main flow with other flows [11].

Looking at the vanes, the transformation between total parameters that takes place without considering effects of mixing is obviously a horizontal line. It is important to note that in the case of the first vane, the cooling processes overall generate a very marked decrease of the outlet flow specific entropy, falling below the corresponding isentropic value. This phenomenon can be justified by applying the entropy conservation equation for an open system consisting of multiple entrances and a single exit.

For the other blades, this effect is always present but much less visible due to the lower secondary flow rates.

Finally, mass balance diagrams can be reviewed to look at the leakages and secondary flows within the machine.

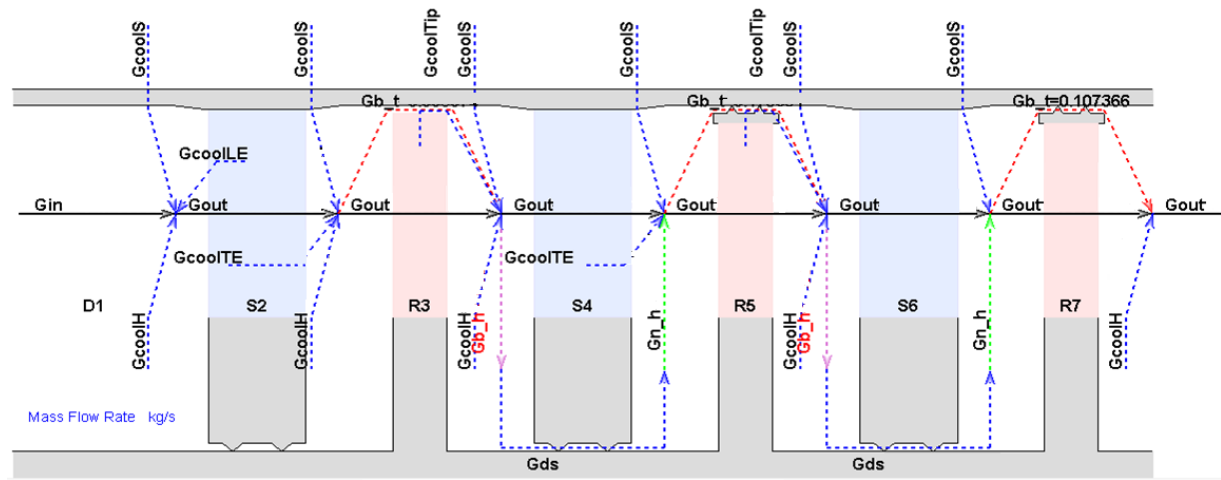


Figure 3.26: Mass balance diagram

4 Compressor thermo-structural FEA

This chapter shows the thermo-structural Finite Element Analysis (FEA) of the last four compressor rotor components, i.e. aft stub shaft and wheels 14 – 15 – 16. FEA is conducted through Ansys, Inc tools, a family software used for Multiphysics computer simulation (e.g. thermodynamic, electromagnetism, structural mechanics, fluid flow, etc.) of structures, electronics, or machine components.

Like any other simulation engineering tool, Ansys is based on the following logical mechanism:

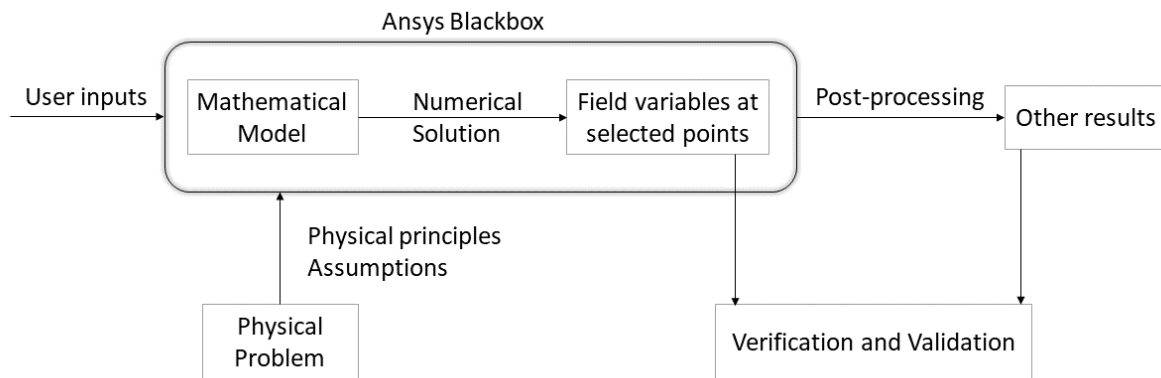


Figure 4.1: Ansys logical scheme

Software solves a mathematical model of the physical problem, based on some key physical principles and assumptions. A numerical solution for selected physics variables at selected points is thus obtained: in a solid mechanics simulation it will be displacements, in a thermal simulation it will be temperatures, in a fluid mechanics simulation it could be pressure and velocity. Everything else is constructed from those outputs at selected points through a process called post-processing. Finally, verification and validation are a systematic step for checking consistency of the results both with the physical principles in the mathematical model and pre-analysis hand/analytical calculation.

4.1 Mathematical model

In general, the mathematical model to be solved is called Boundary Value Problem as it consists of a governing equation, which is a differential equation defined on a domain, and boundary conditions defined at the edges of the domain. The physical problem to be modelled is a thermal-structural coupled system in which temperature field affects the displacement field of the body through the thermal strain.

The first part of the analysis therefore focuses on the thermal and considers a steady state energy equation for an isotropic solid body (constant thermal conductivity):

$$k\nabla^2 T + \varphi_s = 0 \quad 4.1$$

It represents energy conservation for an infinitesimal control volume in which the first term is the net heat flow through the faces of the control volume, whereas the second one represents a heat generation within the control volume.

For the 3D elastic structural part, Ansys uses the following set of governing equations:

- Equilibrium equation

$$\nabla \cdot \sigma + f = 0 \quad 4.2$$

where σ represents the stress tensor and f is a body force (gravity).

- Hooke's Law – relates stresses and strains

$$\begin{Bmatrix} \sigma_x \\ \sigma_y \\ \sigma_z \\ \tau_{yz} \\ \tau_{xz} \\ \tau_{yx} \end{Bmatrix} = \frac{E}{(1+\nu)(1-2\nu)} \begin{bmatrix} 1-\nu & \nu & \nu & 0 & 0 & 0 \\ \nu & 1-\nu & \nu & 0 & 0 & 0 \\ \nu & \nu & 1-\nu & 0 & 0 & 0 \\ 0 & 0 & 0 & \frac{1-2\nu}{2} & 0 & 0 \\ 0 & 0 & 0 & 0 & \frac{1-2\nu}{2} & 0 \\ 0 & 0 & 0 & 0 & 0 & \frac{1-2\nu}{2} \end{bmatrix} \begin{Bmatrix} \varepsilon_x \\ \varepsilon_y \\ \varepsilon_z \\ \gamma_{yz} \\ \gamma_{xz} \\ \gamma_{yx} \end{Bmatrix} - \frac{E}{1-2\nu} \begin{Bmatrix} \alpha\Delta T \\ \alpha\Delta T \\ \alpha\Delta T \\ 0 \\ 0 \\ 0 \end{Bmatrix} \quad 4.3$$

where E , ν , α are Young's modulus, Poisson's ratio, and coefficient of thermal expansion respectively.

- Strain-displacements relations

$$\begin{aligned}\varepsilon_x &= \frac{\partial u}{\partial x}; \varepsilon_y = \frac{\partial v}{\partial y}; \varepsilon_z = \frac{\partial w}{\partial z}; \\ \gamma_{xy} &= \frac{\partial u}{\partial y} + \frac{\partial v}{\partial x}; \gamma_{yz} = \frac{\partial v}{\partial z} + \frac{\partial w}{\partial y}; \gamma_{zx} = \frac{\partial w}{\partial x} + \frac{\partial u}{\partial z};\end{aligned}\tag{4.4}$$

In the structural field the equation set is therefore much more complex, having for each control volume 15 equations for 15 unknowns. In finite element analysis the displacement fields are the primary unknowns from which stresses and strains are subsequently computed.

The two major kinds of boundary conditions are essential (Dirichlet) boundary conditions specify a value for the main variable (e.g. temperature in a heat transfer problem or displacement in a solid mechanics problem), while natural (Neumann) boundary conditions specify a value for the derivative of the main variable (e.g. heat flux or stress).

A third boundary condition later used for convective heat flux, called Robin, specify a linear combination of the main variable and its derivate.

4.2 Numerical solution – FEM

The first step is discretization, moving from the differential equation to a system of algebraic equations.

The computational domain is so divided into a set of simpler non-overlapping subdomains, called finite elements, in which each field variable is expressed locally (at element level) as a linear combination of polynomials, defined in terms of the variable values in the nodes. In this way we reduce the problem to determine variable values at finite number of points (nodes) rather than a function.

Now, substituting the assumed piecewise polynomial function (also called residual function) in the governing equation, we do not get zero, except for the fortunate case when the assumed function is the exact solution. On the contrary we usually obtain an error/residual must be minimized to find the set of nodal values that best fit governing equations and boundary conditions.

$$A(F^*) - f = R\tag{4.5}$$

where A, F* and R are a differential operator, trial piecewise polynomial function and residual, respectively.

For this purpose, the differential form is transformed into a weighted integral form, assembling the integral of the product of the residual and an arbitrary weighting function, and setting it to zero.

$$\int w * (A(F) - f) = 0\tag{4.6}$$

The residual function does not satisfy the weighted integral form for any arbitrary function (except for the case when it coincides with the exact solution), but only for an arbitrary piecewise polynomial variation of w . In this way the arbitrariness of the weighting function is reduced to the arbitrariness of the values it assumes in the nodes.

$$\int w^e * (A(F^*) - f) = 0 \quad 4.7$$

with both w^e and F^* piecewise polynomial function.

Functions used to express the various fields in the original differential equation (also called strong form) must be differentiable up to the order of the PDEs: for example a linear piecewise polynomial assumption cannot be used in 4.1 as it has a second null derivative everywhere and not defined at the nodes. A way to relax this requirement, consists in using a weak form of 4.6. It is a version with fewer restrictions on the assumed shape where integration by parties is applied. This form turns a second-order differential equation in one variable into a first-order differential equation in two variables which requires a weaker continuity on the field variables. By integrating element by element, a set of algebraic equations is obtained. In matrix form:

$$[K]\{x\} = \{f\} \quad 4.8$$

where x is a vector containing nodal variables, K is called stiffness matrix and f is the force vector.

Each equation of the system relates a nodal variable to all its neighbours. Because the gradient at the boundaries appears naturally in the weak form, they get naturally incorporated into the right-hand side of algebraic equations for boundary nodes, and for that reason, this kind of a boundary condition is called a natural boundary condition.

The solution proceeds in 3 steps:

- Firstly, a corresponding variable value is assigned to all the nodes that have essential boundary conditions on them.
- Then a subset system of linear algebraic equations is inverted to get unknown nodal values.
- Variable is found at any point in the domain by interpolation.

Everything else is derived through post processing:

- Differentiating temperature, displacements to get the heat flux, stresses, and strains.
- Computing what is called a reaction in ANSYS, to check whether the solution satisfies fundamental physical principles such as energy conservation or equilibrium.

The figure 4.2 summarizes the numerical procedure performed by Ansys.

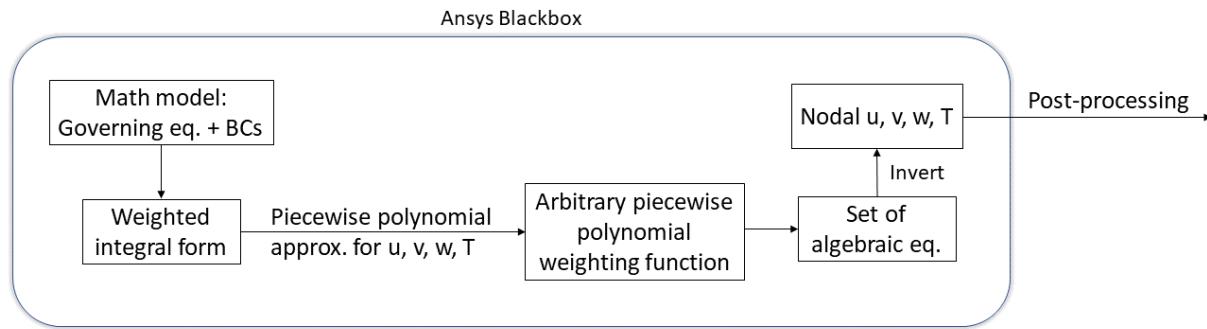


Figure 4.2: Ansys numerical procedure

Having reduced the problem to the calculation of nodal quantities, by adopting a piecewise polynomial distribution of variables in the domain, introduce an error called discretization error. It is easily observable in the case of a linear polynomial trial function, which has a piecewise constant first derivative with discontinuity in the nodes. Even if the shape meets exactly the essential boundary condition, it satisfies the natural one only approximately. So, there is a discrepancy between what was specified and what the solution gives as a result.

It also makes the numerical approach non-conservative locally: net heat flux crosses the element is null and generated heat is only considered in the jump between adjacent elements. Follows energy conservation or equilibrium are not satisfied for each finite element, but in any case, they are satisfied in aggregate.

Discretization error can be reduced by improving our piecewise polynomial approximation. There are two ways to do this:

- Increase number of finite elements.
- Increase the order of the polynomial within each element by using more nodes per element. ANSYS solver puts in the mid-side nodes by default, and uses a second order polynomial, rather than a first order polynomial.

4.3 Creation of the calculation model in Ansys

Ansys simulations are performed using the Ansys Workbench system that contains all the specifications of the current project (figure 4.3).

The study of the individual rotor components involves the use of four main modules: A, B, E, F. Modules A and B, respectively thermal and structural, study the small portion of the wheel containing a single blade. In fact, the simultaneous analysis of several blades would lead to an excessive slowing down of the calculation time, due to their complex airfoil shape which requires the adoption of a large number of nodes. The modules are coupled: the solver first runs the thermal module generating a temperature field which is subsequently imported into the mechanical module, as it affects the displacement field of the body through the thermal strain.

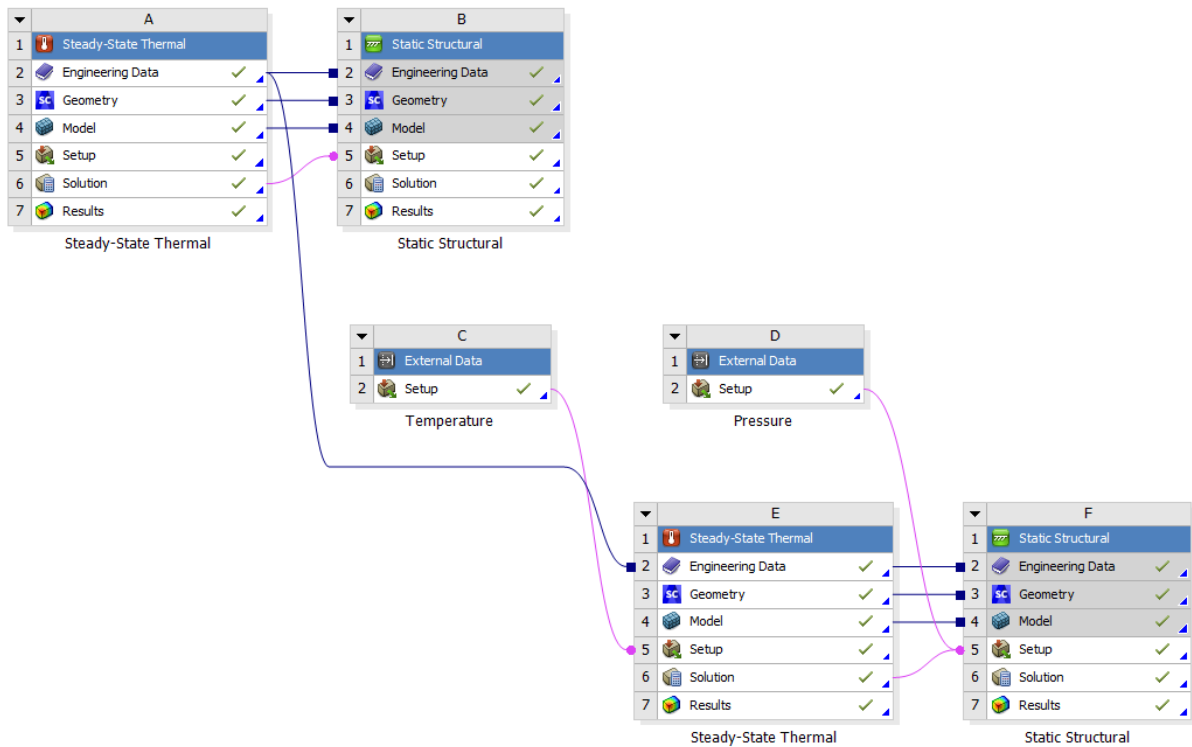


Figure 4.3: Ansys Workbench

The same goes for modules E and F, where, however, the analysis is performed on a larger slice integrate many features not present previously, influent for the real structural behaviour, such as holes for the tie rod, fillets and channels for cooling air flow, that influence stress distribution and could be critical points. Now blade, spacers and slots are suppressed and replaced by equivalent pressure and thermal loads obtained from the previous step and imported through modules C - D.

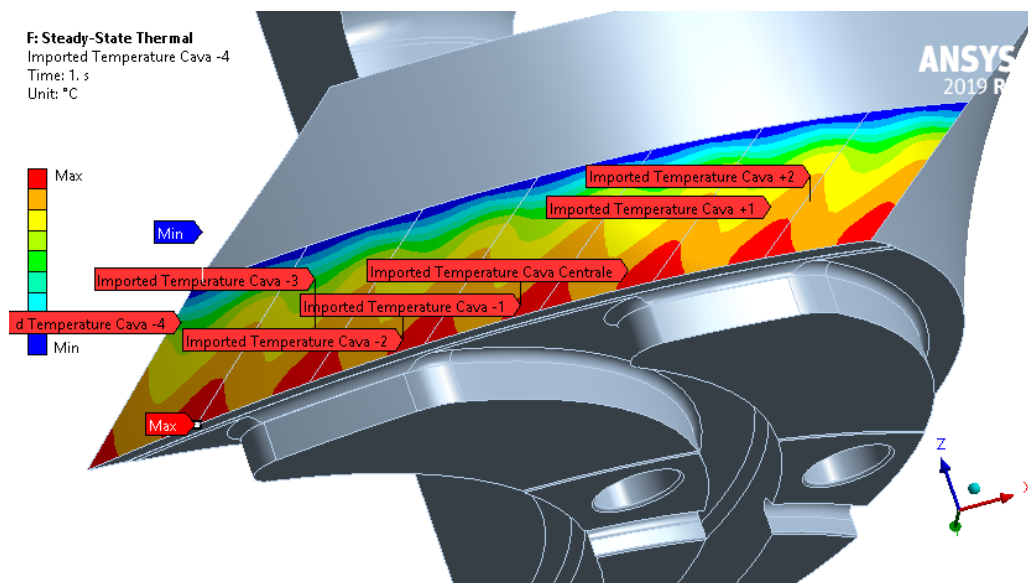


Figure 4.4: Imported pressure and thermal load

The model set up procedure on Ansys can be schematized as:

- Pre-processing:
 - Import of the CAD model defines the domain for boundary value problem.
 - Assign material and correct physical properties to each body of domain.
 - Define a cylindrical coordinate system to study the axial symmetric geometry.
 - Set cyclic symmetry condition allows to study only a part of a body. This considerably reduces the software computational time thanks to a strong reduction in the number of nodes and elements to analyse.
 - Define which are the contact surfaces between the bodies and which type of connection established (Bonded, No separation, Frictionless, Frictional). Particularly important is the dovetail coupling between the blade attachment and the wheel slot, whose surfaces are obtained by broaching. The surfaces in contact during steady state operation, called active surfaces, are determined by the action of the high centrifugal forces, which generate friction forces do not allow any axial movement of the blade.
 - The meshing step represents the discretization of the domain. It is strongly customized to get the best compromise between accuracy, convergence, and calculation speed.

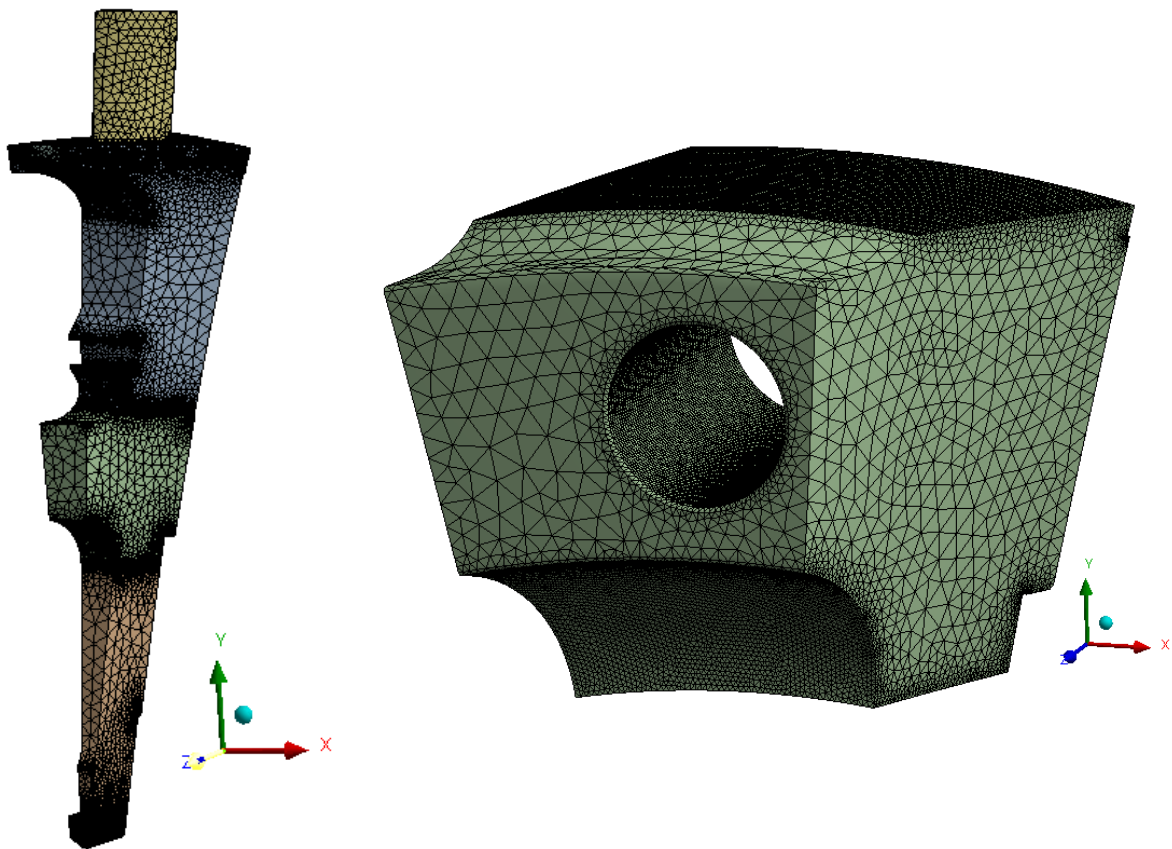


Figure 4.5: Meshing for wheel 16 smaller (left) and larger (right) slice

- Apply boundary conditions at the edges of the domain. In the thermal module, a homogeneous Dirichlet condition is applied to the blade, assuming that in steady state operation the blade has reached the same temperature value as the air flow, already defined in the preliminary analysis. A Robin condition is instead applied to the aft surface of wheel 16 and to the forward side of aft stub shaft, accounting for convective effect of the extracted cooling air. In particular, for the aft stub shaft it is necessary to calculate different values of the convective coefficient due to the particular fan shape. This is done through data provided by the flow network resolution [12].

On the other hand, structural module requires displacement constraints along axial and circumferential directions, leaving the body free to expand along the radial direction, and the application of a centrifugal load, suitably increased to be safe with the over speed.

- Solution: choose the type of solver and the number of steps in which the loads are applied. Using multiple steps allows to compare thermal-structural analysis (primary and secondary loads applied) with one considers only structural load (primary load).
- Post-processing: show solution for temperature, displacements, and stresses fields.

4.4 Post-processing

The main results analysed in this phase are four: temperature, total deformation, maximum principal stress and equivalent stress.

The stress at any point is completely defined by the tri-axial stress tensor, whose components depend on the orientation of coordinate system adopted. It is interesting to find the orientation of the coordinate system whereby the stress tensor at a given point is composed only by diagonal terms. The tensor state is therefore described exclusively by normal stress, called principal stress ($\sigma_1, \sigma_2, \sigma_3$), and no shear stress are present. They are ordered from the highest to the lowest, so that σ_1 is called maximum principal stress. To better understand the severity of the stress tensor, and to verify its acceptability with respect to company design criteria requirements, it is usually transformed in an equivalent (von Mises) tensile stress:

$$\sigma_{VM} = \sqrt{(\sigma_1 - \sigma_2)^2 + (\sigma_2 - \sigma_3)^2 + (\sigma_1 - \sigma_3)^2} \quad 4.9$$

The equivalent stresses relating to the most critical areas are compared with experimental admissible stress curves, represented in a specific chart as a function of temperature.

Mainly they are:

- S_u , ultimate material strength.
- $1.5 \cdot S_m$ and $2 \cdot S_m$, a time independent allowable stress, yielding and ultimate strength function.

- $1.25 \cdot \sigma_t$ at 200kh, a creep allowable stress. Creep is a high temperature phenomenon for which a failure, accompanied by a permanent strain progressively growing in time, may occur even if the material is stressed below the yielding limit.

The stress and maximum temperature values of the analysed critical surface define a $\sigma - T$ point on the graph, which indicates whether the component is safe or not, respects the minimum number of operating hours required, or must be verified through a Low Cycle Fatigue (LCF) analysis.

Finally, the total deformation needs to be checked to verify blade remains clamped to the wheel and to guarantee clearances between elements are respected.

4.4.1 Aft stub shaft

Aft stub shaft and wheel 15 represents the most important object of study as they are subjected to greater thermal stresses due to extraction of cooling air.

Temperature field is strongly affected by the main air flow in contact with the blade, and by the convective action of the extracted flow, which undergoes an expansion in the fan channels. The result (figure 4.6 - dimensionless with respect to compressor discharge temperature) is a gradual cooling of the body from the external diameter towards the centre.

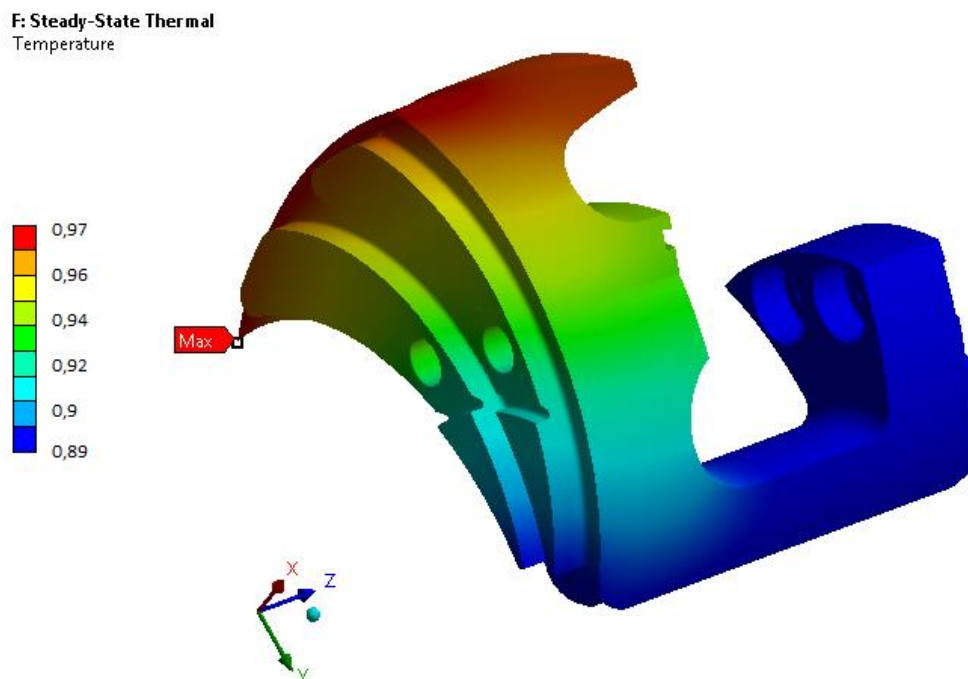


Figure 4.6: Aft stub shaft temperature field

The first structural analysis, involving the portion containing the single blade, highlights high stresses in the dovetail slot sides (figure 4.7 – equivalent stresses dimensionless with respect to material yielding stress evaluated at punctual temperature).

The stress field is both influenced by slot tendency to align its axis with the rotation axis of the machine, and by the expansion it undergoes, different from that of blade attachment as they are made up of different materials.

On the other hand, the structural study performed on the larger slice, shows stresses are mainly concentrated in fillets on the forward surface, due both to the presence of higher temperature gradients and to the action of centrifugal loads acting on a body with non-symmetrical mass distribution, which create a greater bend in this surface. Figure 4.8 displays the most critical areas, in addition to the dovetail slot, which require a comparison with the company design criteria presented in section 4.4.

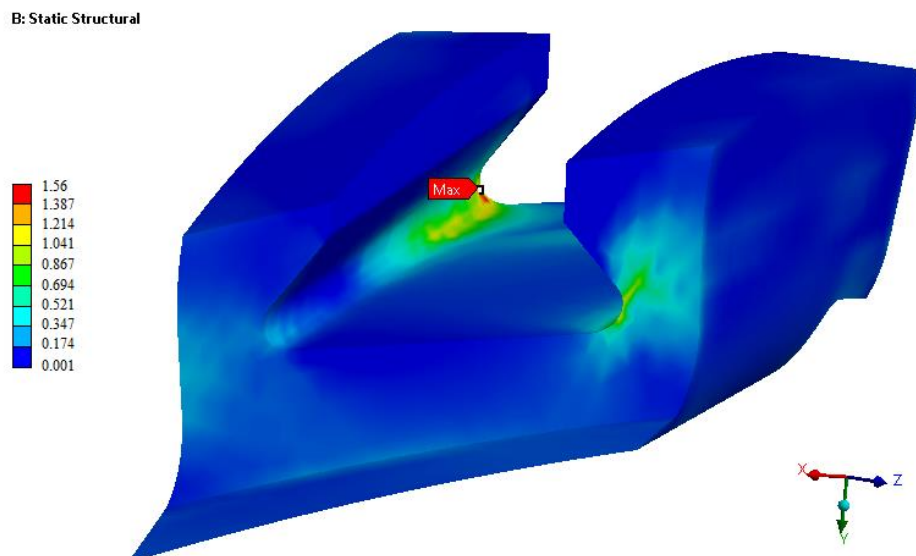


Figure 4.7: Aft stub shaft dovetail slot stress field

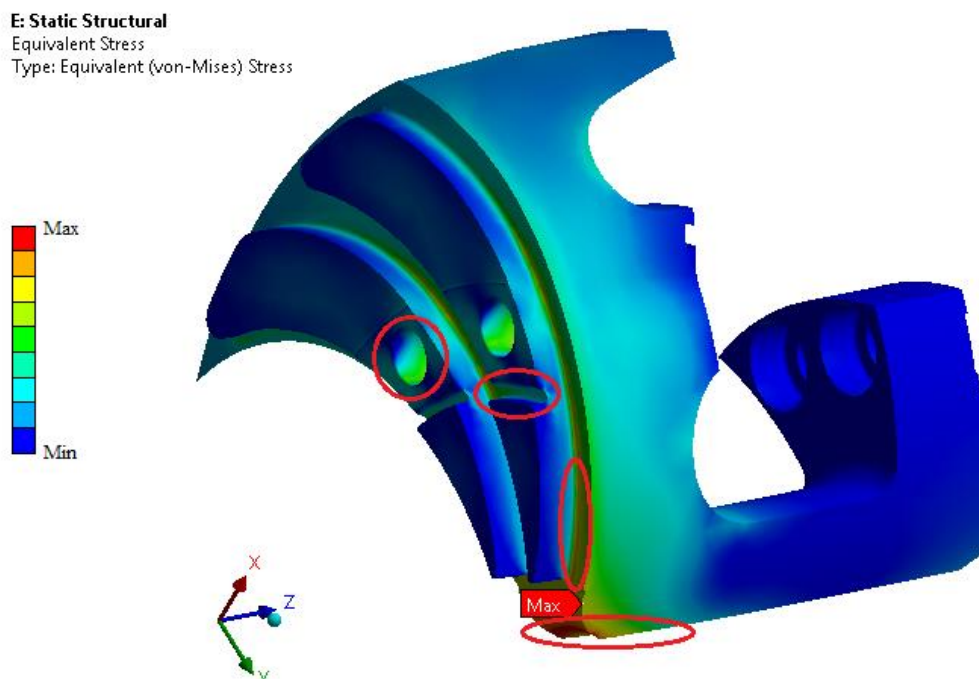


Figure 4.8: Aft stub shaft most critical areas

From the outer diameter towards the centre, they are named:

- Thru bolt hole.
- Centring fillet.
- Fan fillet.
- Bore hole.

For each of them, the maximum temperature, maximum principal, and equivalent stress are extracted.

The company criteria require the equivalent stresses be divided into primary and secondary stress (the latter also consider thermal stress yielded by the internal temperature gradient), as well as mean and peak stress. Mean stresses are those generated in the body to balance external loads such as forces and torques, whereas peak stresses accounts for the local stress increment due to the body geometric discontinuities (holes, notches, fillet and other shape change). With Ansys software it is easy to divide the secondary from the primary stress, but not the same between the primary components. They are opportunely separated in a mathematical way by the help of a 2nd order polynomial interpolation of the results.

There are three main checks to be verified. First, the mean primary stress – max temperature points are entered on the graph, to check if the component respects an admissible stress value and the minimum number of operating hours required (figure 4.9 – in all the graphs presented, σ is dimensionless with respect to material yielding stress at 20°C, whereas T with respect to compressor discharge temperature).

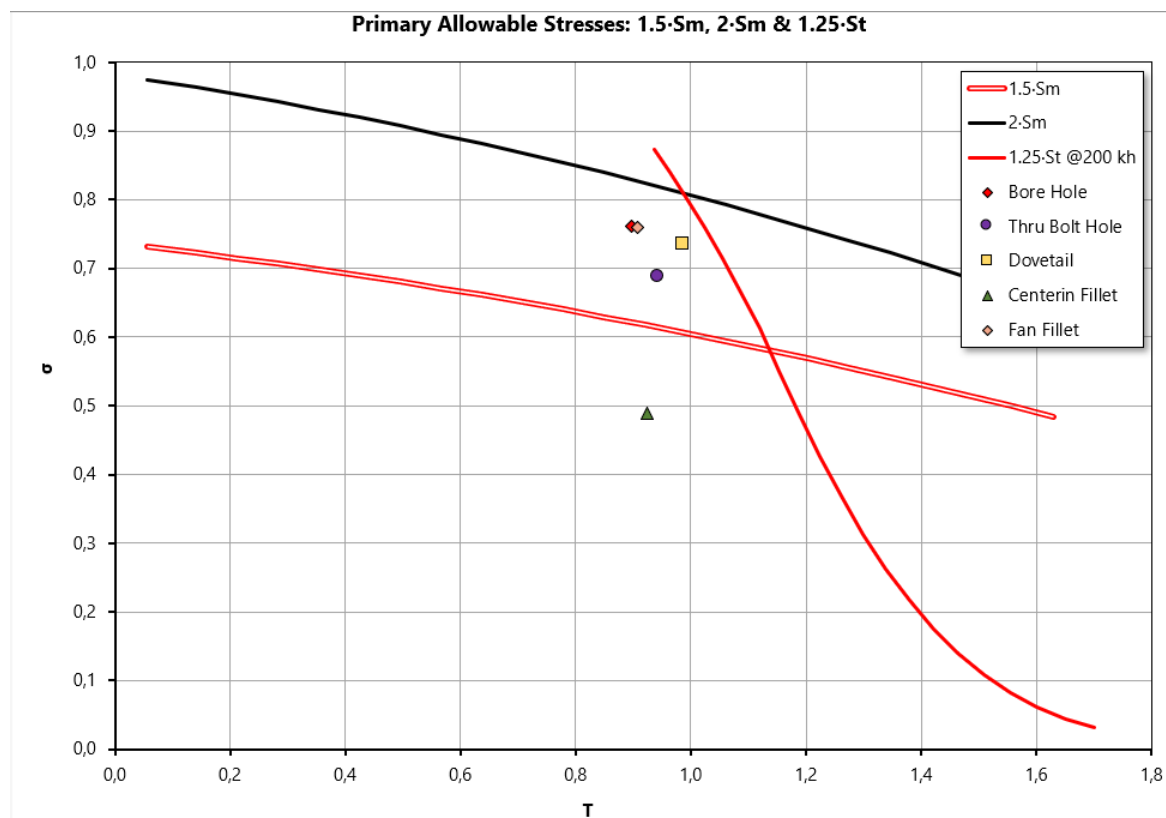


Figure 4.9: Aft stub shaft mean primary and allowable stress

Although all points respect the creep allowable stress, many lie between 1.5 and 2·Sm curves, implying the necessity for further LCF analysis.

Then mean primary + secondary stresses are inserted in another similar graph, which contains yielding and ultimate strength curves to understand if the component is safe or if a wide surface experience a permanent deformation. When a large portion of material exceeds the yielding limit, the linear analysis conducted by Ansys is not reliable and elastic-plastic analysis should be carried-out with a dedicated software. In this case all points correctly lie below the mentioned curves (figure 4.10).

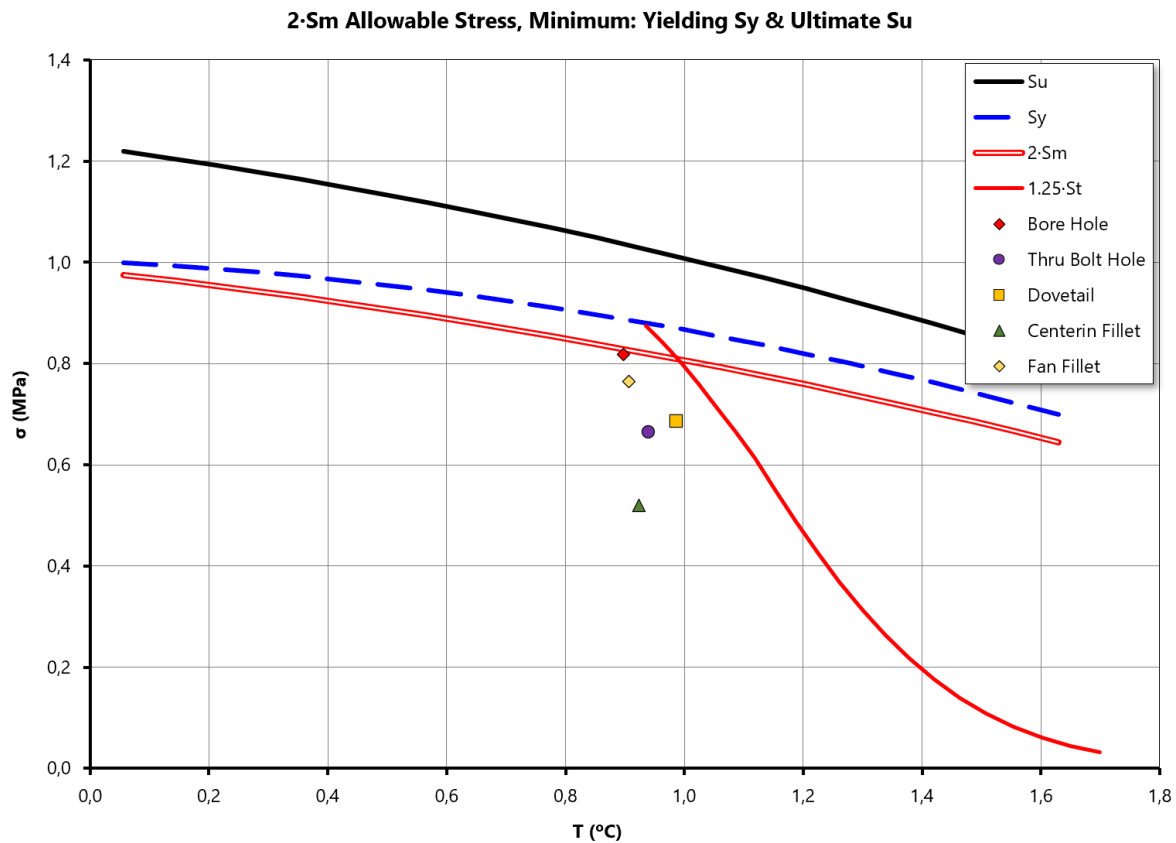


Figure 4.10: Aft stub shaft mean primary + secondary and allowable stress

The structural analyses conducted by Ansys are elastic type, as specified in paragraph 4.1, and therefore stress values going beyond the material yielding strength do not follow a linear stress-strain relationship and require appropriate corrections. This often happens when considering primary + secondary peak stresses, and a clear example can be seen in figure 4.7, on either side of the dovetail slot. They are geometrically concentrated but lead to a local permanent deformation exceeding the 0.2%. When an elastic-plastic deformation occurs in a limited portion of the material, such as stress concentration in a fillet, it is possible to carry-on a stress analysis based on the combined use of Hook's law, Neuber's law and Ramberg-Osgood's equation (figure 4.11). Elastic peak is converted in an elastic-plastic peak, at Neuber's and Ramberg-Osgood's curves cross. The permanent deformation smooths the stress peak sharpness

leading to a redistribution of the load in the surrounding material, preventing the failure also when the elastic value overcomes the ultimate material strength. In this case study the reduced peak values do not exceed S_u but still go beyond the $2 \cdot S_m$ curve (figure 4.12). This reinforces the theory that an LCF analysis is necessary.

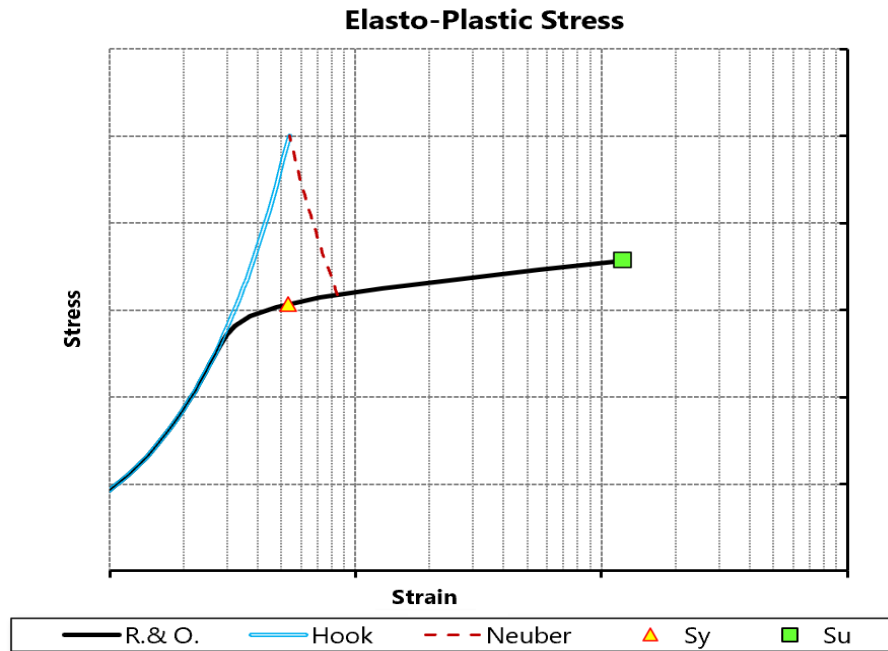


Figure 4.11: Peak stress correction

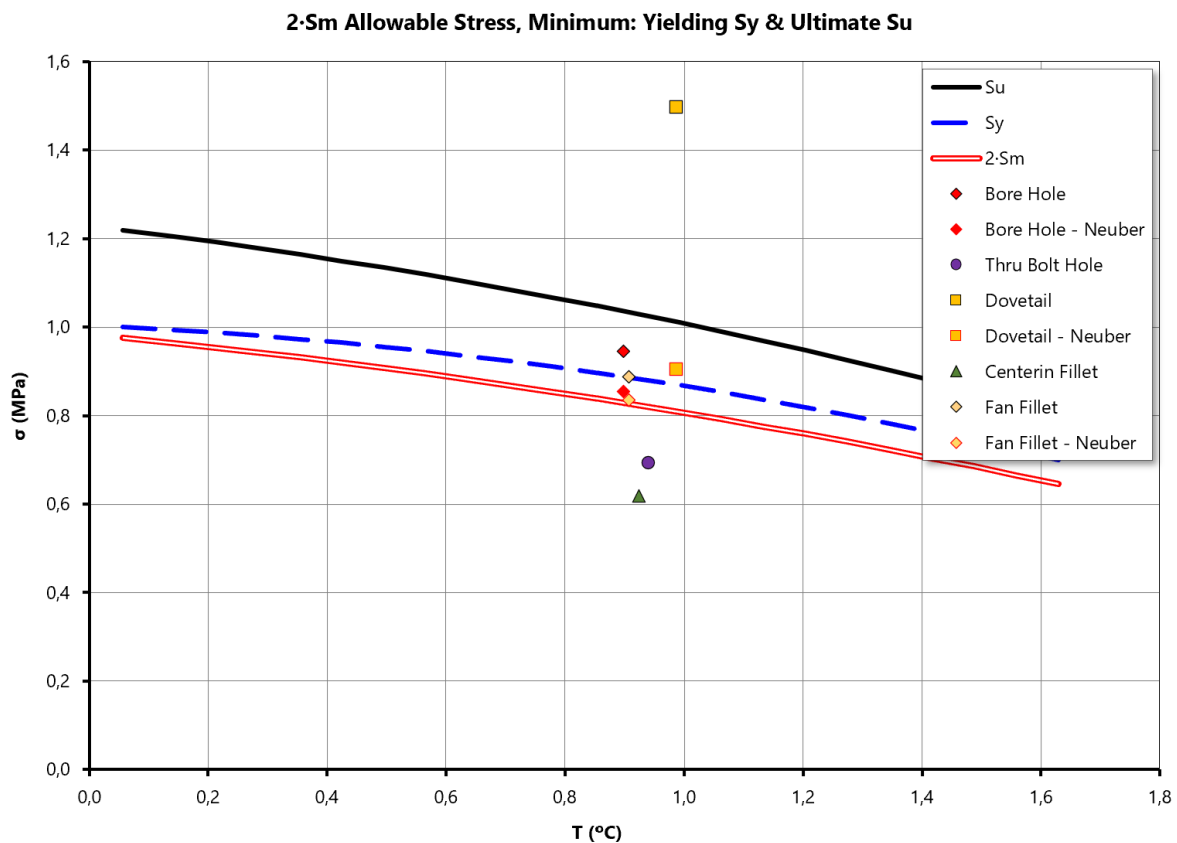


Figure 4.12: Aft stub shaft primary + secondary peak and allowable stress

The low cycle fatigue damage within the duty cycle is evaluated for all the analysed surfaces. The study is based on Smith-Watson-Topper theory where σ_{swt} coincides with the maximum principal stress registered in a cycle.

All the investigated surfaces are characterized by geometric irregularities (such as thru holes, fillets, notches) yielding an important local stress increment. The fatigue tests show that the stress concentration factor between smooth and notched specimens is not the static K_t , but a lower value K_f called fatigue notch factor. The body is less affected by the concentration of tension than in the static case, as the presence of a sensible internal stress gradient makes the material immediately underling the most loaded fibre less stressed and helps to hamper the crack initiation. Maximum principal stress is so reduced by a factor K_f/K_t always lower than unit and used in the material fatigue curve at the specific temperature to extract number of allowable duty cycles (or equivalent start - N) for the considered item. Ratio K_t/K_f is function of many variables such as material, irregularity dimension, nominal stress, and fatigue type field (LCF or HCF).

Finally, considering a service life of 5000 duty cycles (n) the output damage n/N indicates which are the most dangerous areas of the aft stub shaft. They will be subject to possible re-design to extend the component useful life.

	n/N
Bore hole	47.0 %
Thru bolt hole	0.0 %
Dovetail	60.8 %
Centring fillet	0.0 %
Fan fillet	0.0 %

Table 4-1: Aft stub shaft fatigue damage

4.4.2 Wheel 15

The sixteenth rotor stage is also an important object of study due to the extraction of cooling air in its aft side.

The temperature range is therefore very similar to that of the aft stub shaft, with slightly different values due to the different geometric shape and lower temperature of the main air flow. The total deformation peak is obviously located at the top, due to high rotational speed, but it's still contained in the order of a few millimetres (figure 4.13).

Similar considerations to those of the aft stub shaft apply to stress distribution, both for the dovetail slots and for the aft surface, subjected to high thermal gradients as it is affected by the extracted air flow. This body also suffers from a non-symmetrical mass distribution, even though there is no fan and the bore hole is smaller than that of the last stage. The overlapping of these effects requires areas highlighted in the figure below require more in-depth analysis.

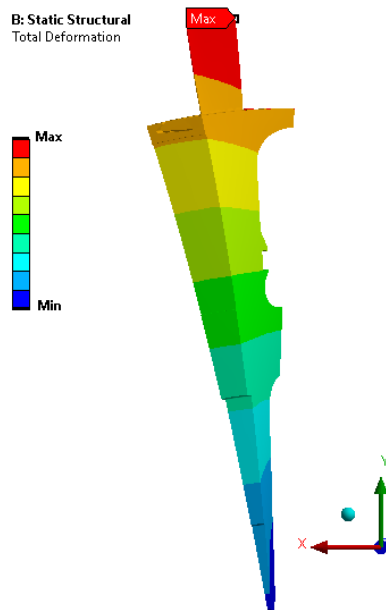


Figure 4.13: Wheel 15 total deformation

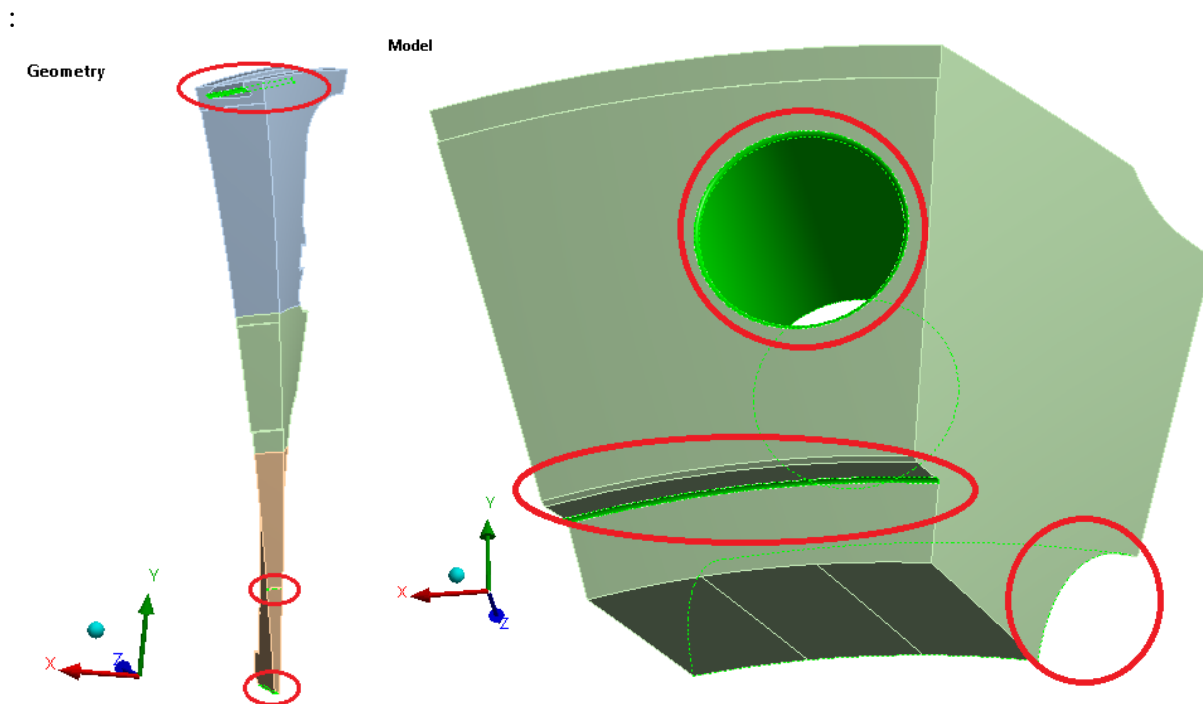


Figure 4.14: Wheel 15 critical areas

They are named respectively:

- Dovetail.
- Facing down round.
- Bore hole.
- Thru bolt hole.
- Armpit AFT.

- Armpit FWD.

Again, for each of them, the maximum temperature, maximum principal, and equivalent stress are extracted and analysed following a procedure identical to that already presented. Figures 4.15, 4.16, 4.17, 4.18 show equivalent stresses dimensionless with respect to material yielding stress evaluated at punctual temperature.

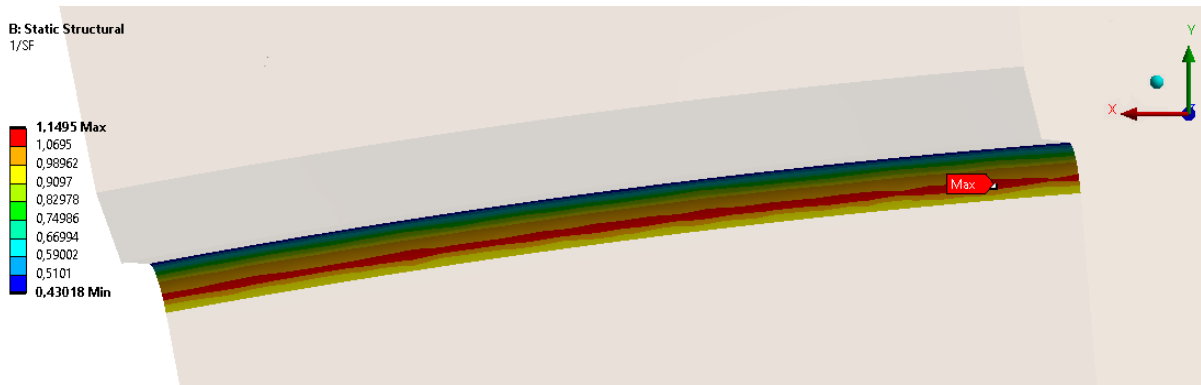


Figure 4.15: Wheel 15 stress field for facing down round

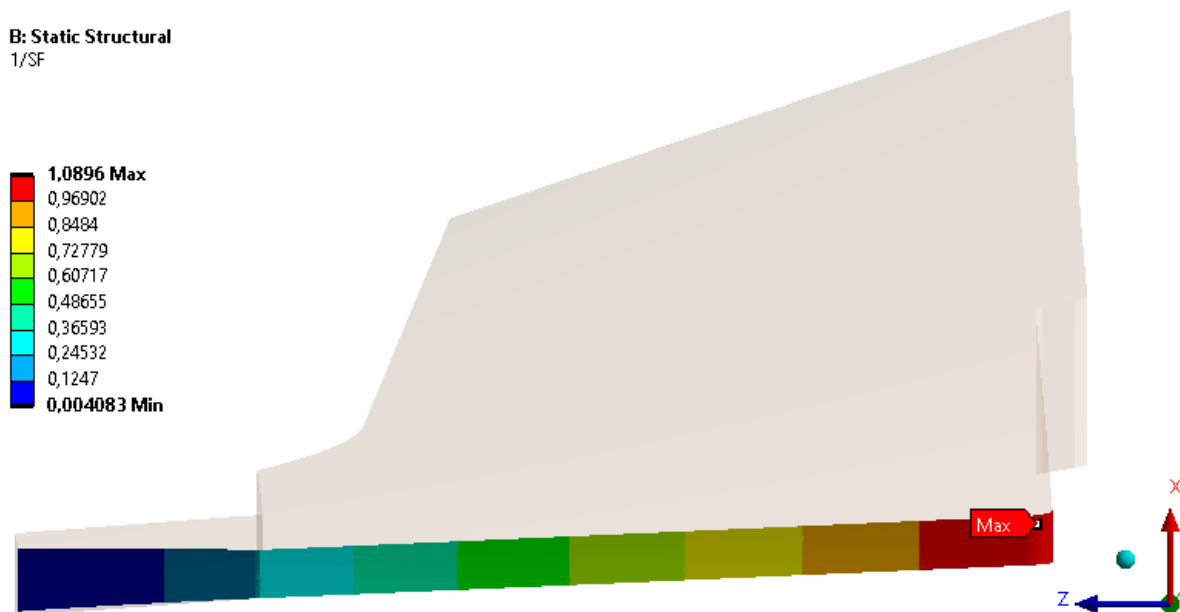


Figure 4.16: Wheel 15 stress field for bore hole

It is useful to note that these bodies, under operating conditions are assembled with other elements: holes for example are not empty but coupled with bolts. This means deformation are limited and tensions are not so critical as in figure 4.17, where peak stress are mainly related to lack of material. However, the distribution of stresses and deformations shows that the hole tends to be squeezed in radial direction.

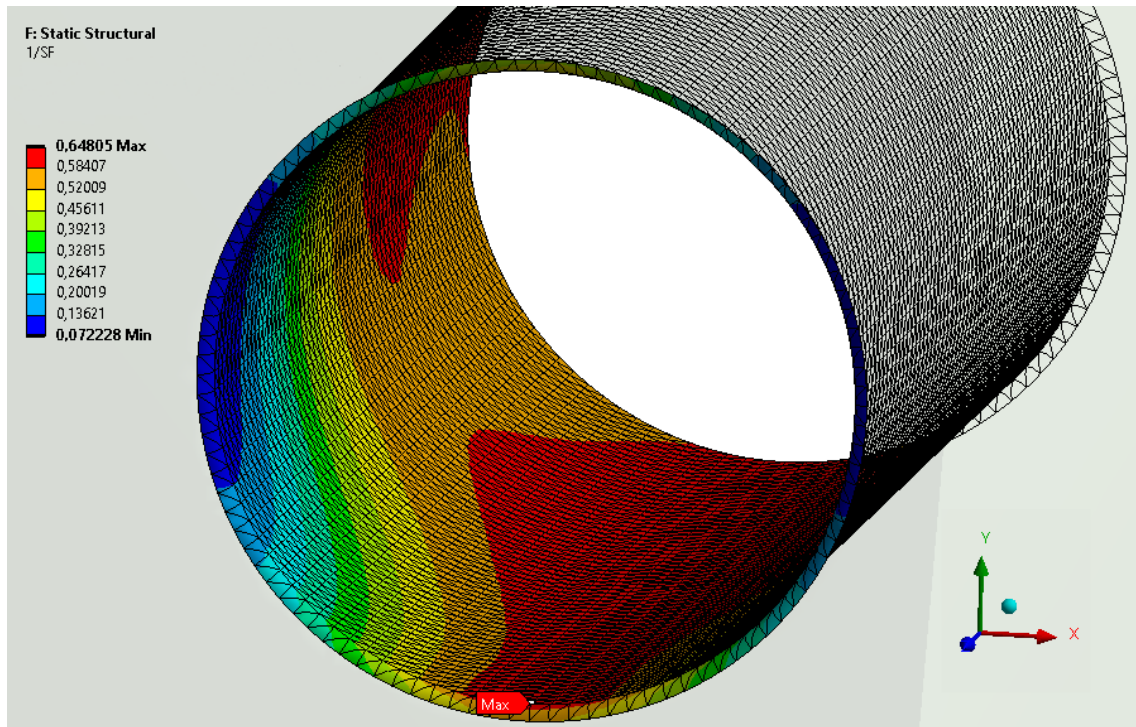


Figure 4.17: Wheel 15 stress field for thru bolt hole

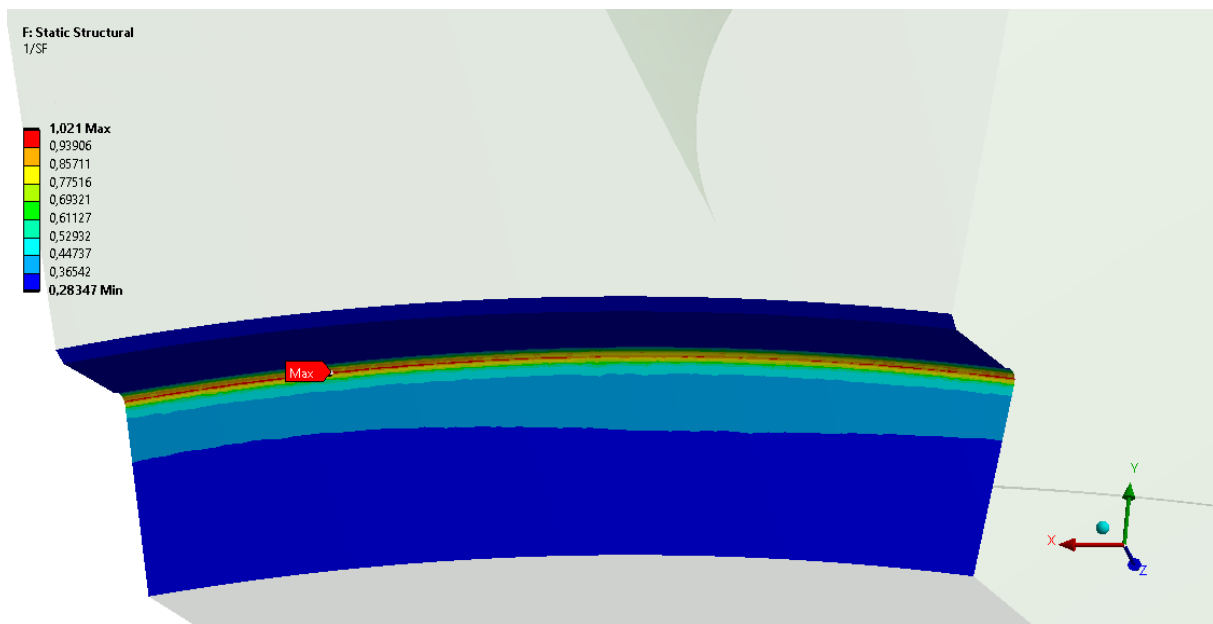


Figure 4.18: Wheel 15 stress field for armpit AFT

The charts below suggest that even if the component is safe, meets the required number of operating hours, and no large area is permanently deformed, an LCF analysis is still necessary.

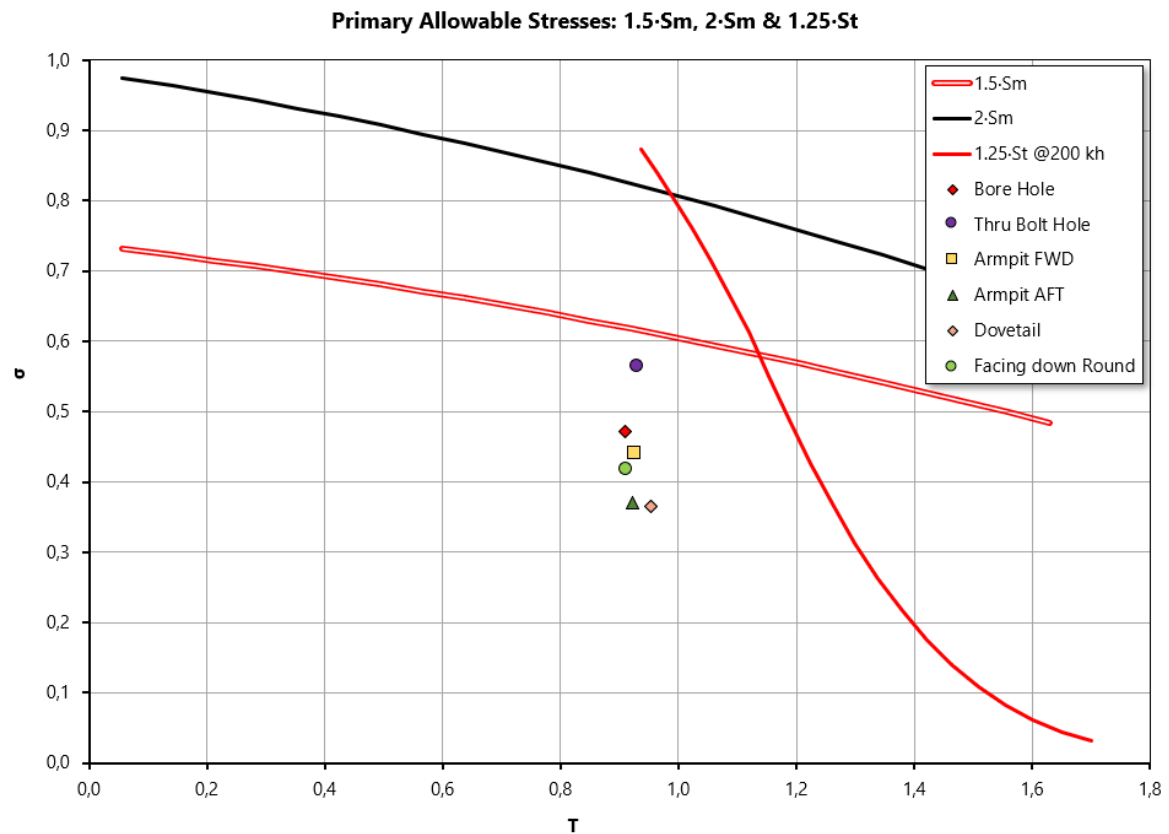


Figure 4.19: Wheel 15 mean primary and allowable stress

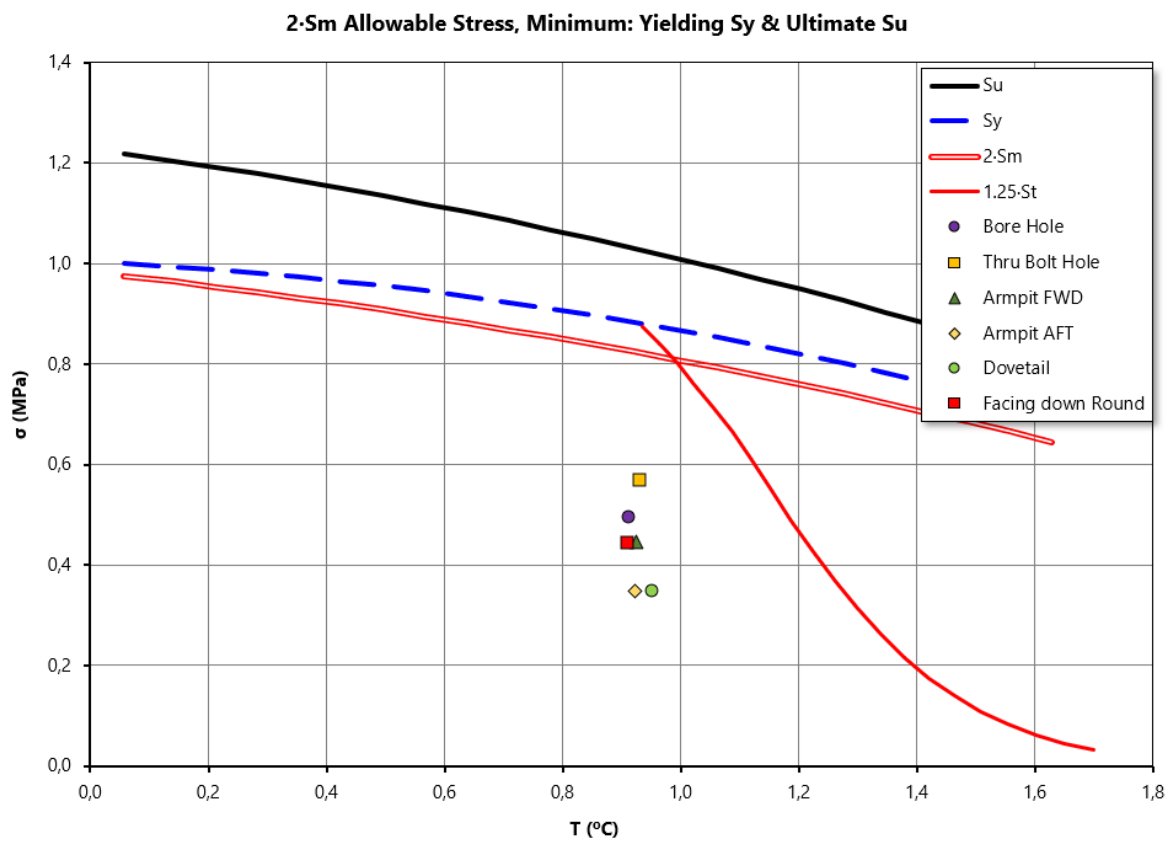


Figure 4.20: Wheel 15 mean primary + secondary and allowable stress

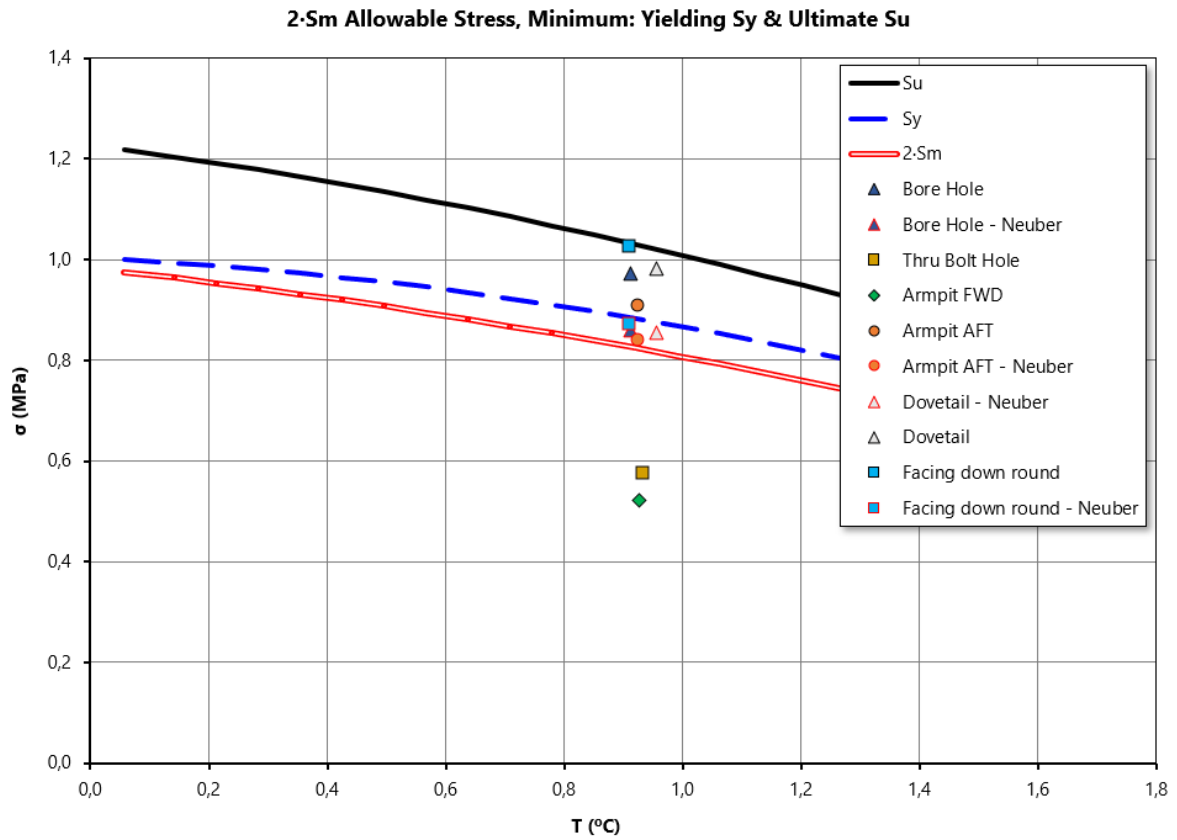


Figure 4.21: Wheel 15 primary + secondary peak and allowable stress

The results of the LCF analysis are summarised in the table below and show the bore hole is the element most subject to fatigue.

	n/N
Bore hole	44.6 %
Thru bolt hole	0.0 %
Armpit FWD	0.0 %
Armpit AFT	0.0 %
Dovetail	0.0 %
Facing down round	0.1 %

Table 4-2: Wheel 15 fatigue damage

4.4.3 Wheel 14 – 13

The fifteenth and fourteenth rotor stages are presented in a single treatment as the results obtained are very similar. In fact, both thermal loads to which they are subjected, and the geometries are similar, with a more symmetrical mass distribution than the previous bodies.

The areas examined are shown in Figure 4.22 and are as follows:

- Dovetail.
- Facing up round.
- Bore hole.
- Thru bolt hole
- Armpit AFT
- Armpit FWD

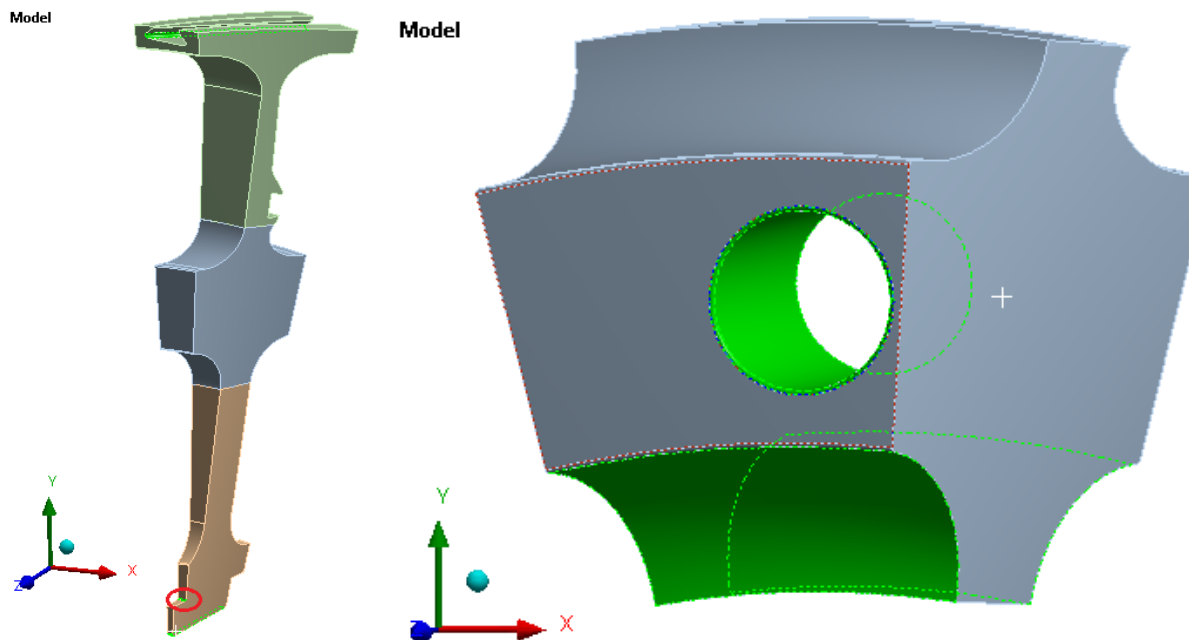


Figure 4.22: Wheel 14 – 13 critical areas

The most stressed areas are the dovetail slot and the facing up round, although the component does not show particular structural problems.

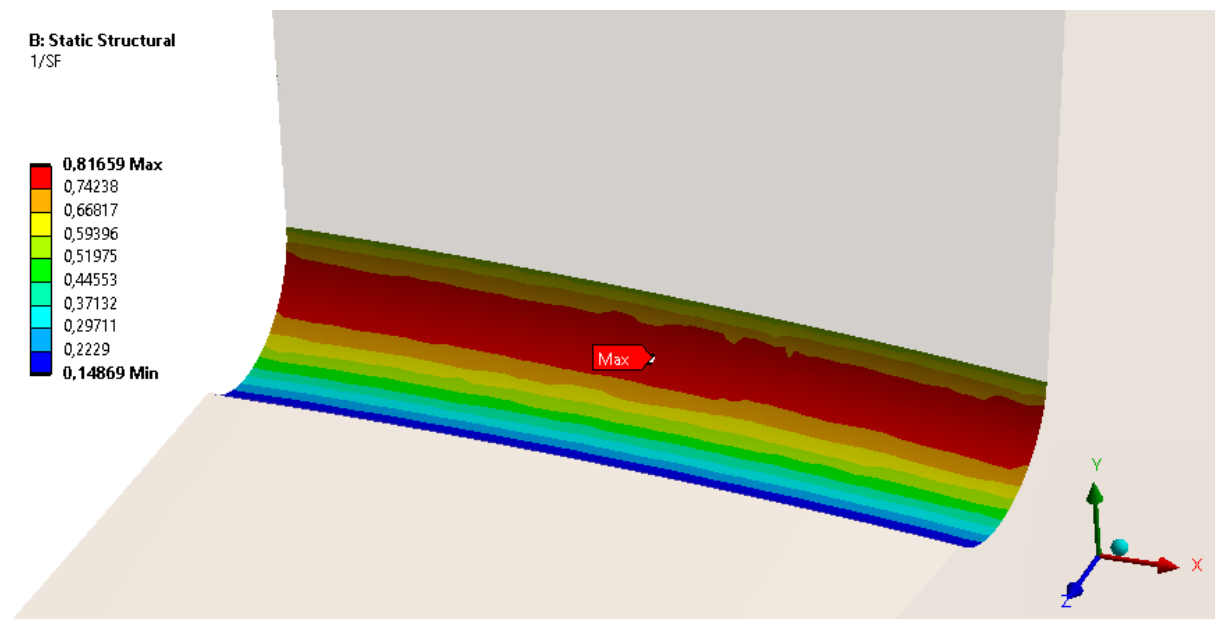


Figure 4.23: Wheel 14 stress field for facing up round

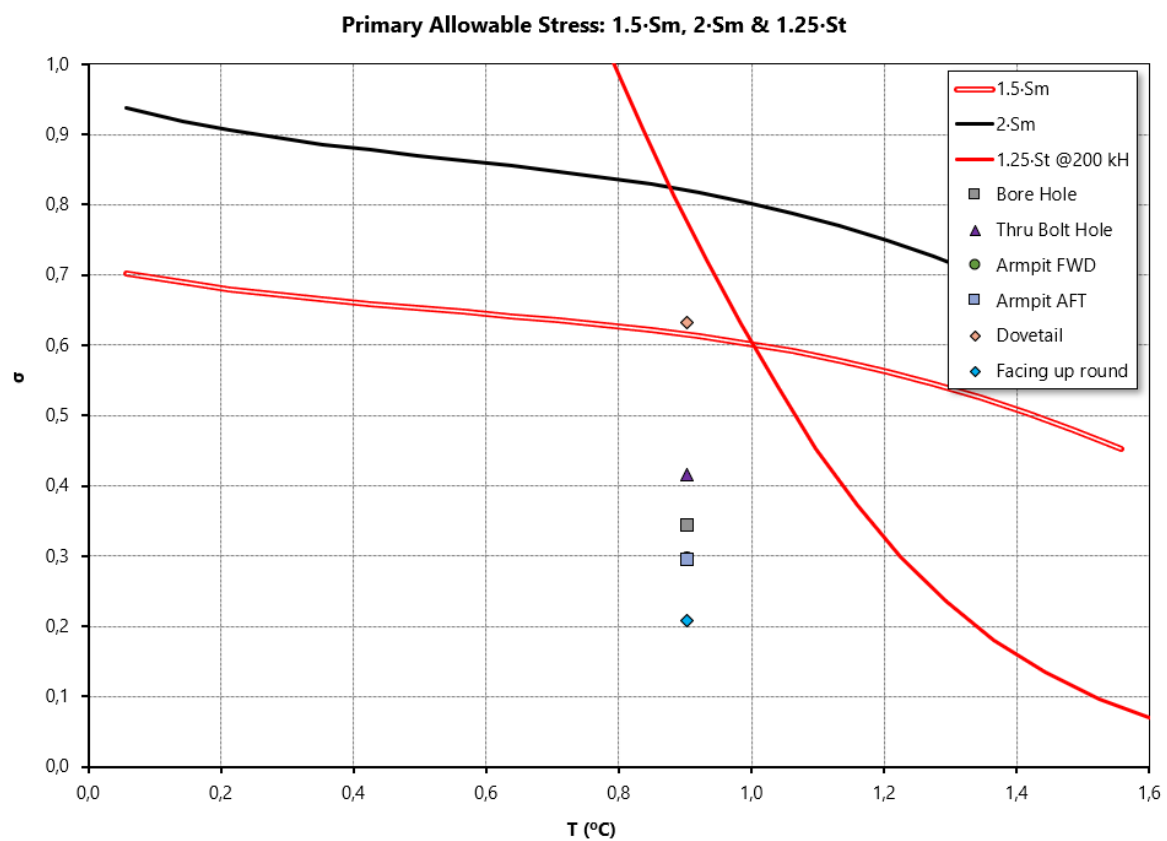


Figure 4.24: Wheel 14 mean primary and allowable stress

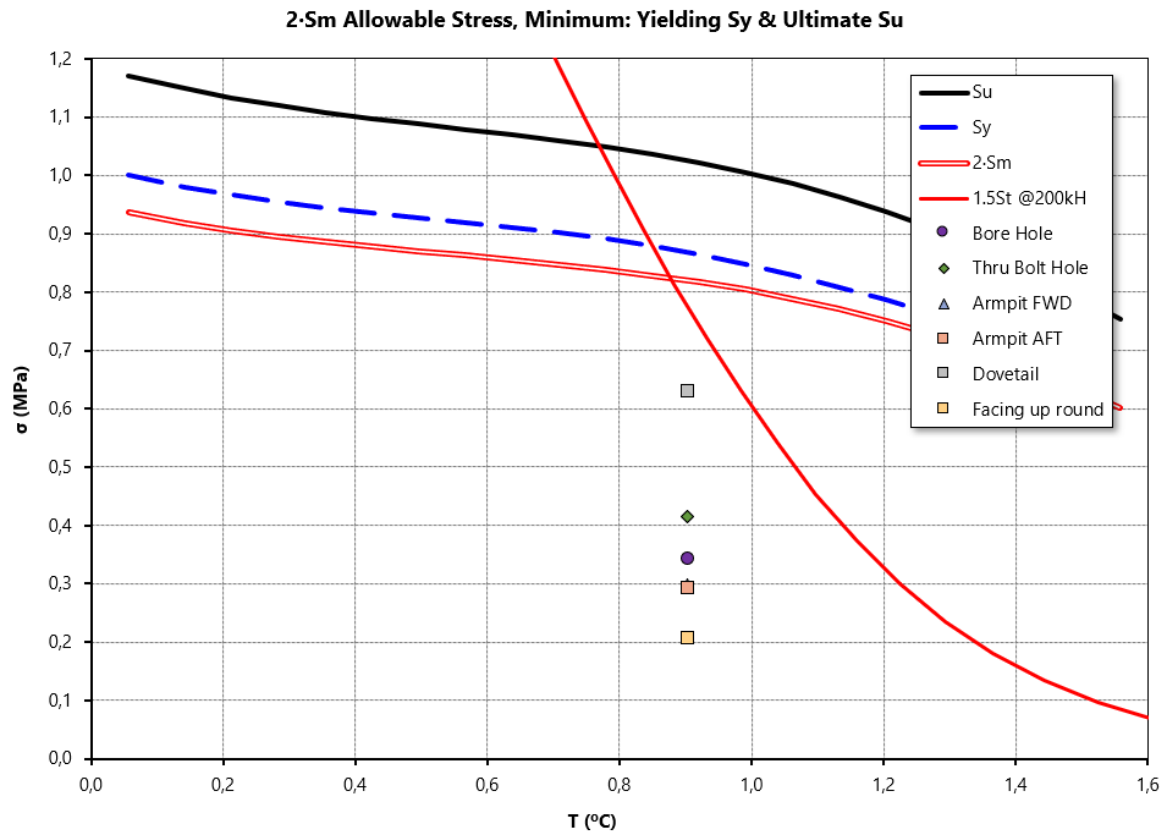


Figure 4.25: Wheel 14 mean primary + secondary and allowable stress

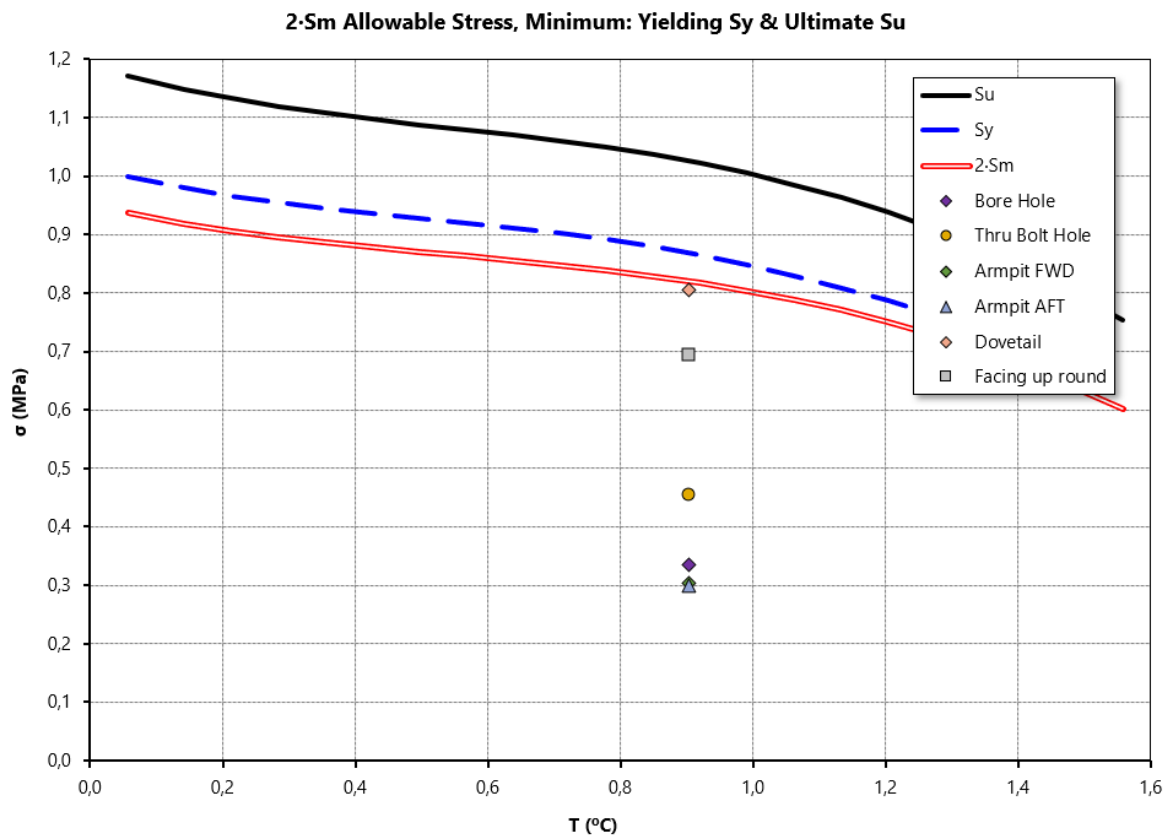


Figure 4.26: Wheel 14 primary + secondary peak and allowable stress

Finally, LCF analysis show dovetail slot and facing up round are the elements most subject to fatigue.

	n/N – wheel 14	n/N – wheel 13
Bore hole	0.7 %	0.7 %
Thru bolt hole	5.8 %	6.6 %
Armpit FWD	0.8 %	0.7 %
Armpit AFT	0.7 %	0.6 %
Dovetail	62.0 %	48.8 %
Facing down round	35.7 %	40.0 %

Table 4-3: Wheel 14 - 13 fatigue damage

5 Conclusions and further Developments

The FR1625 study conducted by Ethos Energy Italia S.p.A. was born in a worldwide context of great development of gas turbine systems market. Despite the progressive advance of technologies based on renewable sources, energy production is still heavily dependent on the use of non-renewable sources. In this scenario natural gas is the fastest growing fossil fuel, gradually replacing the use of coal and oil.

The first part of the work highlights how from a limited amount of information, through appropriate analysis and using operational experience, it is possible to determine many machine operating parameters necessary to conduct subsequent analysis on AxSTREAM.

Meanline output parameters show a full similarity with the average output parameters obtained in the Streamline analysis. Both show a good match with the set target values: the temperatures and power developed by the turbine are practically the same as those estimated, while the higher deviation value, even if within acceptable tolerances, refers to the total pressure at the turbine inlet. The change in the input temperature profile in the Streamline approach does not generate great differences for the output parameters.

Finally, the thermal-structural analysis carried out on the last four rotor components of the compressor shows the presence of critical areas that required a more in-depth static, creep and fatigue analysis. The latter, however, showed compliance with the company's minimum design criteria and will be subject to possible design improvements.

The main development of this thesis work has been the use of Streamline results to define boundary condition for turbine component thermal-structural FEA - ultimately resulting in turbine rotor components life prediction – conducted by Felice Di Palma.

As already anticipated in the abstract, the work carried out in collaboration with Pierfrancesco Angelini and Felice Di Palma, is part of a future company program called Life Time Extension (LTE), whose main goal is the re-design of rotor parts and definition of an opportune maintenance plan allows to extend the useful life beyond that recommended by the OEM.

The calculation model implemented on AxSTREAM is based on numerous assumptions, including the use of ISO compressor input conditions. It could therefore be interesting to study the behaviour of the machine under different ambient conditions.

Finally, streamline results could define input conditions for a CFD analysis of the main flow, to define more accurately the loads acting on the blades.

References

- [1] «Electricity generation,» [Online]. Available: https://en.wikipedia.org/wiki/Electricity_generation.
- [2] «Data and statistics,» [Online]. Available: <https://www.iea.org/data-and-statistics?country=WEOEUR&fuel=Energy%20supply&indicator=Electricity%20generation%20by%20source>.
- [3] «L'evoluzione del mercato elettrico: tutti i dati,» [Online]. Available: <https://www.terna.it/it/sistema-elettrico/statistiche/evoluzione-mercato-elettrico>.
- [4] «Contesto energetico internazionale,» [Online]. Available: <https://www.terna.it/it/chi-siamo/contesto-energetico-internazionale>.
- [5] [Online]. Available: <https://www.iea.org/fuels-and-technologies/gas>.
- [6] «Tracking Power,» [Online]. Available: <https://www.iea.org/reports/tracking-power-2019/natural-gas-fired-power#abstract>.
- [7] F. Jurado, «GAS TURBINES AND ELECTRIC DISTRIBUTION SYSTEM,» in *GAS TURBINES: TECHNOLOGY, EFFICIENCY AND PERFORMANCE*", New York, Nova Science Publishers, Inc., 2011, p. 189.
- [8] F. J. Brooks, «GE Gas Turbine Performance Characteristics».
- [9] R. e. Dow.W.Green, Perry's Chemical Engineers' Handbook, McGraw-Hill.
- [10] «AxSTREAM® Software Platform,» [Online]. Available: <https://www.softinway.com/software/>.
- [11] S. Inc., Tutorial.
]
- [12] P. Angelini, «Analisi dei flussi secondari e analisi FEM 2D del rotore di una turbina a gas,» 2020.
]
- [13] F. D. Palma, «Analisi FEM 3D e verifica statica e a fatica del Rotore di una turbina a gas per applicazioni industriali,» 2020.
]

Figure Index

Figure 1.1: Electricity generation by source in the world – 1990-2017	3
Figure 1.2: Electricity generation by source in Europe – 1990-2017	3
Figure 1.3: Electricity generation by source in Italy [TWh] – 2005-2018	4
Figure 1.4: Electricity generation by source in Italy – 2018	4
Figure 1.5: Electricity generation for fuel in Italy [GWh] – 2000-2018 [3].....	5
Figure 1.6: Changes in natural gas-fired power generation by region - 2018 [6].....	5
Figure 2.1: Single cycle, single shaft gas turbine.....	7
Figure 2.2: Temperature-entropy (TS) and pressure-volume (PV) diagrams for Brayton cycle	8
Figure 2.3: Global efficiency and specific power dependence over β and firing temperature ...	9
Figure 2.4: Effect of ambient temperature.....	9
Figure 2.5: Fan in the forward side of the aft stub shaft.....	12
Figure 2.6: Air extraction for cooling and pressurization process	13
Figure 2.7: Dimensionless discharge temperature for each stage	14
Figure 2.8: Dimensionless discharge pressure for each stage.....	15
Figure 2.9: Thermal resistances isolate hot gas flow	17
Figure 2.10: Wheel spaces pressurization and sealing wings	18
Figure 2.11: First and second stage nozzle	20
Figure 2.12: First stage buckets	20
Figure 3.1: 3D model assembly	24
Figure 3.2: Sectioned 3D models imported on AxSLICE	25
Figure 3.3: 4 of 9 airfoils for the second stage vane	26
Figure 3.4: Automatic slicing and correction process	27
Figure 3.5: Trend of the inlet and the outlet metal angle along the height for the second stage vane.....	28
Figure 3.6: Trend of the inlet and the outlet metal angle along the height for the first stage bucket.....	28
Figure 3.7: Trend of the inlet and the outlet metal angle along the height for the third stage bucket.....	29
Figure 3.8: Final AxSLICE output.....	30
Figure 3.9: Main AxSTREAM database	31
Figure 3.10: Setup window for first stage vane clearances	32
Figure 3.11: Setup window for first stage bucket clearances	33
Figure 3.12: 2D flow path.....	33
Figure 3.13: Main fluid properties	36
Figure 3.14: a) Thermodynamic cooling process for stator and rotor components.	37
Figure 3.15: Stator set up template.....	38
Figure 3.16: Rotor set up template	39

Figure 3.17: Tit° profiles along duct height.....	40
Figure 3.18: Actual plant operating point (P) on the compressor map	42
Figure 3.19: Firing and exhaust total temperature trend along blade height	44
Figure 3.20: Total temperature contour – OEM profile	45
Figure 3.21: Total temperature after optimization – Opt. profile	45
Figure 3.22: Mach number.....	46
Figure 3.23; Reaction degree	47
Figure 3.24: Velocity triangles for streamline 5	47
Figure 3.25: h-s diagram for streamline 5.....	48
Figure 3.26: Mass balance diagram.....	49
Figure 4.1: Ansys logical scheme	50
Figure 4.2: Ansys numerical procedure.....	54
Figure 4.3: Ansys Workbench	55
Figure 4.4: Imported pressure and thermal load	55
Figure 4.5: Meshing for wheel 16 smaller and larger slice	56
Figure 4.6: Aft stub shaft temperature field.....	58
Figure 4.7: Aft stub shaft dovetail slot stress field.....	59
Figure 4.8: Aft stub shaft most critical areas	59
Figure 4.9: Aft stub shaft mean primary and allowable stress.....	60
Figure 4.10: Aft stub shaft mean primary + secondary and allowable stress	61
Figure 4.11: Peak stress correction.....	62
Figure 4.12: Aft stub shaft primary + secondary peak and allowable stress	62
Figure 4.13: Wheel 15 total deformation.....	64
Figure 4.14: Wheel 15 critical areas.....	64
Figure 4.15: Wheel 15 stress field for facing down round	65
Figure 4.16: Wheel 15 stress field for bore hole	65
Figure 4.17: Wheel 15 stress field for thru bolt hole.....	66
Figure 4.18: Wheel 15 stress field for armpit AFT	66
Figure 4.19: Wheel 15 mean primary and allowable stress	67
Figure 4.20: Wheel 15 mean primary + secondary and allowable stress	67
Figure 4.21: Wheel 15 primary + secondary peak and allowable stress	68
Figure 4.22: Wheel 14 – 13 critical areas	69
Figure 4.23: Wheel 14 stress field for facing up round	70
Figure 4.24: Wheel 14 mean primary and allowable stress	70
Figure 4.25: Wheel 14 mean primary + secondary and allowable stress	71
Figure 4.26: Wheel 14 primary + secondary peak and allowable stress	71

Table Index

Table 2-1: Fuel molar percentage.....	11
Table 2-2: Components molar masses.....	11
Table 2-3: Components LHVs	11
Table 2-4: Dimensionless compressor diameter	15
Table 3-1: Stoichiometric moles of air in the combustion reactions.....	34
Table 3-2: Grams of air required for each gram of i-th fuel	35
Table 3-3: Fuel composition [g].....	35
Table 3-4: Air required	35
Table 3-5: Meanline analysis output deviations with respect to targets.....	42
Table 3-6: Streamline analysis output deviations with respect to targets.....	43
Table 4-1: Aft stub shaft fatigue damage	63
Table 4-2: Wheel 15 fatigue damage.....	68
Table 4-3: Wheel 14 - 13 fatigue damage.....	72